Aalto University
School of Chemical
Engineering

Aleksi Matikainen

MIXED-ANION COMPOUNDS: AN UNEXPLORED ALD PLAYGROUND FOR APPLICATIONS

Master´s Programme in Chemical, Biochemical and Materials Engineering

Major in Chemistry

Master's thesis for the degree of Master of Science in Technology submitted for inspection, Espoo, 9 July, 2018.

Supervisor Professor Maarit Karppinen

Instructor Ph. D. Tripurari Sharan Tripathi

Aalto University
School of Chemical
Engineering

Aalto University, P.O. BOX 11000, 00076 AALTO
www.aalto.fi

Abstract of master's thesis

Author Aleksi Matikainen

Title of thesis Mixed-anion compounds: An unexplored ALD playground for applications

Degree Programme Master's programme in Chemical, Biochemical and Materials Engineering

Major Chemistry

Thesis supervisor Professor Maarit Karppinen

Thesis advisor(s) / Thesis examiner(s) PhD Tripurari Sharan Tripathi

Date 09.07.2018 **Number of pages** 89 **Language** English

Abstract

Mixed-anion compounds, such as oxypnictides and oxychalcogenides, are an emerging research subject as functional solid-state materials. Their structures are more complex compared with traditional oxides, which provides novel building blocks for new functional materials. Potential applications include transparent electronics, photovoltaics and thermoelectrics. Atomic layer deposition (ALD) is a possible solution for fabricating mixed-anion thin films with superior properties to bulk mixed-anion compounds.

Oxysulfides are an interesting group of mixed-anion compounds with desirable electrical properties and an inexpensive and non-toxic composition of earth-abundant elements. Their layered structure induces several intriguing properties such as superconductivity, transparent p-type semiconductivity and wide band gap. Only a few oxysulfides have been fabricated with ALD before.

In this work, a novel atomic layer deposition process for fabricating oxysulfide LaOCuS (lanthanum oxide copper sulfide) thin films was implemented. The films were deposited on silicon and borosilicate glass substrates and the precursors used for depositions were $La(thd)_2$, ozone, $Cu(acac)_2$ and elemental sulfur. Different cycle numbers were utilized along with varying deposition temperatures and pulse/purge lengths to find the optimal deposition conditions. X-ray reflectivity (XRR) and grazing incidence X-ray diffraction (GIXRD) were used for characterization of the films. Both as-deposited and annealed films were characterized. Thin films of LaOCuS were successfully fabricated: partial crystallinity was observed in the deposited films and their phase composition was examined by comparing the XRD data of the films and the powder XRD data corresponding bulk compounds.

Keywords ALD, thin films, mixed-anion compounds, oxysulfides, lanthanum oxide, copper sulfide

Aalto-yliopisto
Kemian tekniikan
korkeakoulu

Aalto-yliopisto, PL 11000, 00076 AALTO
www.aalto.fi
Diplomityön tiivistelmä

Tekijä Aleksi Matikainen

Työn nimi Useamman anionin yhdisteet ja niiden käyttö ALD-sovelluksissa

Koulutusohjelma Master's programme in Chemical, Biochemical and Materials Engineering

Pääaine Chemistry

Työn valvoja Professori Maarit Karppinen

Työn ohjaaja(t)/Työn tarkastaja(t) PhD Tripurari Sharan Tripathi

Päivämäärä 09.07.2018 **Sivumäärä** 89 **Kieli** englanti

Tiivistelmä

Useamman anionin yhdisteet, kuten oksikalkogeenit ja oksipniktidit, ovat kasvava tutkimuskohde funktionaalisina kiinteän faasin materiaaleina. Koska niiden rakenne on monimutkaisempi kuin oksideilla, niitä voidaan käyttää lähtöaineina uusille funktionaalisille materiaaleille. Muutamia mahdollisia käyttökohteita ovat läpinäkyvä elektroniikka sekä valosähköiset ja termosähköiset materiaalit. Atomikerroskasvatuksella (ALD) on mahdollista valmistaa korkealaatuisia useamman anionin ohutkalvoja, joilla on paremmat ominaisuudet kuin vastaavilla bulkkiyhdisteillä.

Yksi useamman anionin yhdisteiden alaryhmä ovat oksisulfidit, joilla on erinomaisia elektronisia ominaisuuksia. Lisäksi ne ovat edullisia ja koostuvat myrkyttömistä ja yleisistä alkuaineista. Oksisulfidien suprajohtavuus, läpinäkyvyys, p-tyypin puolijohtavuus ja laaja energia-aukko ovat seurausta niiden kerrosrakenteesta. Vain muutamia oksisulfideja on valmistettu atomikerroskasvatuksella.

Tässä työssä valmistettiin LaOCuS-ohutkalvoa (lantaanioksidikuparisulfidi) käyttämällä uutta atomikerroskasvatusprosessia. Kalvot kasvatettiin pii- ja borosilikaattilasisubstraateille ja lähtöaineina käytettiin $La(thd)_2$:ta, otsonia, $Cu(acac)_2$:a ja alkuainerikkiä. Kasvatuksissa vaihdeltiin syklien määrää, kasvatuslämpötilaa ja pulssipituuksia optimaalisten kasvatusolosuhteiden löytämiseksi. Sekä lämpökäsitellyt että käsittelemättömät ohutkalvot karakterisoitiin. LaOCuS-ohutkalvon kasvatus atomikerroskasvatuksella onnistui. Ohutkalvot todettiin osittain kiteisiksi ja niiden faasirakennetta tutkittiin vertailemalla kalvojen XRD-dataa vastaavien bulkkituotteiden pulveri-XRD-dataan.

Avainsanat ALD, atomikerroskasvatus, ohutkalvot, oksisulfidit, lantaanioksidi, kuparisulfidi

Preface

The experimental research of this thesis was carried out at the Laboratory of Inorganic Chemistry at Aalto University School of Chemical Engineering between February 2018 and June 2018.

First, I would like to express my gratitude for my supervisor, Professor Maarit Karppinen, for trusting me with this opportunity in her research group. Secondly, I say thanks to my advisor, PhD Tripurari Sharan Tripathi, for advice on my interesting thesis topic and for his expertise on the laboratory equipment. Many thanks to the friendly people at the Research Group of Inorganic Chemistry, especially Juho Heiska, who gave me valuable information on the master's thesis, ALD reactors and data analysis, as well as Otto Mustonen and Professor Antti Karttunen who have helped me with theories behind superconductivity and crystallography. Kudos to my fellow workers in the School of Chemical Engineering, especially J-J, Kim and Erkka (for helping me with the gas cylinders).

Finally, I would like to (and will) say thank you to my friends from the Polytech Choir for all the wonderful experiences during my studies and for providing me with a musical environment during my free time. I also thank my family for supporting me during my studies. Special thanks to my lovely voice teacher Tuire, for patiently working with me during the past seven years.

Espoo 9.7.2018

Aleksi Matikainen

Table of contents

Symbols and Abbreviations

ALD	Atomic Layer Deposition
ALE	Atomic Layer Epitaxy
SALD	Spatial Atomic Layer Deposition
PVD	Physical Vapor Deposition
GPC	Growth per cycle
XRD	X-ray diffraction spectroscopy
XRR	X-ray reflectivity
GIXRD	Grazing incidence X-ray diffraction
acac	Deprotonated acetylacetone
thd	2,2,6,6-tetramethyl-3,5-heptanedione
LED	Light-emitting diode
MRI	Magnetic Resonance Imaging
R-SPE	Reactive solid-phase epitaxy
VESTA	Visualization for Electronic and STructural Analysis
eV	Electron Volt
T_c	Superconducting transition temperature
Å	Ångström (10^{-10} m or 0.1 nm)
TG	Thermogravimetry

1 Introduction

Mixed-anion compounds in bulk or thin film form are a less researched group of functional solid-state materials that have a variety of novel properties and applications. Research has been conducted on electrical applications [1,2], coatings [3,4], microbatteries [5], and various thin films [6]. Atomic Layer Deposition (ALD) provides an opportunity of synthesizing highly conformal structures, which helps improving or discovering new physicochemical properties in the compounds. [7]

Mixed-anion compounds offer an interesting basis for compounds sought for new functionalities. Their feature of containing multiple anions instead of a single oxide ion (in traditional oxides) makes them more interesting candidates for optical and electronic applications because of their broader coordination geometry. Applications include energy conversion, catalysis, battery electrodes, superconducting materials and thermoelectrics. Additionally, the anionic species (such as N, P, S, Cl and O) are usually light and earth-abundant. Controlling multiple anion ratio changes the dimensionality of these compounds, permitting modifications to compound functions. [8]

The main goal of the literature part of this thesis is to review different mixed-anion compound groups, compare the properties of similar compounds variations in properties across groups. In addition, the most common applications of mixed-anion compounds are examined.

The experimental part of the thesis focuses on the novel ALD deposition process of the inorganic quaternary oxysulfide LaOCuS that has been synthesized by various solid-state [9] and sputtering synthesis methods [10] but not yet with ALD.

Generally, very few mixed-anion thin films have been deposited with ALD and the particular LaOCuS compound has never been deposited. Toxic precursor substitution is a goal of the experimental part: the commonly utilized H_2S has been successfully substituted for elemental sulfur in ALD processes recently and

elemental sulfur is also used in the experimental part of this thesis as the source of sulfur [11].

LITERATURE PART

2 Mixed-anion compounds

Mixed-anion compounds are a group of compounds that contain two or more different anions. Two terminologies, mixed-anion and heteroanion compounds, are used for the same group of compounds [12] but to be consistent, only the term mixed-anion compounds is used in this thesis. Mixed-anion compounds contain more than one kind of an anion: usually two different anions are present but especially doped and substituted compounds may contain three or more anions [13,14].

In this thesis, the focus is on quaternary compounds that contain oxygen as one anion and another element from groups 15, 16 or 17 as the other (such as sulfur in oxysulfides). Generally, the format M_1OM_2A (where M_1 and M_2 are metal ions in the oxide and anion phases respectively) is used in representing the stoichiometry of the compounds. For ternary compounds, M_2 is omitted.

Oxygen is an element with which almost all other elements form compounds. The Earth's crust is abundantly composed of oxides, which are commonly found everywhere. Oxides are stable and easy to synthesize (usually by high-temperature solid-state reactions) and present diverse chemical and physical properties: catalysis, magnetism electronic properties, and high-temperature superconductivity are a few to name. [8,15]

Oxygen-containing mixed-anion compounds may also be called suboxides, i.e. they include an excess of electropositive metals compared to electronegative oxygen. As a result, the accommodation of more metals in the mixed-anion compound structures may be difficult. [16,17]

Synthesis methods of bulk mixed-anion compounds mainly include high-temperature solid-state reactions, where the typical temperature varies between

500°C and 1200°C and the synthesis is executed in silica or quartz ampoules [9,18–20]. Other methods include hydrothermal synthesis [21], high-pressure synthesis [22] and ammonolysis for oxynitrides [23]. There are various methods for synthesizing mixed-anion thin films, of which pulsed-laser deposition (PLD) [24], radio-frequency sputtering (RF sputtering) [10,25] and chemical vapor deposition (CVD) [26] are most common. Some atomic layer deposition (ALD) [27–29] processes have been reported as well. The synthesis of mixed-anion compounds may be complex because of their metastability [30]. Adaption for applications and devices requires chemical stabilization of the phases in these compounds, which may be possible by combining various synthesis methods, e.g. high pressure and high temperature, or by utilizing multi-step processes. [8]

Currently, mixed-anion compounds provide a new possible materials platform that may have new functionality compared to traditional single anion oxide compounds. The coordination geometry of mixed-anion compounds is different, which provides new building blocks for seeking novel compounds and functions. [8]

This thesis concentrates on the following mixed-anion groups, whose naming is based on the two different anions included in the compound: oxychalcogenides (oxide-chalcogenides), oxypnictides (oxide-pnictides) and oxyhalides (oxide-halides). [8]

2.1 Properties

Mixed-anion compounds have various electronic and optical properties, e.g. semiconductivity, which is observed in oxysulfides (wide-band gap semiconductivity in LnOCuQ (Q = S, Se) [31]) and oxynitrides, and superconductivity, which is observed especially in oxypnictides. On the other hand, oxyselenides have been studied for their thermoelectric properties [32,33] and oxynitrides and some oxysulfides for photocatalytic applications [34–36]. The number of different mixed-anion compounds is limited even with a wide range of

structural possibilities. Currently, there are roughly 3000 mixed-anion compounds recorded in the ICSD database (the number of different oxide compounds is over 50 000). [8]

In cation-based single-anion compounds, the building units are common coordination polyhedra, such as CuO_4 square planes. In mixed-anion compounds, one or more oxide anions are replaced with other anions, which results in novel coordination geometries and flexibility for material functions due to the different properties of anions: ionic radius, electronegativity, polarizability and valence. For example, the square planar Fe_2O layers in the oxychalcogenide $A_2F_2Fe_2OQ_2$ (A=Sr, Ba; Q=S, Se) affect the properties of the material. Metal ion substitution is a common method for controlling the bond properties and electron count in mixed-anion compounds. [8,15,37]

Several mixed-anion compounds consist of alternating layers of metal oxides and metal chalcogenides or pnictides, creating a stack of alternative layers. Layered oxychalcogenides include alternating layers of an oxide and a chalcogenide: for example, the structure of LaOAgS contains layers of LaO and AgS with weak La-S bonds between them. The sulfur atoms are located on two parallel planes close to each other, whereas the Ag atoms are located inside the tetrahedral of S atoms. [14,38] Not all mixed-anion compounds possess a heteroleptic (transition metal or main group compounds having more than one type of ligand [30]) coordination geometry around a transition metal: some structures are also composed of alternative layers with homoleptic (transition metal or main group compounds having only one type of ligand [30]) coordination by a different anion. A homoleptic example is $Sr_2MnO_2Cu_{1.5}S_2$ that has alternating layers of Sr_2MnO_2 and $Cu_{1.5}S_2$. In general, crystallography explains the structural relationships between different mixed-anion compounds. The crystal structures of layered oxychalcogenides and oxyhalides are related to Ruddlesden-Popper structures where the oxide ions in the rock-salt-type layers are replaced by larger anions and oxypnictides have cations inserted into tetrahedral holes in the layers that large anions form. [8,15]

In layered structures, low dimensionality in structural and physical properties is achieved when two anions order within a material. Different anion types commonly arrange in layers, which leads to two-dimensional conductivity or magnetic correlations when cations with unpaired electrons are present. The structure type that a mixed-anion compound adopts, affects its properties: for example, ZrCuSiAs type structures include various high-T_c (high superconducting transition temperature) superconductors. [8]

Control of the electronic communication between the oxide and chalcogenide layers provide novel and unusual properties complementary to those found in oxides and chalcogenides. For example, in CaOZnS the structure contains two hexagonal layers of CaO and ZnS with similar topology, which increases its piezoelectric coefficient. [14,39]

Band gap engineering is possible for a variety of mixed-anion compounds that exhibit semiconductivity. Mixed crystal preparation is one technique to utilize with mixed semiconductor systems. In $LaOCuS_{1-x}Se_x$, the formation of solid solutions allowed the band gap engineering without affecting the band gap emission feature or p-type conductivity of the oxychalcogenide compound. [40,41] The semiconductivity for wide band gap optoelectronic materials has been studied for mixed-anion compounds and novel transparent p-type semiconducting mixed-anion compounds have been found. For example, $La_{1-x}Sr_xOCuS$ and LaOCuS are optically active, transparent and wide-gap materials and thus are new candidate materials as p-type semiconductors. These could be applied in transparent transistors, LEDs or solar cells. [42]

Mixed-anion systems often adopt anion-ordered structures with transition metal cations in unusual oxidation states and coordination environments. If the oxide layer is thicker or the structure is similar to $Sr_2ZnO_2Cu_2S_2$, a transition metal ion may be integrated in the place of Zn in the oxide layers. This affects the orbitals and may result in various magnetic properties in the compounds, because of localized magnetic moments on the transition metal ions. Further, examples of

unusual coordination environments include square planar systems in $A_2CoO_2Cu_2S_2$ (A = Sr, Ba) and distorted octahedral FeO_2Se_4 coordination environment in $La_2O_3Fe_2Se_2$. [15,31] Studies of the crystal structures and emerging computational research [43–46] have provided up to date information on the magnetic properties of mixed-anion compounds. Some mixed-anion compounds have exhibited ferromagnetism [34,47,48]. However, antiferromagnetism and paramagnetism seem to be the most common attributes. [18,49]

2.2 Classes and subgroups

This thesis concentrates on mixed-anion compounds that contain oxygen as one anion. Mixed-anion compounds can further be divided into subgroups where the naming of the subgroup is derived only from the other anionic element (from groups 15-17) besides oxygen. An example of this are oxyfluorides (oxide-fluorides), which are a subgroup of oxyhalides. [8]

2.2.1. Oxypnictides

Oxypnictides contain both oxide anions and the anions of a heavier pnictogen (P, As, Sb, Bi). The term pnictide is a common term for naming compounds of the pnictogens (or pnicogens). There are over 100 oxypnictides reported, which include 30 distinct elements. The typical synthesis of bulk oxypnictides require high temperature [50] or high pressure [51] conditions. In addition, pulsed laser deposition (PLD) and molecular beam epitaxy (MBE) have been common methods for oxypnictides thin films synthesis. [16,39,52–54]

The characteristic structure of oxypnictides is different from the structure of simpler oxides: the crystal structures are composed of alternating layers. The coexistence of both oxygen and a pnictogen in these compounds forms polyatomic anions, pnictates, of which examples are phosphates, arsenates, bismuthates and antimonates (PnO_4^{3-}, where Pn=P, As, Bi or Sb). The structure-property relationship of layered d-metal oxypnictides is studied by investigating both inter-

and intralayers in the structure and selecting suitable cations for interlayers and pnictide ions for intralayers. Most usual structures of d-metal oxypnictides include fluorite or antifluorite type layered structures. Figure 1 shows two basic oxypnictide structures and common crystallographic sites for species to occupy. [16]

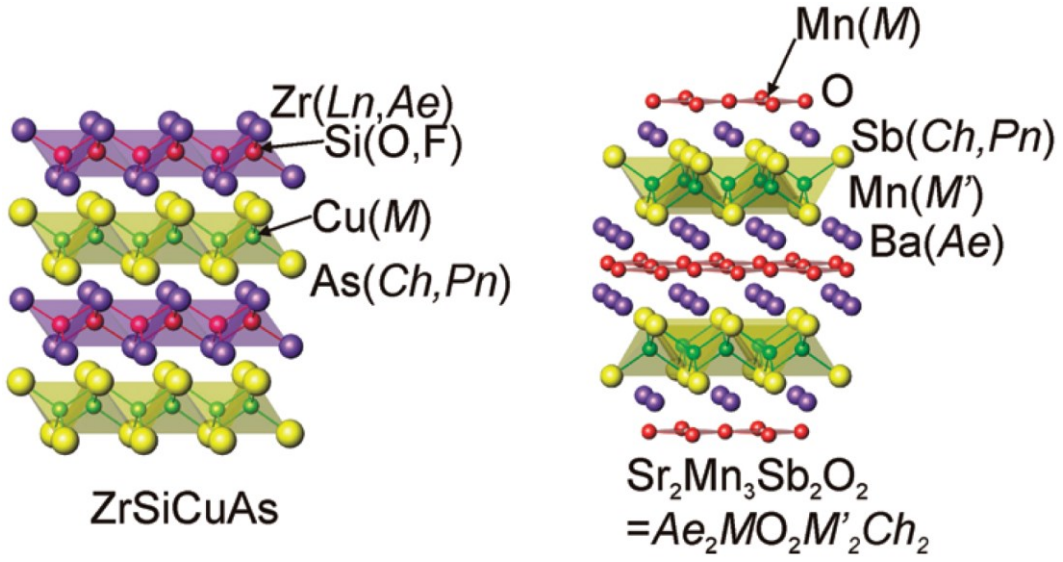

Figure 1. Oxypnictide ZrSiCuAs (left) and $Sr_2Mn_3Sb_2O_2$ (right) structures, which show crystallographic sites for species to occupy. These species include Ln (lanthanides), Ae (alkaline earth metals), M/M' (transition or main group metals), Ch (chalcogenides) and Pn (pnictides). [15]

Concerning electronic properties, the oxide and pnictide layers in layered oxypnictides are rather electronically distinct. The difference depends on the size of the cations in the compound structure due to varied distance between the metal and the pnictogen atom. Thus, the pnictide anion may be more or less engaged in bonding interactions with the metal. [15]

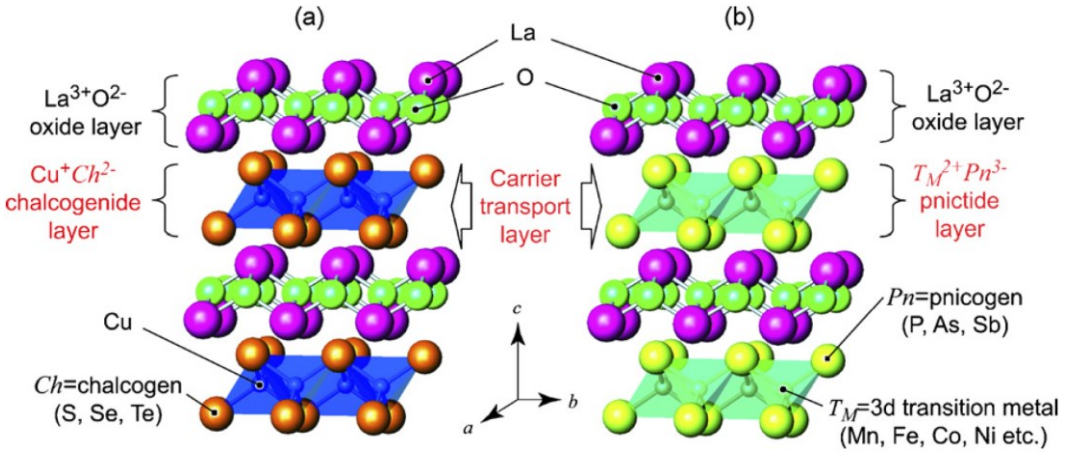

Figure 2. The crystal structures of a layered oxychalcogenide LaOCuCh (Ch = chalcogen) is similar to a layered oxypnictide LaOTMPn (TM = divalent 3d transition metal, Pn = pnictogen). The chalcogenide and pnictide layers work as carrier transport layers. [55]

The layered structures of oxypnictides are similar to the structures of oxychalcogenides, as presented in Figure 2. It also shows the oxidation states of lanthanum and copper in the layered oxychalcogenide LaOCuCh (Ch = chalcogen). La^{3+} and Cu^{+} indicate that lanthanum layer of the mixed-anion compound has more positive charge than the copper layer. The CuCh layer between the oxide layers works as a transport path for hole carriers, which are generated in the LaO layer. Orbital hybridization broadens the hole conduction paths. [55,56] Also, the copper deficiency in compounds implies that the transition metal or lanthanide in the compound is oxidized. The Cu ion also has variable occupancy in the tetrahedral sites of the chalcogenide layer. [15]

Transition metal-based oxypnictides $LaOT_MP$ (T_M=Fe, Ni) are isostructural to layered oxychalcogenides LaOCuCh. The layer composed of the transition metal and a pnictogen in oxypnictides is expected to conduct the carrier transport similar to the layer composed of copper and a chalcogen in oxychalcogenides. This has helped in finding novel superconductors such as LaOFeP and LaONiP. Like oxychalcogenides, oxypnictides have promising electrical properties as transparent conductors and battery materials. In addition, oxypnictides are also supposed to have similar ferromagnetic properties to oxychalcogenides. [15,55]

The first oxypnictide superconductor, $La[O_{1-x}F_x]FeAs$, was discovered by Kamihara in 2006 [50]. Other $R[O_{1-x}F_x]FeAs$ (R=rare-earth metal) iron pnictides have been found to exhibit superconductivity too, which has led to an intensive search for new transition metal based superconductors. Many oxypnictides and oxychalcogens share the same ZrCuSiAs structure (with space group P4/*nmm*): those compounds exhibit superconductivity and have interesting magnetic and transparent p-type semiconducting properties. [53,57] Doping and substitution have been vital in searching for higher superconducting temperatures, of which one example is superconducting state in $BaOTi_2Sb_2$ achieved with Na substitution [58]). One of the highest superconducting transition temperatures has been reported for $Sm[O_{1-x}F_x]FeAs$ fluorine-doped iron oxypnictides with T_c = 55 K [59]. For LaCoOAs, the transition temperature has been estimated for as high as 66 K but apparently not physically confirmed [48]. Another research interest has been in the field of pnictides that contain $[CuO_2]^{2-}$ -layers, because other compounds of this type are known to exhibit superconductivity [16,60]. Figure 4 shows a collection of oxypnictides and their superconducting transition temperatures. In Table 2, a selection of oxypnictide compounds and their properties can be found.

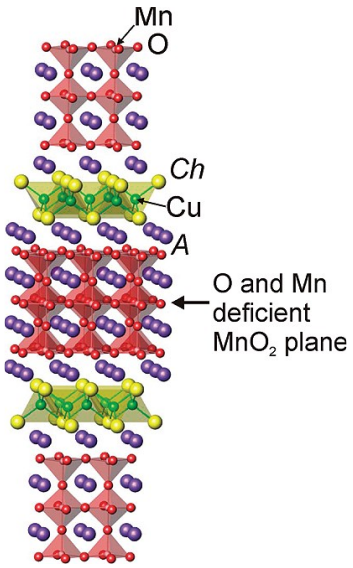

Figure 3. The crystal structure of $A_4Mn_2O_{7.5}Cu_2Ch_2$ (A = Sr, Ba; Ch = S, Se). The oxide block includes a plane with Mn and oxide deficiencies. The mean oxidation state of manganese is +3. [15]

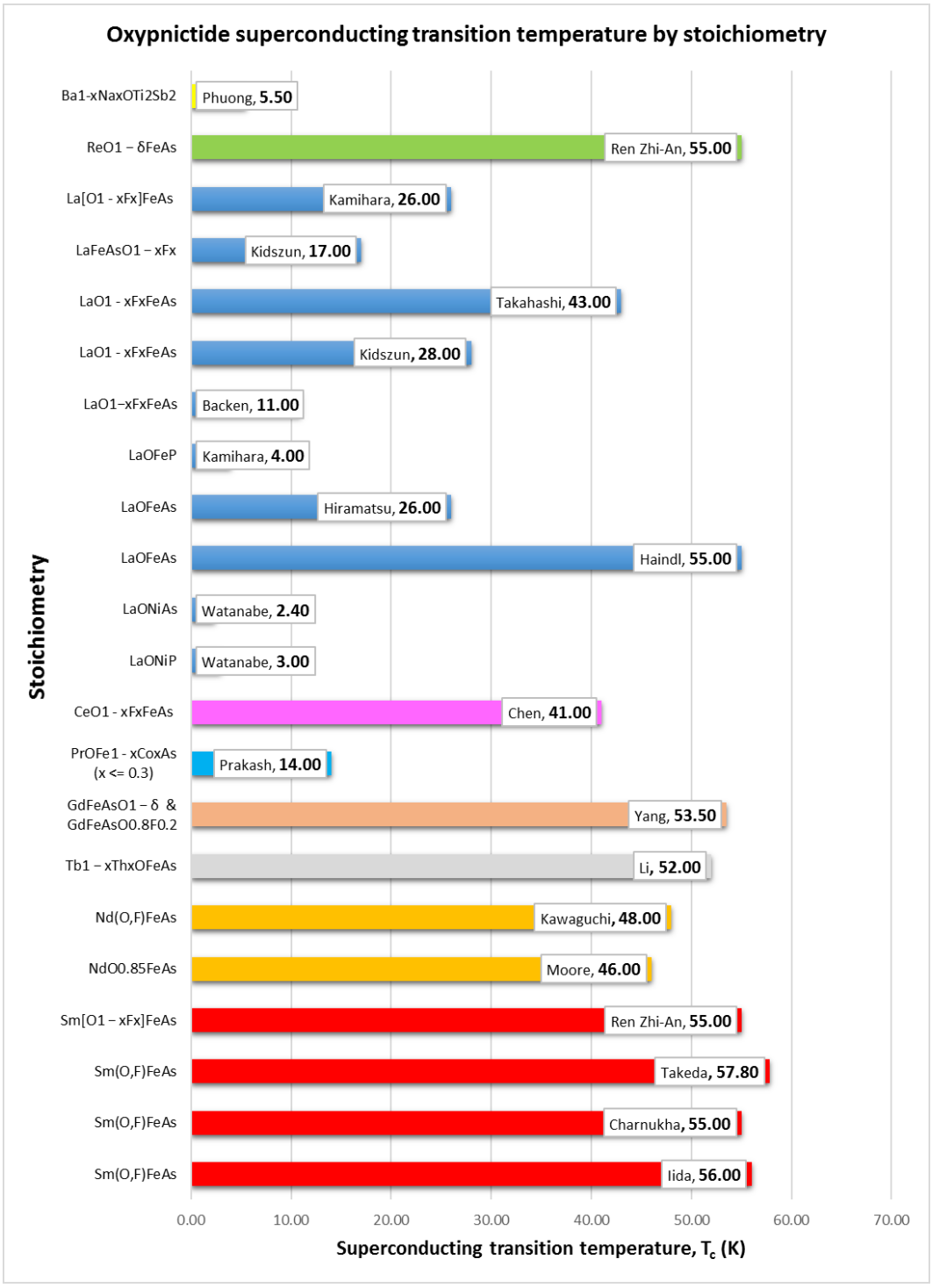

Figure 4. Oxypnictide superconducting transition temperatures (K).

Studies of the magnetic properties of oxypnictides frequently go in line with the superconductivity studies. For instance, perfect diamagnetism was observed in LaOFeP and this verified the occurrence of the superconducting transition in the compound [50]. Diamagnetism and its onset is also determined in other studies, from the field cooling (FC) curves [59,61–63]. Antiferromagnetic ordering of ion magnetic moments are observed in low temperatures for $CeO_{1-x}F_xFeAs$ [64] and $Tb_{1-x}Th_xOFeAs$ [65], and ferromagnetism in LaOCoX (X=P,As) compounds [48].

2.2.1.1 Oxynitrides and oxyphosphates

Oxynitrides are a relatively new class of compounds that may exhibit the properties of both oxides and nitrides. The optical and electrical properties of oxynitrides have not been extensively studied; however, oxynitrides have been reported as either semiconductors or insulators with carrier concentrations of 10^{13} – 10^{21} cm^{-3} and Hall mobilities of up to 200 $cm^2V^{-1}s^{-1}$ [66,67]. Most common applications include oxynitrides glasses (where nitrogen incorporation increases the resistance, elastic modulus, tenacity and hardness of the glass) [68], thin films [29,67,69,70] and photocatalytic applications. Oxynitrides are suitable for catalysis because of their high corrosion resistance and electrical conductivity. Silicon oxynitrides have also been utilized in steel coatings. [34,71]

Metal oxynitrides are intriguing in the field of photocatalytic processes, such as water splitting for hydrogen evolution, because of their small band gaps that lead to activity in the visible light-driven photoreactions. Only a few oxynitrides have been reported as ferromagnetic: these include $EuNbO_2N$ [23] and $EuWON_2$ [72]. Common oxynitrides include metals such as titanium, niobium, zirconium, gallium and tantalum. Gallium-zinc oxynitride is a solid solution of GaN and ZnO, while tallium oxynitride (TaON) is hepta-coordinate with monoclinic crystal structure and has two anion sites occupied by O and N (Figure 5). Perovskite structured oxynitrides have also been prepared. Lithium phosphorus oxynitride LiOPN (LiPON) is a compound utilized in Li-ion microbattery electrolytes. This compound

has also been deposited as a thin film with ALD. See Table 1 for more oxynitride compounds and their properties. [34,73]

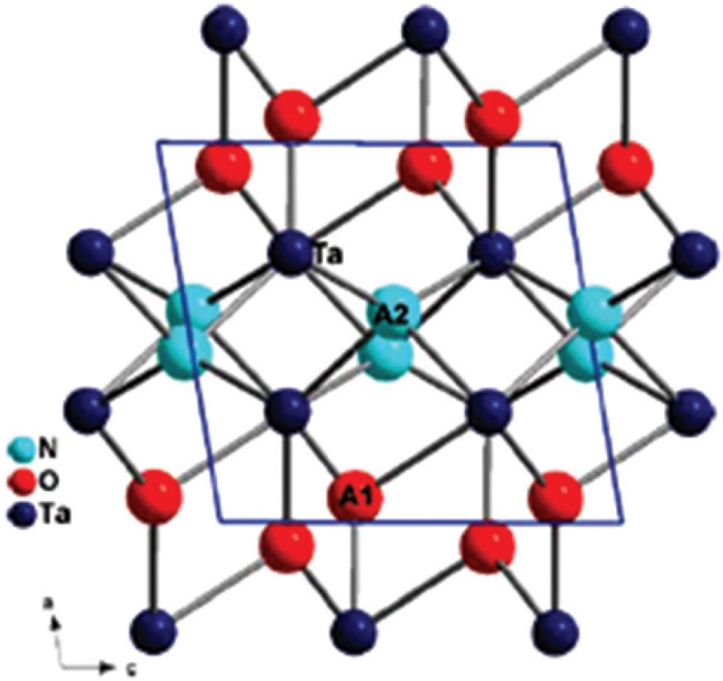

Figure 5. The crystal structure of TaON.

Oxyphosphates include a phosphate anion in addition to the oxide anion. Zinc oxyphosphate has been extensively used in dentistry [74], other examples include quaternary NdOZnP [75], ternary antiferromagnetic MO_5FeP (M = Co, Ni, Cu) [76], as well as superconductors LaONiP [77] and LaOFeP [50]. Mixed phosphate crystals have also been studied for their luminescent properties [78].

Table 1. Oxynitride compounds and their properties.

Stoichiometry	Carrier conc. [n] (cm^{-3})	Mobility [μ] ($cm^2V^{-1}s^{-1}$)	Conductivity [σ] (S/cm)	Type	Optical band gap [E] (eV)	Ref.
LiOPN		very small	$3.8 * 10^{-10}$ - $1.67 * 10^{-6}$			[69], [79], [73]
CaO_2TaN					2.43	[80]
BaO_2TaN				I		[81]
stainless steel 316 + O + N			$3.1*10^{-6}$ - $7.0*10^{5}$	C & Se	1.78	[82]
SiOxNy:H	10^{15}		$4.5*10^{-3}$	Se	2.3	[83]
Examples: **TaON, $Ti_3O_3N_2$, $Zr_3O_3N_2$**				Se	3	[34]
ZnON	10^{17} - 10^{19}	2 - 10	0.1	Se	3.2	[84]
ZnON	10^{16} - 10^{21}	0 - 50		Se		[66]
ZnOSnN	$6 * 10^{13}$	2.8	$2.3 * 10^{-6}$	Se	3.2	[70]
ZnO_xN_y	10^{19}	200		Se		[67]
TiN:O, TiO_xN_y & TiO_2:N			**$sigma_{300K}$ =** $7.14 * 10^{4}$ Sm^{-1}	Se		[85]
ZrO_xN_y				Se	3.6	[86]
$TaO_{2.42}N_{0.25}$				Se	2.3	[87]
LaO_2HfN NdO_2HfN SmO_2HfN			1.0^{-10}	I	3.4	[35]
LaO_xTiN_y				Se	2.05 - 2.35	[88]
LaO_2TiN				Se	2.1	[89]
$EuNbO_2N$ & $EuTaO_2N$				I		[23]

Table 2. Oxypnictide compounds and their properties.

Stoichiometry	Conductivity [σ] (S/cm)	*Type	Optical band gap [E] (eV)	[T_c] (K)	Magnetic properties	Ref.
$BaOTi_2Sb_2$, $Ba_{0.90}ONa_{0.10}Ti_2Sb_2$, $Ba_{0.85}ONa_{0.15}Ti_2Sb_2$	0.2 – 1	Su		5.5	**$BaTi_2Sb_2O_{(1-x)}F_x$:** AFM	[63]
$Ba_2OTi_2Cr_2As_4$	2.3	C			AFM	[87]
MO_5FeP (M = Co, Ni, Cu)		I			AFM	[79]
$ReO_{1-\delta}FeAs$	0 – 2	Su		55	Diamagnetic	[69]
ROZnP (LaOZnP)						[78]
Tb(O,F)FeAs & Dy(O,F)FeAs	0 – 1.25			45.9		[59]
$PrOFe_{1-x}Co_xAs$ (x <= 0.3)	0 – 0.14	Su		14	**Diamagnetic below T_c	[67]
$GdFeAsO_{1-\delta}$ & $GdFeAsO_{0.8}F_{0.2}$	0 – 1	Su		53.5	Diamagnetic	[68]
$Lu_xY_{1-x}O_4P$		Se	5.6			[81]
LaOFeAs & SmOFeAs		Su		55		[17]
LaOFeAs	0 – 0.8	Su	**LaOCuS:** 3.241 **LaOCuSe:** 2.925	26	Perfect diamagnetism	[66]
$LaO_{1-x}F_xFeAs$		Su		28		[32]
$LaFeAsO_{1-x}F_x$		Su		17		[62]
$La[O_{1-x}F_x]FeAs$	0 – 0.2	Su		26	Diamagnetic susceptibility 50%	[85]
$LaO_{1-x}F_xFeAs$	0 – 3.33	Su		43	Magnetic instability	[87]
LaOFeP		Su				[58]
LaONiP	0.83	Su		3	Pauli paramagnetism	[80]
LaONiAs	0.29	Su		2.4	Pauli paramagnetism	[89]
LaOCoP & LaOCoAs	40				Ferromagnetic	[54]
LaOZnAs & YOZnAs		Se	**LaOZnAs:** 0.65 **YOZnAs:** 1.3			[91]
$CeO_{1-x}F_xFeAs$ (x <= 0 - 0.20)	0 – 0.5			41	AFM	[71]
bulk: **Pr(O,F)FeAs** thin film: **Sm(O,F)FeAs**	0 – 1.11	Su (thin film)		55		[90]
$NdO_{0.85}FeAs$		Su		46	Paramagnetic background	[83]
Nd(O,F)FeAs	0.1 – 1	Su		48		[18]
$NdO_{1-x}F_xMnAs$ & $PrO_{0.95}F_{0.05}MnAs$	**$PrO_{0.95}F_{0.05}$ MnAs:** 3.30	Se	**$NdMnAsO_{1-x}F_x$:** 0.023 **$PrMnAsO_{0.95}F_{0.05}$:** 0.048		AFM	[88]
$Sm[O_{1-x}F_x]FeAs$	0 – 0.4	Su		55	Diamagnetic	[64]
Parent compound: **SmOFeAs** Film: **Sm(O,F)FeAs**	0 – 1	Su		56	Critical current density: $J_c > 10^5$ A/cm^2	[82]
Sm(O,F)FeAs	0 – 0.83	Su		57.8		[89]
$Tb_{1-x}Th_xOFeAs$	0.04 – 0.2	Su		52	AFM	[70]

*legend: Su=superconductor, Se=semiconductor, C=conductor, I=insulator, AFM=antiferromagnetic

**diamagnetic: diamagnetic transition is observed when determining the superconducting transition temperature

2.2.2. Oxyhalides / Oxohalides

Halide (or halogenide) is a generic term for naming compounds of halogens. Oxyhalides are mixed-anion compounds containing one or more elements combined with oxygen and halogen atoms (F, Cl, Br, I, At). Most metals form oxyhalides, but the alkali metals are an exception. Some of the most common oxyhalides in this group include nitrogen, phosphorus and sulfur oxyhalides. [52,90,91]

Especially bismuth-containing oxyhalides such as BiOCl, BiOBr and BiOI [92–94] and oxyfluorides such as YOF [95,96] have been studied comprehensively. The applications of oxyhalides include new cathode materials [95,97], photocatalytic applications of bismuth oxyhalides [98–100] as well as optoelectronic materials [101].

Mixed-anion oxyfluorides are an emerging material group for high-capacity cathodes. They are studied as an alternative to pure fluorides because of their enhanced cyclability via oxygen substitution. Complex electrochemical reactions are attributed to the cycling in mixed-anion compounds and their electrochemical properties are altered with substitution. For example, the higher oxidation state of Fe in oxygen-substituted FeO_xF_{2-x} is expected to be the reason of its improved electrical conductivity. [97]

Oxyfluorides are also strong fluorinating agents that react violently with water and phosphorus. Examples include selenium oxyhalides $SeOF_2$ and $SeOFI_2$. [90]

The oxidation state of phosphorus affects the preparation and composition of phosphorus oxyhalides. The most desirable is the +5 oxidation state of phosphorus, of which compounds such as POF_3, $POCl_3$ and $POBr_3$ and $POClF_2$ are produced. +3 is also a well-known oxidation state of phosphorus for mixed chlorofluoride and bromofluoride compounds. Furthermore, the oxidation state of sulfur is typically +4 in SOX_2 thionyl or sulfur(IV) oxyhalides or +6 in SO_2X_2 sulfuryl or sulfur(VI) oxyhalides. [90]

In an iron oxyfluoride compound FeO_xF_{2-x}, the Fe_2O_3 and FeO_xF_{2-x} are found to coexist for $x \leq 0.7$ but FeO_xF_{2-x} still remained as a single phase. Maximum oxygen substitution is assessed to improve the electrochemical reversibility and electric conductivity of the material so x=0.7 is the most viable amount. The product is shown to have a good capacity retention with reasonable cyclability and its working potential can be compared with sodium-sulfur or sodium-air systems. [95] Similar results have been received for the compound of same stoichiometry and the oxygen substitution is believed to sustain an oxygen-rich layer on the compound surface. This would enhance the cycling stability as well as the electrochemical activities in FeO_xF_{2-x} electrodes. [97]

As an addition, the carrier transport properties of Tl, Pb and Bi based oxyhalides are attributed to their ions (6p and 5p ions with an outer configuration of ns^2). Thus, the less toxic Bi^{3+} based oxyhalides have been studied for their wide band gaps that allow various optoelectronic applications. Computational researches, which usually concentrate on the electrical and optical properties of the compounds, have also been conducted. [101]

Table 3. Oxyhalide compounds and their properties.

Stoichiometry	[n] (cm^{-3})	Conductivity [σ] (S/cm)	*Type	Optical band gap [E] (eV)	*Magnetic properties	Ref.
Oxyfluorides						
Sr_2O_4Ru F-doped: **$Sr_2O_3RuF_2$**		**$Sr_2RuO_3F_2$**: 0.024	**Sr_2RuO_4:** Su **$Sr_2RuO_3F_2$:** I		**Sr_2RuO_4:** ferro-magnetic	[102]
$SrFeO_{3-x}F_x$ (0.6 ≤ x ≤ 1)			***cis* $SrFeO_2F$**: I	**$SrFeO_{3-x}F_x$**: 2.4 **$LaFeO_3$:** 2.1	G-type AFM	[103]
$FeO_{0.7}F_{1.3}$			Conductor			[97]
YOF			Se	> 5		[96]
CeO_xF_y			Se	3.1 - 3.2		[104]
NdO_3Ni F-doped: **$NdO_{3-x}NiF_x$**	**Non-doped:** ~10^{22}	**F-doped:** 0.0001	**Non-doped:** C **F-doped:** I	**F-doped:** 2.1		[105]
Other oxyhalides						
$BiO_{0.1}F_{2.8}$			Se	2.47 - 4.02		[98]
BiOX (X = Cl, Br, I)			Se			[92]
BiOX (X = Cl, Br, I)			Se	**BiOCl:** 3.4 **BiOBr:** 2.8 **BiOI:** 1.8		[99]
BiOX			Se	**BiOCl:** 3.3 **BiOBr:** 2.7 **BiOI:** 1.8		[94]
BiOI			Se			[106]
$BiOCl_xBr_{1-x}$ and $BiOCl_xBr_{1-x}$ /alumina composite			Se	2.94		[107]
BiOCl, BiOBr, BiOI			Se	**BiOCl**: 3.5 **BiOBr:** 2.92 **BiOI:** 1.90 **BiOF:** ~4		[93]

*legend: Su=superconductor, Se=semiconductor, C=conductor, I=insulator, AFM=antiferromagnetic

2.2.3. Oxychalcogenides

Oxychalcogenides contain both oxide anions and the anions of a chalcogen from group 16 (S, Se or Te). Oxysulfides found in chapter 2.2.3.3 are the main point of focus here. [39,52] Oxychalcogenides have versatile electrical conductivity ranging from nearly insulating to metallic conduction with carrier mobility as high as 40 $cm^2V^{-1}s^{-1}$ for Zn-based materials. The tunability of layered oxychalcogenides is high owing to the alteration of distinct layers. With Zn(O,S) oxysulfide buffer layers, the tunability of their conduction band offset is high, while tuning with binary compounds (simple oxides) is not possible. Thermoelectric applications are also possible because the compounds exhibit low-dimensionality together with ionic and covalent bonding. [14,108–110]

LnOCuCh (Ln = a lanthanide such as La, Ch = S, Se, Te) are the most extensively researched layered oxychalcogenides. They have exhibited optical properties such as transparent p-type semiconductivity, large band gaps and large exciton binding energies ("quantum-well-like" materials because of a charge-carrying chalcogenide layer separated by an insulating oxide layer). Potential applications are LEDs and optoelectronic devices. In this thesis, the experimental focus is on the oxysulfide LaOCuS thin film. The layered structure of an oxychalcogenide MCuOCh (M = Bi, La; Ch = S, Se, Te) is shown in Figure 6. [15,57]

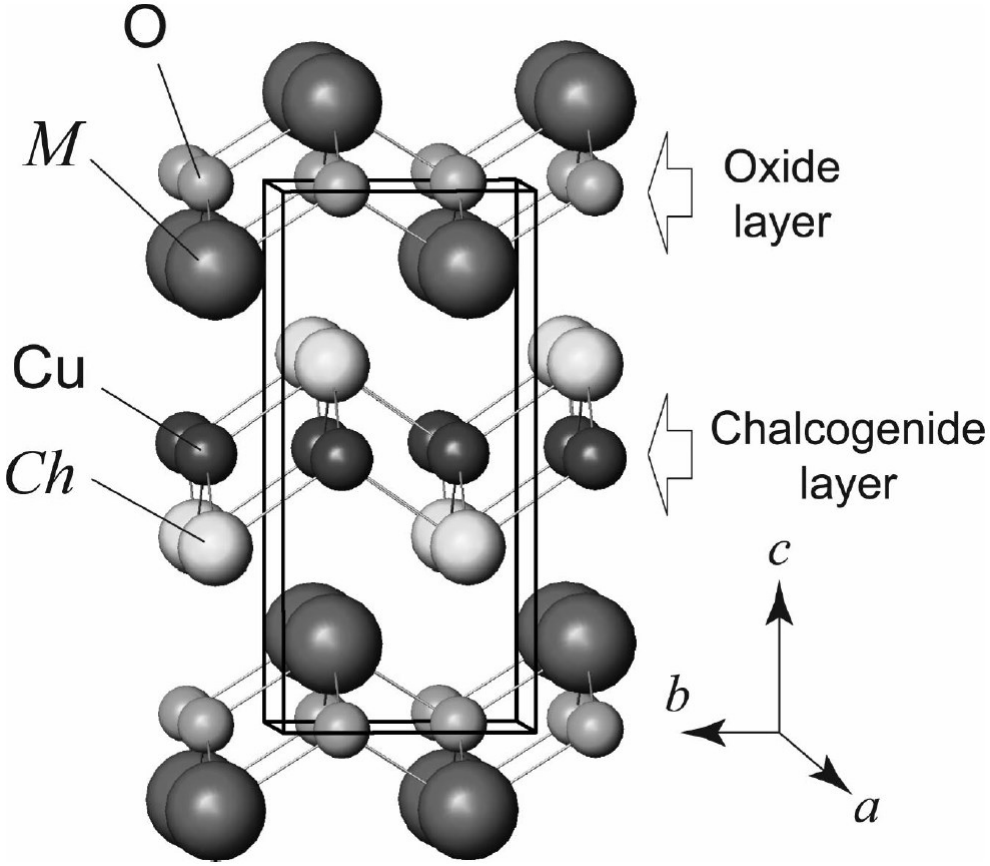

Figure 6. The crystal structure of MCuOCh (M = Bi, La; Ch = S, Se, Te) and its unit cell, with space group of P4/nmm. [111]

2.2.3.1 Oxysulfides

Oxysulfides (M_1OM_2S) contain sulfur as the other anion besides oxygen. In oxysulfide syntheses, hydrogen sulfide (H_2S) has been a common precursor as an affordable sulfur source, but unfortunately, it is an extremely toxic gas, which requires careful chemical handling. Recently, elemental sulfur has been studied as a safer alternative precursor and thin films have successfully been deposited by utilizing it. With elemental sulfur, ALD processes are also faster and produce more uniform phases. Elemental sulfur has also been utilized as a precursor in solid-state syntheses of various bulk oxysulfides [112–114]. Another possibility has been to utilize metal sulfides as precursors [9,49]. [11,27]

Structures

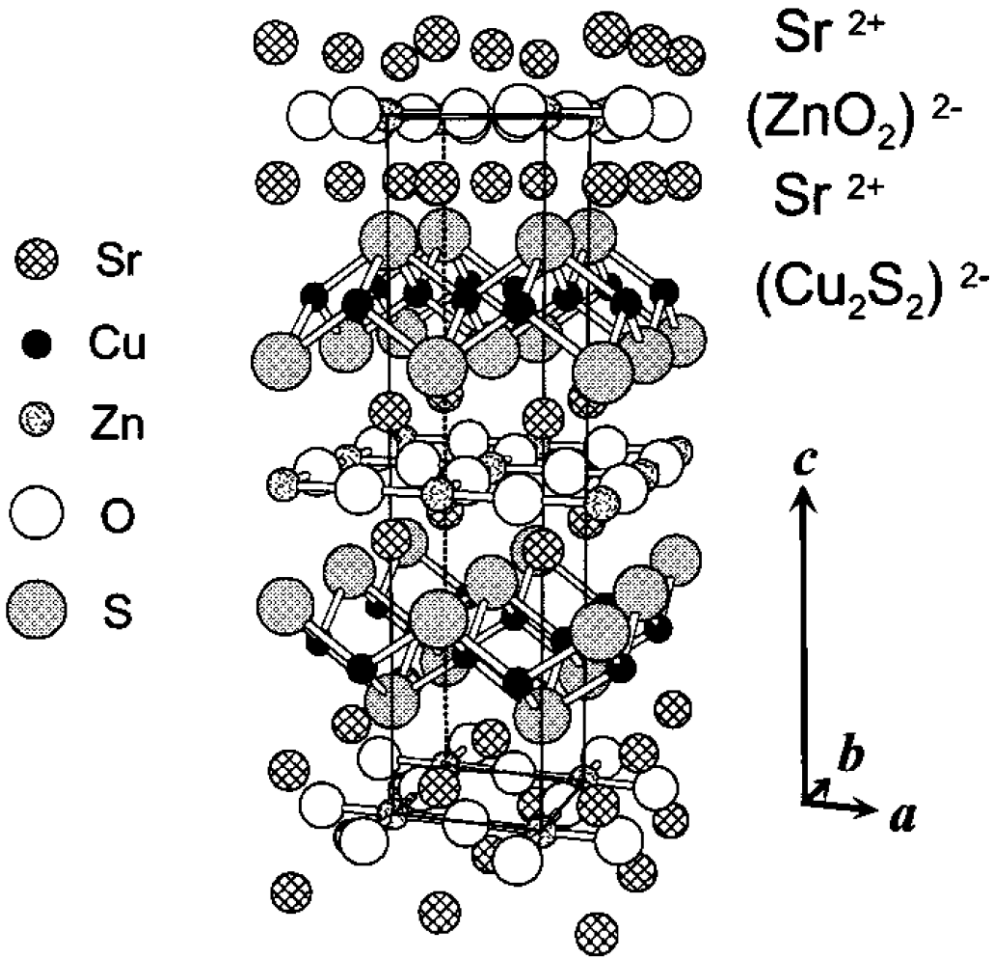

Figure 7. Crystal structure of the layered oxysulfide $Sr_2Cu_2ZnO_2S_2$. Sr layers separate the Cu_2S_2 and ZnO_2 layers. [115]

Many oxysulfides have a layered structure, where functional sublattices include a two-dimensional structure. Sulfides are also considered more polarizable than oxides, causing ordering of different anions. As a result, the compounds exhibit interesting electrical properties such as superconductivity and high magnetoresistance. [15,115] The crystal structure of a quinary oxysulfide $Sr_2Cu_2ZnO_2S_2$ (SCZOS) is shown in Figure 7 (antitype structure). The structure contains $(ZnO_2)^{2-}$ and $(Cu_2S_2)^{2-}$ layers of which the latter are same sublattices that are found in LaOCuS. A similar compound Sr_2CuMO_3S (M = Ga, In) also contains an SrO layer [116]. Both oxysulfides are proposed have similar optical and electrical properties due to the common layers. For example, SCZOS is a p-type

semiconductor and Na-doping increases its electrical conductivity. Based on the photoemission spectroscopy studies of the material, $(Cu_2S_2)^{2-}$ layers are viewed as the conduction paths for positive holes, while the $(ZnO_2)^{2-}$ layers perform the transport of electrons (Figure 8). [115]

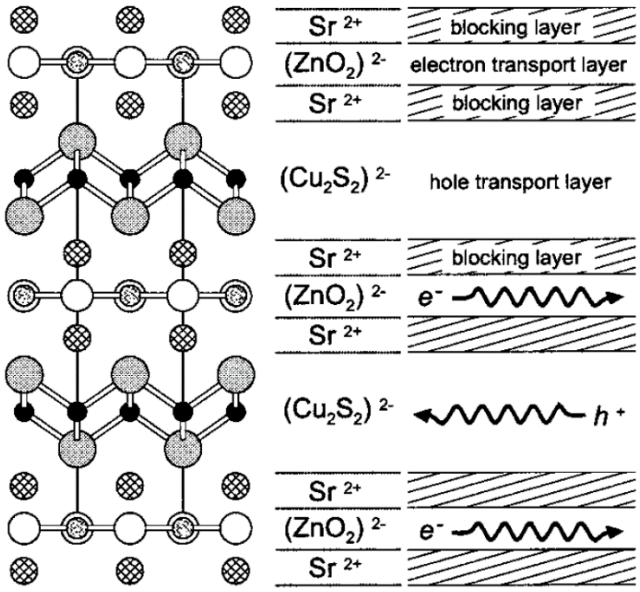

Figure 8. Hole and electron transport functions for each layer of $Sr_2Cu_2ZnO_2S_2$ (SCZOS). [115]

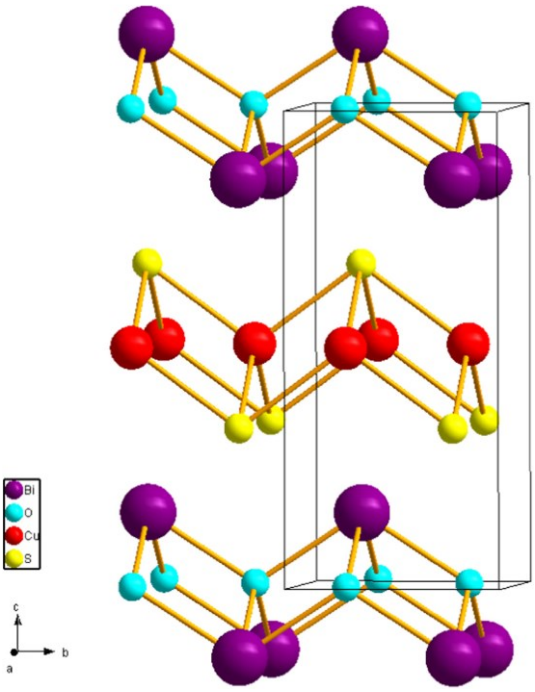

Figure 9. The BiOCuS crystal structure with stacked $[Bi_2O_2]^{2+}$ and $[Cu_2S_2]^{2-}$ layers. [114]

A copper deficient $BiOCu_{1-x}S$ ($x < 0.20$) oxysulfide has a structure with stacking fluorite-like $[Bi_2O_2]^{2+}$ and antifluorite-like $[Cu_2S_2]^{2-}$ layers. The crystal structure (Figure 9) is a ZrCuSiAs-type. The copper deficiency amount is fixed at $BiCu_{0.95}$. Charge transfer between these layers exists and the oxidation state of Bi is probably required to be higher than +3.

A semiconducting oxysulfide compound $Sr_2MnO_2Cu_{1.5}S_2$ includes manganese, which is suggested to have an oxidation state between +2 and +3. High mobility of Cu ions in the thicker CuS layers is suggested for the compound also for its low-temperature cation/vacancy-ordered superstructure: the copper ions are exchangeable by lithium ions at room temperature. The structure of this compound, visualized with VESTA (Visualization for Electronic and Structural Analysis) [117], is shown in Figure 10. [15,118]

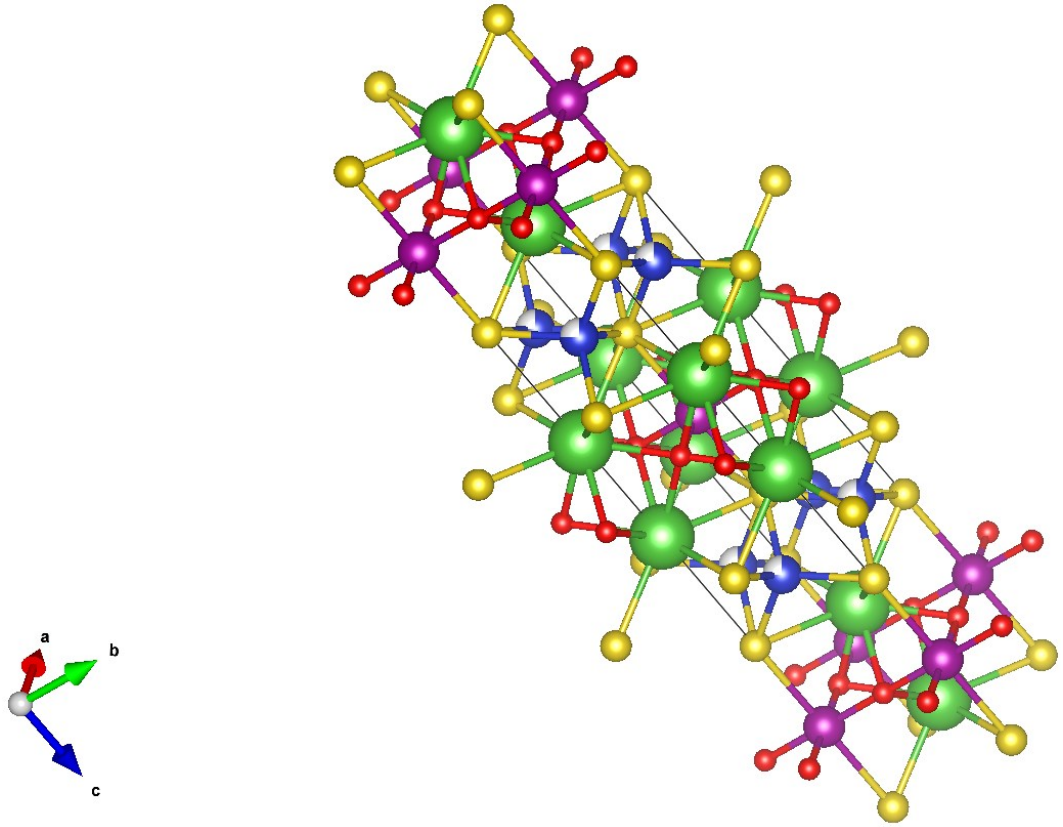

Figure 10. The oxysulfide $Sr_2MnO_2Cu_{1.5}S_2$ visualized in VESTA. Green = Sr, red = O, blue = Cu, yellow = S, purple = Mn. [118]

Moreover, first mixed cationic sites on a titanium oxysulfide compound were observed in $Gd_{6+x}Ti_{4-x}S_{10-y}O_{6+y}$. In this compound, half of the titanium cations are Ti^{3+} and half Ti^{4+}, with a structure of stacking of ribbons of Gd- and Ti-polyhedra (Figure 11). [20]

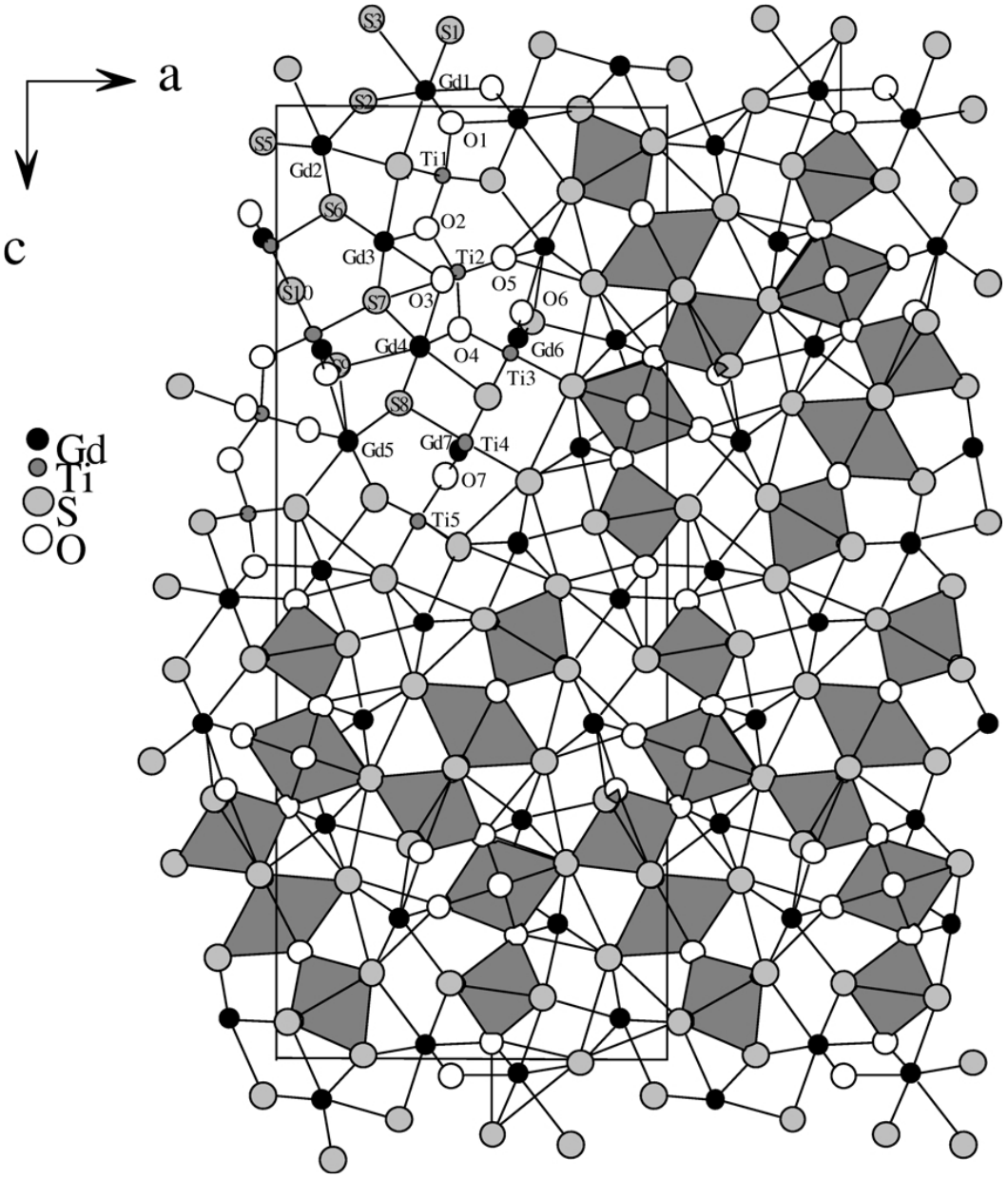

Figure 11. The structure of $Gd_{6.044}Ti_{3.956}S_{9.732}O_{6.268}$ compound on the (ac) plane. The stacking of Gd- and Ti-ribbons alternates along the a-axis. [20]

Properties & Applications

Oxysulfides are important compounds because of their inexpensiveness and low toxicity. Especially zinc oxysulfide [Zn(O,S)] has been applied as a buffer material in solar cells and is a very promising material due to its composition of earth-abundant and non-toxic elements [27,109]. Another example of low toxicity are gadolinium compounds, which have been used as MRI agents. Gadolinium oxysulfide exhibits a lower toxicity compared to oxides in this application, because of its lower solubility [119]. Conformal molybdenum oxysulfide thin films have also been electrochemically deposited via a simple and inexpensive process [120]. Nevertheless, the most common synthesis method is a solid-state reaction in high temperature and/or pressure for bulk oxysulfides [22,39] along with sputtering methods [10,121], PLD [122,123] and ALD [27,124,125] that have been utilized for thin films.

Layered oxychalcogenides with stoichiometry LnOCuCh (Ln = lanthanide, Ch = S, Se, Te) have wide optical band gaps (around 3 eV for oxysulfides), which can be tuned by changing the chalcogenide or the lanthanide ion. For the oxysulfide LaOCuS, the band gap is the highest among the chalcogen ions, 3.1 eV, compared to LaOCuSe (2.82 eV) and LaOCuTe (2.31 eV). The band gap values result from the different electronegativities of the chalcogenide ions. Moreover, decreasing the lanthanide ion size will result in a decreasing band gap value. [15] An even larger band gap value of 5.6 eV has been found by computational calculations for LiOAlS layered oxysulfides. The large band gap value ensures a wide electrochemical window, which means that LiOAlS is an excellent solid-state electrolyte. [126] Ab initio studies have also showed that changing the anions in the alternating Cu-Ch layers stabilize the variation of optical properties in compounds with the stoichiometry LaOCuCh [127]. A collection of oxysulfide band gaps can be found in Figure 12.

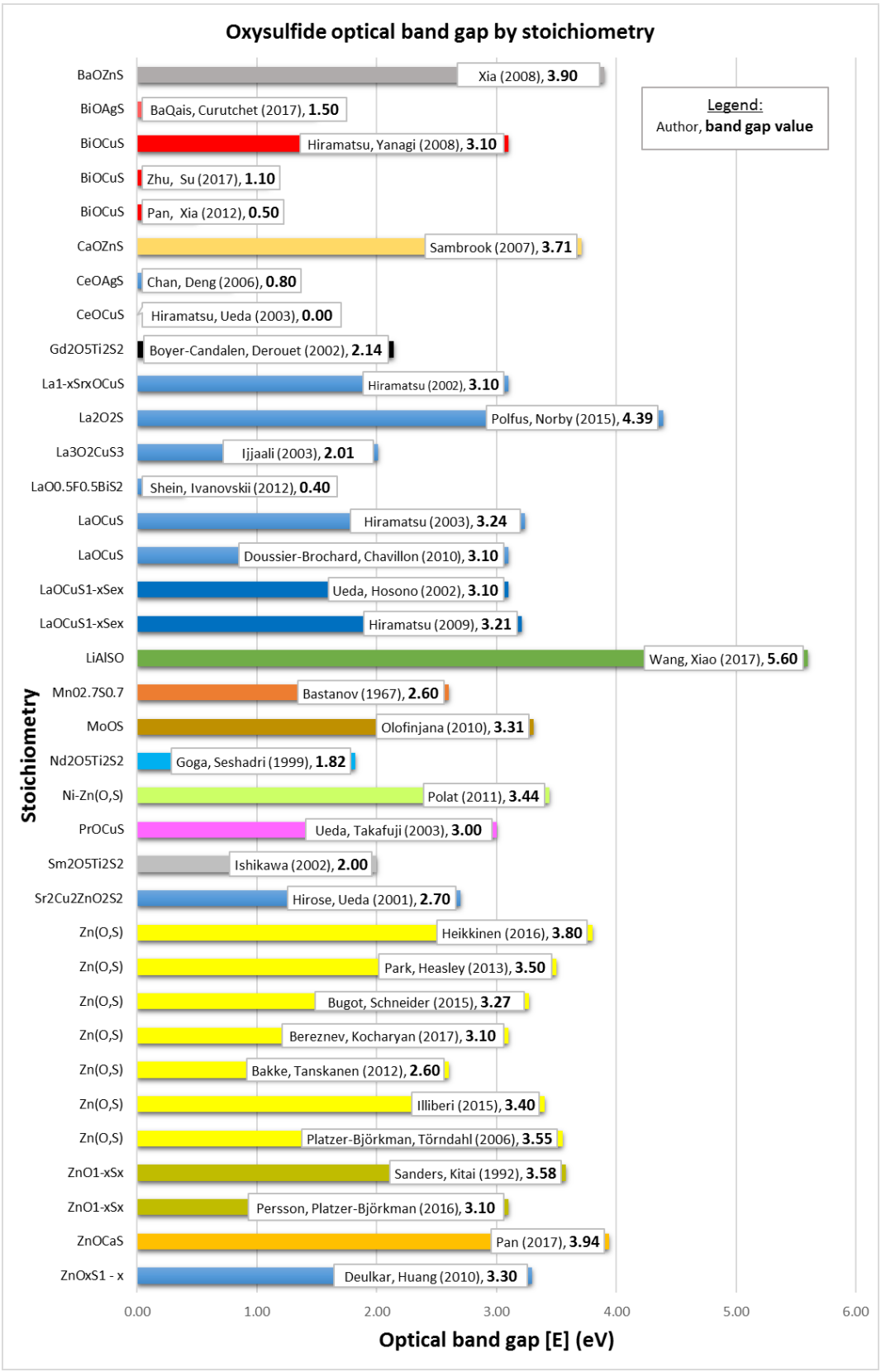

Figure 12. Oxysulfide optical band gaps (eV).

The electrical conductivity of oxysulfides with CuS layers can be modified via Sr^{2+} substitution by Na^{+}. In $Sr_{2-x}Na_xCu_2ZnO_2S_2$ and $Sr_{2-x}Na_xCuGaO_3S$, the substitution changed their electrical conductivity from insulating to semiconducting. This was confirmed by increasing the Na^{+} concentration and observing an increase in the electrical conductivity. The mixed valency of Cu^{+} and Cu^{2+} ions was suggested as the reason for reflectance decrease in the compounds while the ionization of Na^{+} ions at the Sr^{2+} ion sites generates positive holes in the valence band. [116]

The magnetic properties of oxysulfides have also been studied, commonly together with superconductivity studies in low temperatures. Antiferromagnetism is frequently observed in Sr and Mn based oxysulfides, where antiferromagnetic coupling is found between the MnO_2 sheets [18,128], and rare-earth metal based oxysulfides [47,49,129], where Nd-Cr interactions have prominent impact. Ferromagnetism has been observed also in Zn(O,S) thin films [130] in addition to rare-earth metal based oxysulfides $LaoCrS_2$ [47]. Lanthanide based oxysulfides have been shown to exhibit paramagnetic behavior with occasional long range magnetic order at low temperatures, like lanthanide compounds in general. [49]

Superconductivity

Various superconductivity studies of oxychalcogenides and oxypnictides have been conducted over the past ten years. The discovery of $LaO_{1-x}F_xFeAs$ superconductor with FeAs layers has drawn attention to structures with similar layers in finding new superconducting materials. The utilization of high pressure, crystallographic studies and replacing non-magnetic elements with magnetic elements has led to novel discoveries. [131]

The superconducting properties of BiS_2-based layered compounds appears to be connected to the crystal structure. Doping electrons into the BiS_2 conduction layers induces the superconductivity. An example is the oxysulfide $LaOBiS_2$, whose crystal structure is shown in Figure 13. The structure includes BiS_2 double layers stacked with a blocking LaO layer. For superconductivity to occur in $REOBiS_2$-based (RE=rare earth metals) compounds, electron carriers are essential: a common

strategy for electron carrier generation is partial substitution of O^{2-} by F^{-}, which has also been used in FeAs-based oxypnictide superconductors. By substituting O with F, the resistivity decreases and the superconducting transition is observed at 3 K for $LaO_{0.5}F_{0.5}BiS_2$. High pressure annealing will further enhance its superconducting properties: this was reported to be partly due to crystal structure transition from tetragonal to monoclinic. Another way to enhance the superconducting properties is increasing the length of the a-axis by changing the blocking layer. While lanthanum in the compounds mentioned is the largest rare earth metal, other metals and blocking layers should be studied to reach better superconducting properties. [132]

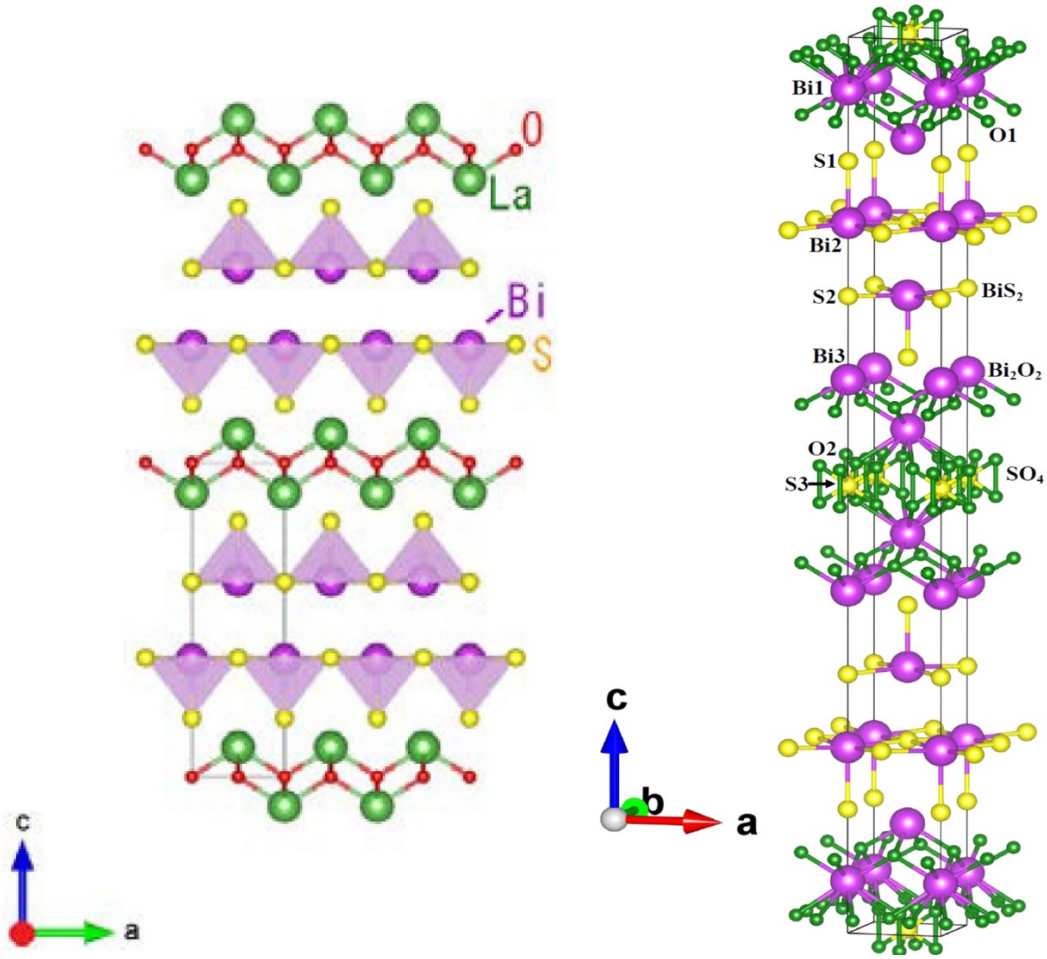

Figure 13 (left). The crystal structure of $LaOBiS_2$. [132]

Figure 14 (right). The crystal structure and unit cell of the $Bi_4O_4S_3$ oxysulfide. Violet=Bi, yellow=S, green=O. [133]

A ternary oxysulfide, $Bi_4O_4S_3$, has been confirmed to be a bulk superconductor (T_c = 4.4. K) by utilizing AC and DC magnetization measurements. Its structure is also layered, with alternating layers of Bi_2O_2, Bi_2S_4 and SO_4 (Figure 14). The BiS_2 layers induce superconductivity, through hybridization of the 6p orbital of Bi and 3p orbital of S. [133]

Another BiS_2-based superconductor is $LaO_{1-x}F_xBiS_2$ (T_c = 10.6 K), whose layered structure is equivalent to the $Bi_4O_4S_3$ superconductor. The two compounds both include BiS_2 layers, implying that the BiS_2 layer could be a basic structure for a novel layered superconducting family, similar to CuO_2 plane of cuprate superconductors and Fe_2An_2 layer for Fe-based superconductors. Bulk superconductivity for $LaO_{1-x}F_xBiS_2$ is achieved by increasing the fluorine concentration slightly above x = 0.5. Superconductivity would be achieved by optimizing carrier-doping techniques and doping levels by changing the spacer layer structures. [134]

Superconductivity in some bismuth oxysulfides have also been shown to appear due to copper vacancies. For example in $BiCu_{1-x}O$; for x > 0.05, structural nanodefects are detected and are a possible explanation for $BiCu_{1-x}OS$ superconductivity. [114] However, Cu^{2+} accommodation is difficult in the less electronegative oxychalcogenides compared to more electronegative oxides. [16]

The oxysulfide $Sm_2Ti_2S_2O_5$ has been studied for its visible light driven photocatalytic properties. The Ruddlesden-Popper type structure includes layers of S-(TiO_2)-O-(TiO_2)-S double octahedral. The structure did not decompose while visible light ($\lambda \leq 650$ nm) was utilized for O_2 and H_2 evolution from an aqueous solution. Thus, it is a stable photocatalyst for oxidation of water while a sacrificial electron donor or acceptor is present. [36] In addition, other titanate oxysulfides with Sm replaced with Nd, Pr or Sm have been suggested as candidate materials for photocatalytic splitting of water. [15]

See Table 4, Table 5 and Table 6 for a selection of oxysulfide compounds and their properties.

LaOCuS

The LaOCuS oxysulfide is built upon slates of $[LaO]^{+}$ and $[CuS]^{-}$, which form a tridimensional edifice. The oxide ion is coordinated tetrahedrally by the electropositive La ion only and the chalcophilic monovalent Cu ion is tetrahedrally coordinated by the sulfide only. As mentioned before, the stacking of layers are the origin of intriguing electrical properties such as intense exciton emission, high p-type conductivity and absorption threshold. Invisible (transparent) electronics are a potential application for LaOCuS based materials. [15,135]

Another study shows that the crystal structures of other rare earth oxysulfides CeOCuS, PrOCuS and NdOCuS crystallize in the same crystal structure as LaOCuS. Thus, they may also exhibit similar optical and electrical properties. Among these compounds, CeOCuS has highest electrical conductivity without doping and a unique electronic structure because of no observed photoluminescence peak. This is suggested to originate from an unoccupied band near the Fermi level. [136]

The crystal structure of the simple unit cell of solid LaOCuS is visualized in Figure 15. In addition, the layered structure of the compound is more clearly visualized in Figure 16, where the unit cell is expanded. From Figure 16 it can be observed that there are two [LaO] layers for every [CuS] layer in the same plane (along the c-axis).

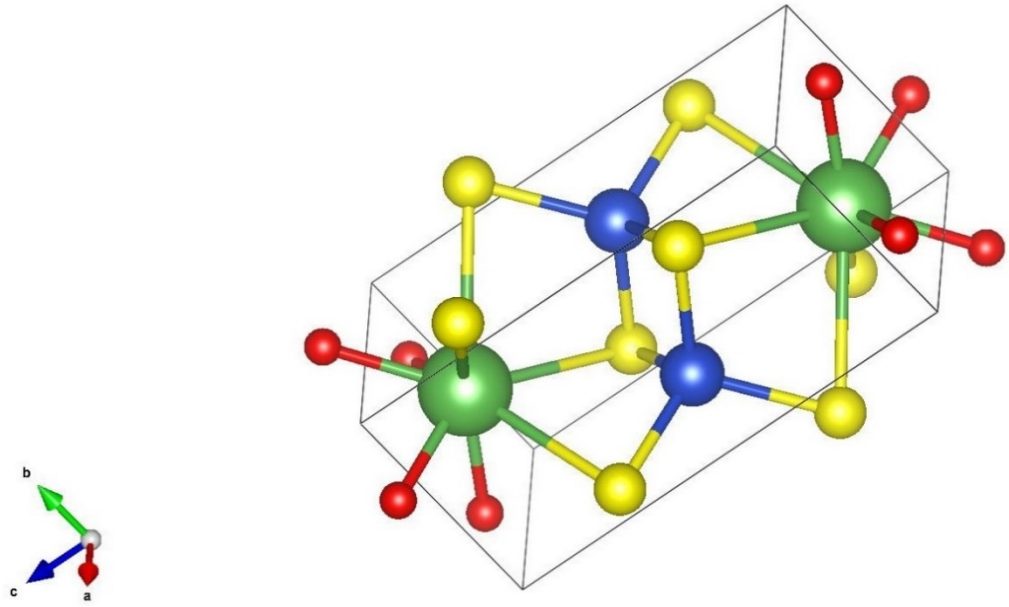

Figure 15. The crystal structure and one unit cell of LaOCuS visualized in VESTA. Red=O, green=La, yellow=S, blue=Cu. [19]

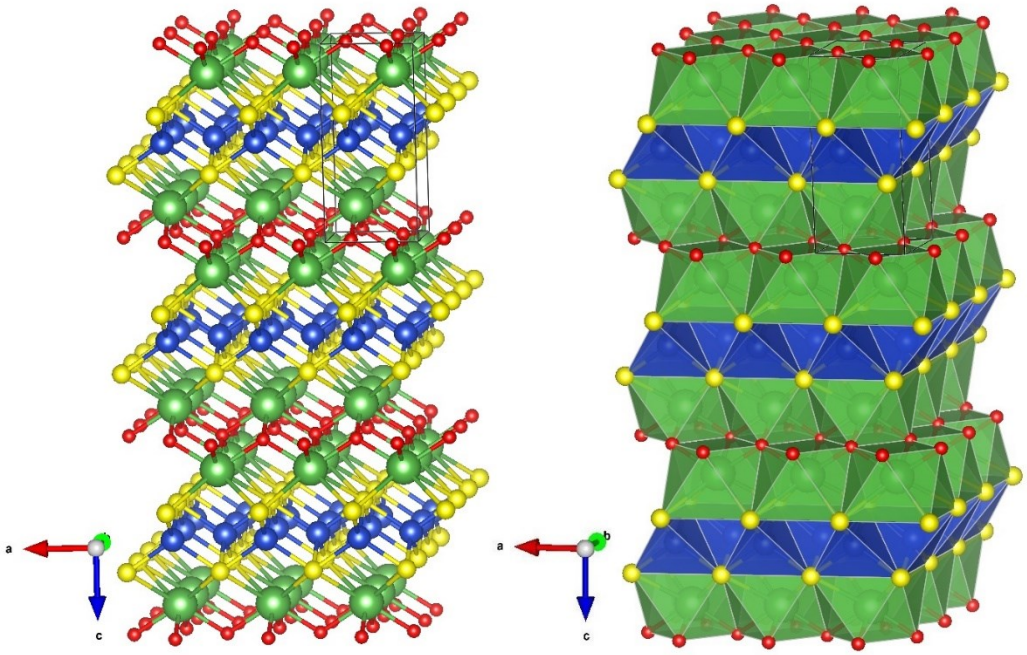

Figure 16. The crystal structure and unit cell of LaOCuS, showing the layered structure in ball-and-stick (left) and polyhedral (right) models in VESTA. Red=O, green=La, yellow=S, blue=Cu. [19]

The layered structure of LaOCuS has been studied for its transparent p-type semiconducting properties as its band gap lies at the edge of the visible region. The antibonding crystal orbitals of Cu-3d/S-3p are able to accommodate holes generated, for instance, by the substitution of La^{3+} ions by Sr^{2+} ions. [15,39,137] The Sr^{2+} ion doping has been confirmed to enhance the p-type electrical conductivity significantly [42,113], indicating that acceptor doping by cation substitution is efficient. Thus, LaOCuS is also a promising luminescent material for optical applications.

LaOCuS is a promising transparent p-type semiconductor and it could be an addition to the transparent semiconductors in addition to oxides such as $CuAlO_2$ and $SrCu_2O_2$. Oxysulfides in general are suitable for this because they usually include highly electropositive ions and have a suitable energy level of np^6 orbitals. The high optical transparency of LaOCuS is likely to be related to band-to-band transitions: an interband transition was suggested to generate a sharp photoluminescence peak. The electrical conductivity of LaOCuS was also found controllable by acceptor doping. [42]

The optical band gap of LaOCuS typically varies between 2.0 and 3.0 eV. The value has been explained by the layered crystal structure and the orbital configurations. The band gap has also been studied computationally [127] with a value of approximately 3.2 eV (see also Figure 12).

Table 4. Carrier concentrations, Hall mobilities, and Seebeck coefficients of selected oxysulfides.

Stoichiometry	Carrier concentration [n] (cm^{-3})	(Hall) Mobility [μ] ($cm^2V^{-1}s^{-1}$)	Seebeck coefficient [S] (μVK^{-1})	Ref.
Zn				
Zn(O,S)	$9.3*10^{19}$	2 - 32		[138]
Zn(O,S)	$\leq 10^{20}$	0.1 - 10		[139]
$ZnO_{1-x}S_x$	$4.8*10^{19}$ (x=0) $1.7*10^{18}$ (x=0.25) $1.66*10^{19}$ (x=0.56) $2*10^{17}$ (x=0.66)	13.2 (x=0) 36.1 (x=0.25) 32.2 (x=0.56) 24 (x=0.66)		[28]
n-ZnO:B & i-ZnO	$2.22*10^{18}$	$5.7*10^{18}$ & $5*10^{16}$		[140]
Zn(O,S)		43		[109]
Zn(O,S) & ZnO:Al		5		[124]
Sr				
$Sr_2Cu_2ZnO_2S_2$ & $Sr_{1.9}Na_{0.1}Cu_2ZnO_2S_2$	**$Sr_2Cu_2ZnO_2S_2$:** 2.2 * 10^{18} **$Sr_{1.9}Na_{0.1}Cu_2ZnO_2S_2$:** 1.1 * 10^{18}	**$Sr_{1.9}Na_{0.1}Cu_2ZnO_2S_2$:** 0.74	**$Sr_{1.9}Na_{0.1}Cu_2ZnO_2S_2$:** 310	[116]
Bi				
$BiOCu_{1-x}S$			700-750	[114]
BiOCuCh	$>10^{21}$	> 3.5	**nondoped BiOCuS**: 400	[111]
BiOCuCh (Ch = S, Se, Te)	**BiOCuS:** $4.00(3)*10^{18}$	**BiOCuS:** 0.139	**BiOCuS:** ~600	[22]
La & Rare-earths				
LaOCuS	10^{15} - 10^{20}	0.5	55 - 713	[10]
$LaOCuS_{1-x}Se_x$	> 10^{21}	0.1 – 11 $\mu(cm^2V^{-1}s^{-1})$	~250	[25]
$LaOCuS_{1-x}Se_x$			*nondoped: **1350-1450** *Sr-doped: **150-1200**	[40]
$(La_{1-x}Sr_xO)CuS$			x=0: **713** x=0.03: **44**	[113]
LnOCuS			> 0	[136]
Ce				
CeOCuS			12	[136]

Table 5. Resistivities, type and optical band gap of selected oxysulfides.

Stoichiometry	Conductivity [σ] (S/cm)	*Type	Optical band gap [E] (eV)	Ref.
Ca				
CaOZnS		Se		[141]
CaOZnS		Se	3.71	[39]
CaOZnS (host)		Se		[142]
Ti				
$TiO_{0.3}S_{1.5}$		C		[121]
Mn				
$MnO_{2.7}S_{0.7}$			2.6	[143]
$Sr_2O_2MnCu_{2m-6}S_{m+1}$	**$Sr_2O_2MnCu_{1.5}S_2$:** 0.67 **$Sr_2O_2MnCu_{3.5}S_3$:** 0.71 **$Sr_2O_2MnCu_{5.5}S_4$:** 0.71	Se		[118]
Fe				
$Fe_2OLa_2O_2Q_2$ (Q=S, Se)		Mott I		[31]
Zn				
Zn(O,S)		Se	2.6 - 3.8	[27]
Zn(O,S)	0.2 – 1	Se	2.6	[2]
Zn(O,S)	77	Se	~3.27	[138]
Zn(O,S)		Se	3.2 - 3.5	[139]
Zn(O,S) buffer layer	23 – 588	Se	2.6 - 3.55	[125]
$ZnO_{1-x}S_x$	208 (x=0) 9.9 (x=0.25) 23.8 (x=0.56) 0.78 (x=0.66)	Se	3.58	[28]
n-ZnO:B & i-ZnO		Se	3.3	[140]
Zn(O,S), AZO, CBD-CdS buffer layers		Se		[110]
Zn(O,S)	286	Se	~3.1	[109]
Zn(O,S) & ZnO:Al	333		**Zn(O,S):** 3.4	[124]
ZnO_xS_{1-x}		Se	3.3	[123]
Ni-Zn(O,S)			**Non-doped:** 3.44 **Ni-doped:** 3.38	[130]
ZnOCaS		Se	3.94	[144]
Sr				
$Sr_2MnO_2Cu_{1.5}S_2$ & $Sr_2MnO_2Cu_{3.5}S_3$		Se		[128]

Stoichiometry	Conductivity [σ] (S/cm)	*Type	Optical band gap [E] (eV)	Ref.
$Sr_2Cu_2ZnO_2S_2$ & $Sr_{1.9}Na_{0.1}Cu_2ZnO_2S_2$	**Conductivity:** **$Sr_2Cu_2ZnO_2S_2$:** $2.1 * 10^{-8}$ **$Sr_{1.9}Na_{0.1}Cu_2ZnO_2S_2$:** $1.2 * 10^{-1}$	Se		[116]
$Sr_2O_2Cu_2MS_2$		Se		[18]
$Sr_2Cu_2ZnO_2S_2$		Se	2.7	[115]
Nb				
$K_4ONb_2S_{10}$ and $Rb_4ONb_2S_{10}$		Se	**$K_4ONb_2S_{10}$:** 1.99 **$K_4Nb_2S_{11}$**: ~2.1	[145]
Mo				
$Mo_{21}S_2O_{76}$			3.31	[26]
MoO_yS_z		Se		[5]
Ba				
$Ba_3O_3V_2S_4$		C		[146]
BaOZnS		Se	3.9	[147]
Bi				
$Bi_4O_4S_3$		Su		[133]
BiOCuS		I		[148]
BiOCuS		Su		[149]
$BiOCu_{1-x}S$	**$Bi_{0.5}OPb_{0.2}CuS$:** 14	Se / Su		[114]
BiOCuCh		Se	**BiOCuS:** 1.1eV & 3.1eV **BiOCuSe:** 0.5eV & 2.6eV **BiOCuTe:** 2.4eV	[111]
BiOCuCh (Ch = S, Se, Te)	**BiOCuS:** ~10 **BiOCuSe:** ~900 **BiOCuTe:** ~10000	**BiOCuTe:** conductor **others:** Se	**BiOCuS:** 1.1 **BiOCuSe:** 0.8 **BiOCuTe:** 0.4-0.5	[22]
BiOAgS & BiOCuS		Se	**BiOCuS:** 1.1 **BiOAgS:** 1.5	[21]
La & Rare-earths				
LaOCuS		Se		[10]
LaOCuS		Se	3.1	[135]
LaOCuS & LaOCuSe		Se		[19]
$La_3O_2CuS_3$			2.01	[9]

Stoichiometry	Conductivity [σ] (S/cm)	*Type	Optical band gap [E] (eV)	Ref.
$LaOCuS_{1-x}Se_x$	0.1 - 11	Se		[25]
$LaOCuS_{1-x}Se_x$		**Nondoped:** Se **Sr-doped:** metal / Se	3.1 - 2.8	[40]
$La_{1-x}Sr_xOCuS$	x=0: $6.4*10^{-5}$ x=0.03: 20	Se	3.1	[113]
$La_{1-x}Sr_xOCuS$		Se		[42]
$LaOCrS_2$ & $LaOCrSe_2$				[47]
$La_{20}O_6Ti_{11}S_{44}$				[150]
LnOCuS (Ln = La, Pr & Nd		**Nondoped:** Se **Sr 5 at. % doped:** metallic / Se	3	[136]
LnOCuCh		I / Se	3.24	[151]
$Ln_2O_5Ti_2S_2$ & $Tb_2O_5Ti_2S_2$				[49]
$Ln_2O_5Ti_2S_2$		Se	**$Y_2O_5Ti_2S_2$**: 2.00 **$Gd_2O_5Ti_2S_2$**: 2.14	[152]
$Ln_2O_5Ti_2S_2$		Se	1.82	[112]
$LnOBiS_2$		Su		[129]
$LaO_{1-x}F_xBiS_2$	0.167	Su		[134]
$LaOBiS_2$, $LaO_{0.5}F_{0.5}BiS_2$ & $Bi_4O_4S_3$	**$LaOBiS_2$:** 0.03 **$LaO_{0.5}F_{0.5}BiS_2$:** 0.2	**$LaOBiS_2$:** Se **$LaO_{0.5}F_{0.5}BiS_2$:** Su		[132]
PrCuOS, NdCuOS, LaCuOS		Se		[127]
$Sm_2O_5Ti_2S_2$			~2	[36]
Ce				
$Ce_3O_4NbS_3$				[153]
$CeOCu_{0.8}S$ & CeOAgS		Se	**$CeOCu_{0.8}S$** *optical band gap E_g < 0.73 eV **CeOAgS** *direct band gap 0.8 eV	[154]
CeOCuS	0.61	degenerate Se		[136]

Table 6. Magnetic properties of selected oxysulfides.

Stoichiometry	*Type	T_c (K)	Magnetic properties	Ref.
Ca				
CaOZnS	Se		*Polar but non-ferroelectric *Very small pyroelectric coefficient	[39]
Mn				
$Sr_2O_2MnCu_{2m-\delta}S_{m+1}$	Se		A-type antiferromagnetic	[118]
Fe				
$Fe_2OLa_2O_2Q_2$ (Q=S, Se)	Mott I		Antiferromagnetic	[31]
Zn				
Ni-Zn(O,S)			Ni–Zn(O,S) films: **ferromagnetic**	[130]
Sr				
$Sr_2MnO_2Cu_{1.5}S_2$ & $Sr_2MnO_2Cu_{3.5}S_3$	Se		**Below 30 K:** A-type antiferromagnets	[128]
$Sr_2O_2Cu_2MS_2$	Se		**$Sr_2O_2Cu_2MnS_2$:** antiferromagnetic ordering at about 29 K	[18]
Mo				
MoO_ySz	Se			[5]
Bi				
$Bi_4O_4S_3$	Su	4.4		[133]
BiOCuS	Su	5.8	none	[149]
La & Rare-earths				
$LaOCrS_2$ & $LaOCrSe_2$			**$LaOCrS_2$ & $LaOCrSe_2$:** Ferromagnetic **$NdOCrS_2$:** antiferromagnetic	[47]
$Ln_2O_5Ti_2S_2$ & $Tb_2O_5Ti_2S_2$			Antiferromagnetic (T_N < 10K)	[49]

Stoichiometry	*Type	T_c (K)	Magnetic properties	Ref.
$Ln_2O_5Ti_2S_2$	Se		Paramagnetic susceptibility	[152]
$LnOBiS_2$	Su	**$LaO_{0.5}F_{0.5}BiS_2$:** 3.1 **$CeO_{0.5}F_{0.5}BiS_2$:** 1.89 **$PrO_{0.5}F_{0.5}BiS_2$:** 4.29 **$NdO_{0.5}F_{0.5}BiS_2$:** 4.37 **$YbO_{0.5}F_{0.5}BiS_2$:** 5.3	**$YbO_{0.5}F_{0.5}BiS_2$**: probable antiferromagnetic order at ~2.7 K	[129]
$LaO_{1-x}F_xBiS_2$	Su	10.6		[134]
$LaOBiS_2$, $LaO_{0.5}F_{0.5}BiS_2$ & $Bi_4O_4S_3$	**$LaOBiS_2$:** Se **$LaO_{0.5}F_{0.5}BiS_2$:** Su	3 - 10.6		[132]
Ce				
$Ce_3O_4NbS_3$			***Weakly antiferromagnetic**	[153]

*legend: Su=superconductor, Se=semiconductor, C=conductor, I=insulator

ALD preparation

Zinc oxysulfide thin films grown with SALD (Spatial Atomic Layer Deposition) have shown potential for replacing toxic cadmium sulfide, CdS, in photovoltaic applications. The continuous mode of the SALD deposition process would also reduce processing costs and make the use of oxysulfides industrially feasible. [27] A previous ALD experiment, in which H_2S was utilized, has also shown an increase in the aluminum content in aluminum-incorporated Zn(O,S) thin films. It was possible to adjust the carrier concentration with aluminum incorporation and the band gap value was increased. [139] For electrical applications, ALD is proposed to be a superior method because the substrate is not exposed to high energy species. The deposited films have less crystallographic defects than films deposited with traditional sputtering processes that include high-energy ion bombardments. With ALD, it is possible to deposit highly uniform transparent films (for example Al:ZnO) with photovoltaic properties, with the minor setback of a low deposition rate. This has been overcome by utilizing spatial ALD where the substrate sequentially moves into each different space-divided zones of the reactor. [124]

Solar energy applications are common for zinc oxysulfides, Zn(O,S). Buffer layers of these compounds deposited with ALD have been shown to have improved properties without changes in their composition. [155] Generally, mixed-anion compound research has a focus on the basic research concepts at the moment and various phase compositions are yet to be experimented with in applications. Only a few mixed-anion compounds have been studied by ALD, so it remains an interesting field for novel applications.

2.2.3.2 Oxyselenides

Much like other mixed-anion systems, oxyselenides (M_1OM_2Se, where M_1 and M_2 are metal ions in the oxide and anion phases respectively) also exhibit interesting properties compared with oxides. These include layered structures and the possibility of preparation with uncommon cation coordination environments, usually with low oxidation states. The structure of many oxyselenides is similar to superconducting pnictides and chalcogenides. [156] A novel oxyselenide superconductor $LaO_{0.5}F_{0.5}BiSe_2$ with T_c = 2.6 K has also been synthesized [157].

The synthesis of oxyselenides must be conducted more carefully than traditional oxide syntheses, which are usually easily conducted in air environment. In oxyselenide synthesis, oxidation of selenium and selenide reagents to higher oxidation states of Se must be avoided. Additionally, selenium is a toxic material and it is volatile above 640°C: therefore, in solid-state syntheses, low heating rates and low temperature dwell should be utilized to prevent pressure build up in the reaction chamber or tube. [156]

BiOCuSe is one of the most explored oxyselenides, which crystallizes in a layered crystal structure composed of conductive $(Cu_2Se_2)^{2-}$ layers and insulating $(Bi_2O_2)^{2+}$ layers along the c axis (Figure 17). Consequently, anisotropy is expected for their thermal and electrical transport properties and higher carrier mobility along the a,b plane (in-plane) is observed after synthesis. The thermoelectric figure of merit value (ZT) of BiOCuSe oxyselenides is considerably larger than that of other oxides because of low oxyselenide thermal conductivity. Hole doping with barium has increased the electrical transport properties and hence the thermoelectric performance of BiOCuSe. [8,158,159]

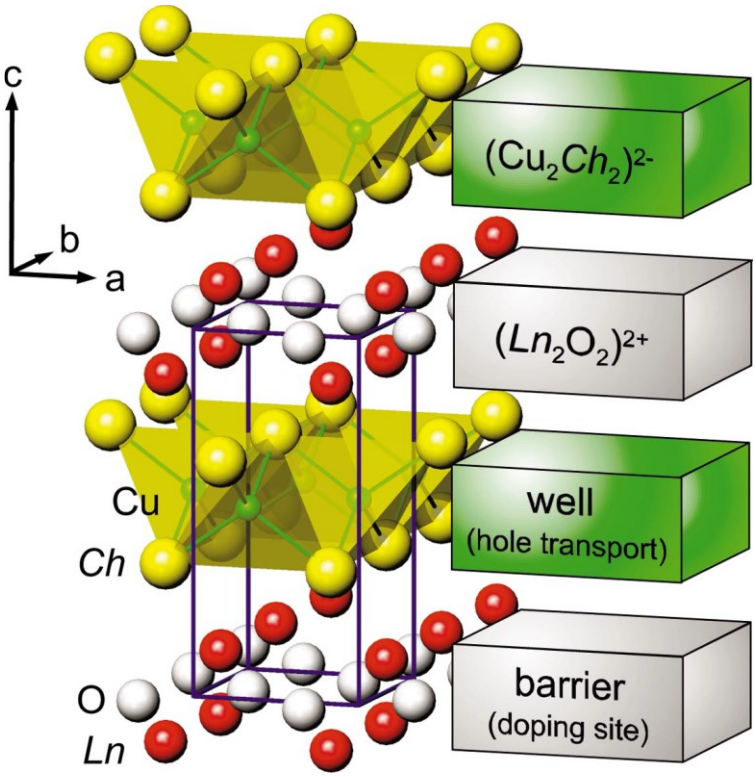

Figure 17. The crystal structure of LnCuOCh (Ln=lanthanide, Ch=S, Se, Te) with space group P4/nmm. The multiple quantum well structure is formed by alternately stacking $(Cu_2Se_2)^{2-}$ and $(Bi_2O_2)^{2+}$ layers. [159]

A typical optical band gap for Bi-based oxyselenides varies from 0.8 to 2.0 eV [13,160]. Substituting Se with S indicates a large change in the band gap value: the optical band gap for the $BiOCuS_{1-x}Se_x$ is wider with a value ranging from 2.8 to 3.1 eV [40]. The origin of this wide band gap has been studied with energy band calculations, which have shown that $[Cu_2Se_2]^{2+}$ layers and their antibonding states have the largest effect. These results demonstrated that the insulating $[La_2O_2]^{2+}$ layers confine the hole carriers to the $[Cu_2Se_2]^{2-}$ layers, which causes notable two-dimensional character. The large tuning in the band gap energy also indicates that LnCuOCh (Ln=lanthanide, Ch=S, Se, Te) compounds can be promising candidates for transparent p-type semiconductors. [159]

As an addition to thermoelectric performance improvement by barium doping [158], similar methods have also been utilized. Na doping has been confirmed to increase BiOCuSe carrier concentration significantly [161]. Fluorination and

oxygen de-intercalation have been utilized to tune the antiferromagnetic ordering temperature for $Sr_4Mn_3O_{7.5}Cu_2Ch_2$ (Ch = S, Se), and lithium exchange [128] has been used to tune the magnetic and electrochemical properties. Superconductivity of FeSe has been tuned by ammonia intercalation [162]. [156] See Table 7, Table 8 and Table 9 for selected oxsyselenides and their properties.

Table 7. Carrier concentrations, Hall mobilities and Seebeck coefficients of oxyselenides.

Stoichiometry	[n] (cm^{-3})	[μ] ($cm^2V^{-1}s^{-1}$)	[S] (μVK^{-1})	Type	Ref.
CaOFeSe				Semiconductor	[163]
$LaOCuS_{1-x}Se_x$			**nondoped samples:** 1350-1450 **Sr-doped samples:** 150-1200	**nondoped sample:** semiconductor **Sr-doped sample:** metal or degenerate semiconductor	[40]
$LaOCuS_{1-x}Se_x$				Semiconductor	[19]
LaOCuSe	up to 1.7 * 10^{21}	~ 8		Semiconductor	[164]
LaOCuSe(:Mg)	**LaOCuSe** ~2 × 10^{20} cm^{-3} **LaOCuSe:Mg** hole concentration 1.7*10^{21} cm^{-3}	**undoped LaOCuSe:** 8.0 **LaOCuSe:Mg** 3.5	positive for all films	Semiconductor	[55]
$La_2O_2CdSe_2$				Insulator	[108]
$La_{1-x}Sr_xOCuSe$ (x=0 to 0.2)			**x=0:** 140-290 **x>0:** 80-150	**nondoped:** semiconductor **Sr-doped:** p-type metal	[165]
$A_4O_4TiSe_4$ (A = Sm, Gd–Er, Y)				**A=Gd–Ho, Y:** semiconductors	[166]
Bi_2O_2Se	1.5 - 3.0 * 10^{13}	120 - 11000		Semiconductor	[167]
BiOCuSe	10 - 180 * 10^{18}	0.5 - 10	**x=0:** 350-400 **x=0.15:** 75-125	Semiconductor	[168]

Stoichiometry	[n] (cm^{-3})	[μ] ($cm^2V^{-1}s^{-1}$)	[S] (μVK^{-1})	Type	Ref.
BiOCuSe	1 - 1000*10^{18}	2.5 - 22	**x=0:** 300-400 **x=0.1:** 100-200	Semiconductor	[33]
BiOCuSe	10^{18} - 10^{21}	2.5 - 25	**lowest for x=0.1:** 100-150	Conductor	[169]
BiOCuSe & $Bi_{1-x}M_xOCuSe$ (M = Mg, Ca, Sr and Ba)	1 - 1000 * 10^{18}	22	349	Semiconductor	[160]
$Bi_{0.875}Ba_{0.125}CuSeO$	1 * 10^{21}	1 - 4	75 - 200	Conductor	[158]
BiOCuCh (Ch = S, Se, Te),	**BiOCuS**: 4 **BiOCuSe**: 12.65 **BiOCuTe**: 116.25	**BiOCuS**: 0.13 **BiOCuSe**: 2.20 **BiOCuTe**: 4.22	**BiOCuS**: 300-600 **BiOCuSe**: 350 **BiOCuTe**: 100-150	Semiconductors	[22]
$Bi_{1-x}La_xOCuSe$	0.8 - 1.8 * 10^{19}	2 - 35	150 - 300		[170]
$Bi_{1-x}ONa_xCuSe$	0.92 * 10^{18}	8	310 - 450	Semiconductor	[161]
BiOCuSe & $Bi_{0.75}Ba_{0.25}OCuSe$	**highest for heavily doped $Ba_{0.25}$:** > 10^{21}	**highest for modulation doping $Ba_{0.125}$:** 4.1	50-400	Semiconductor	[32]
$Bi_{1-x}Mg_xOCuSe$ & $Bi_{1-x}Ba_xOCuSe$	**$Bi_{1-x}Mg_xCuSeO$:** <10*10^{18} **$Bi_{1-x}Ba_xCuSeO$:** <1000*10^{18}	2.5 - 22	353 - 420	Semiconductor	[171]
$Bi_{0.875}Ba_{0.125}OCuSe$	**for BiCuSeO:** 1*10^{18}	**for BiCuSeO:** 22	**x=0:** 350-400 **x=0.125:** 100-150	Semiconductor	[172]
$Bi_{1-x}Sr_xOCuSe$	10^{18} - 10^{21}	0.2 - 21	50 - 150	Semiconductor	[13]
$Bi_{1-x}Sr_xOCuSe$			**x=0:** 350-400 **x=0.15:** 75-125	Semiconductor	[173]

Table 8. Electrical properties and band gaps of oxyselenides.

Stoichiometry	Type	Conductivity [σ] (S/cm)	Band gap [E] (eV)	Ref.
CaOFeSe	Semiconductor	**6.6 * 10 $^{-5}$**	1.8	[163]
$LaOCuS_{1-x}Se_x$	**nondoped sample:** semiconductor **Sr-doped sample:** metal or degenerate semiconductor		~2.8 - ~3.1	[40]
$LaOCuS_{1-x}Se_x$	Semiconductor		3.1	[19]
LaOCuSe	Semiconductor		2.8	[164]
LaOCuSe(:Mg)	Semiconductor	**LaOCuSe:Mg:** 910 Scm^{-1} (for 40 nm-thick films)	**$LaCuOS_{1-x}Se_x$:** emission energy of 2.89-3.21 eV	[55]
$La_2O_2CdSe_2$	Insulator	very small	3.3	[108]
$La_{1-x}Sr_xOCuSe$ (x=0 to 0.2)	**nondoped:** semiconductor **Sr-doped:** p-type metal	**Sr-doping:** 30 – 50 **no doping**: ~ 1		[165]
$A_4O_4TiSe_4$ (A = Sm, Gd–Er, Y)	**A=Gd–Ho, Y:** semiconductors	**A=Gd–Ho, Y:** 1 – 3	**A=Gd–Ho, Y:** 0.25 - 0.37	[166]
Bi_2O_2Se	Semiconductor		1.4 - 1.9	[167]
BiOCuSe	Semiconductor	**lowest for BCSO:** 0-10 **highest for BCSO1500**: 5-55		[168]
BiOCuSe	Semiconductor	**x=0:** 1-10 **x=0.1:** 100-500	0.82	[33]
BiOCuSe	Conductor	**x=0:** 1-10 **x=0.1:** $3*10^4$ - $6*10^4$		[169]
BiOCuSe & $Bi_{1-x}M_xOCuSe$ (M = Mg, Ca, Sr and Ba)	Semiconductor	1.12	0.8	[160]
$Bi_{0.875}Ba_{0.125}CuSeO$	Conductor	**100 - 700**		[158]
BiOCuCh (Ch = S, Se, Te),	Semiconductor	**BiOCuSe**: 0.0005	**BiOCuSe**: 0.8	[22]
$Bi_{1-x}La_xOCuSe$		**10 - 60**	0.2 - 1.2	[170]
$Bi_{1-x}ONa_xCuSe$	Semiconductor	**x=0:** 1-11 **x=0.015**: 80-110		[161]

BiOCuSe & $Bi_{0.75}Ba_{0.25}OCuSe$	Semiconductor	**Ba_0:** 1-2 **$Ba_{0.25}$:** 400-900		[32]
$Bi_{1-x}Mg_xOCuSe$ & $Bi_{1-x}Ba_xOCuSe$	Semiconductor	**Mg-doping:** 32 **no doping**: 1.12	*large for BiOCuSe*	[171]
$Bi_{0.875}Ba_{0.125}OCuSe$	Semiconductor	**x=0**: 0-10 **x=0.125**: 200-450		[172]
$Bi_{1-x}Sr_xOCuSe$	Semiconductor	> 40000	0.8	[13]
$Bi_{1-x}Sr_xOCuSe$	Semiconductor	**x=0:** 1000 **x=0.15:** ~80000	0.8	[173]

Table 9. Superconducting oxyselenides and their properties.

Stoichiometry	Electrical properties	Type	Band gap [E] (eV)	T_c [K]	Magnetic properties	Ref.
$LaO_{1-x}F_xBiSe_2$	**El. resistivity:** 0.3 - 1.0 Ωcm	Superconductor	0.17	3.1	diamagnetic	[174]
$LaO_{0.5}F_{0.5}BiSe_2$	**El. resistivity:** 0 - 0.10 mΩcm (T=2.0-3.0 K)	Superconductor		2.6	diamagnetic	[157]

2.2.3.3 Oxytellurides

Like oxyselenides, oxytellurides (M_1OM_2Te) exhibit thermoelectric performance but they are not as well studied. However, it is shown that substitution of Se by Te in BiOCuCh oxychalcogenides leads to an increase in electrical conductivity and a reduction in thermal conductivity. Thus, the thermoelectric performance of BiOCuTe is higher than that of BiOCuSe. The ternary compound Bi_2O_2Te also has a remarkably low thermal conductivity (0.91 $Wm^{-1}K^{-1}$ at room temperature) for a crystalline material. [175]

EXPERIMENTAL PART

Bulk LaOCuS was originally reported by Palazzi [137] in 1981. The goal of the experimental part to optimize the novel ALD process for fabricating crystalline inorganic quaternary oxysulfide LaOCuS thin films. The objective was to find optimal deposition parameters and analyze the structural properties and phase composition of the thin films. The composition of the films was compared with corresponding bulk structures from the literature, and thin films with different deposition parameters were compared to each other. The films were also annealed to see if it has an effect on the phase uniformity.

3 Motivation

A typical ALD process for metal sulfide deposition includes the use of hydrogen sulfide gas, H_2S. Due to its toxicity, special precautions are needed for safe use. Additionally, ALD processes based on H_2S are slow: growth rates vary between 0.20 and 0.94 Å/cycle. These kind of copper sulfide processes yield Cu(I) sulfide as the main phase whereas efficient ALD processes for high-quality Cu(II) sulfide thin films are an interesting concept for the future. With a novel ALD process, crystalline single-phase thin films of CuS have been deposited, up to the deposition temperature of 230°C. This was one of the first processes (along with some early ALD processes), where elemental sulfur was used instead of H_2S as the sulfur source. [11]

As noted in the literary part of this thesis, mixed-anion compounds have interesting electrical properties and consequently, are intriguing materials for electronic applications. The electric transport properties (for example, transparency, semiconductivity, superconductivity and large band gap) reported for bulk mixed-anion compounds, such as LaOCuS, are encouraging for future applications. The conformality of the layers deposited by ALD [7] permits the fabrication of thin film structures that possibly have superior properties compared

with their bulk equivalents. Furthermore, ALD is a vital process for miniaturization: especially the semiconductor industry could find mixed-anion compounds beneficial in manufacturing more efficient semiconducting high aspect ratio structures. [176]

With the scarcity of quaternary oxysulfide thin films that have been deposited so far, this thesis provides a new perspective to thin film synthesis. Moreover, almost none of the mixed-anion thin films have been synthesized with ALD, which is why the deposition processes have not been optimized yet and numerous thin film phase compositions are unknown. Previously reported mixed-anion thin film syntheses include zinc oxysulfide thin film depositions with spatial ALD [27,155], yttrium oxysulfide thin films with atomic layer epitaxy (ALE) [177] as well as aluminum oxynitride [29] and lithium phosphorus oxynitride [73] deposition with ALD.

4 Experimental details

In this section, precursor synthesis and their properties are discussed. After that the chemistry behind the ALD process is shortly described and the experimental details of the deposition processes are explained.

4.1 Synthesis of precursors

$La(thd)_2$ and $Cu(acac)_2$ were used as metal precursors, elemental sulfur as the sulfur source and ozone (O_3) as the oxygen source in the thin film depositions. $La(thd)_2$ was chosen as a precursor because of its low reactivity in air atmosphere, observed for thd-based compounds in previous studies. $Cu(acac)_2$ was chosen as a source for the copper metal based on previous studies on ALD depositions of CuO. [178–180]

$La(thd)_2$ (thd = 2,2,6,6-tetramethyl-3,5-heptanedione, Figure 18) was synthesized during 22.3.-27.3.2018 in the laboratory. First, sodium hydroxide (NaOH) was added to 15.5 mL of H(thd) in 30 mL EtOH (96 m-%) and lanthanum nitrate

hexahydrate (in 96 m-% EtOH) was added drop by drop to the flask while stirring. The white precipitate was filtered and washed with water, then dried in a vacuum oven (Heraeus RVT 350) overnight in 50°C. Finally, the dried powder was sublimated in 180°C. The synthesized $La(thd)_2$ powder was stored in fridge.

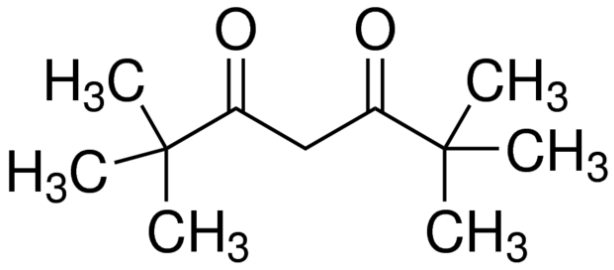

Figure 18. thd = 2,2,6,6-tetramethyl-3,5-heptanedione. [181]

The sublimation temperature of the synthesized $La(thd)_2$ precursor was verified by thermogravimetric analysis (TG). Perkin Elmer TGA 7 was used for the analysis, which yielded approximately 170-180°C as the sublimation temperature of $La(thd)_2$ (Figure 19).

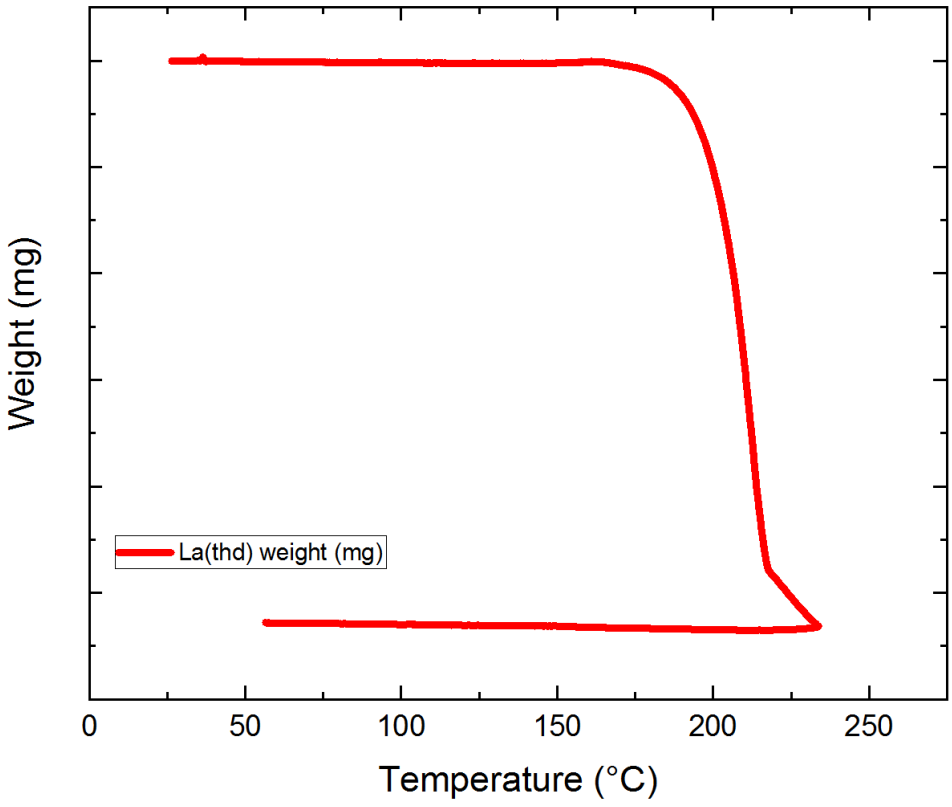

Figure 19. $La(thd)_2$ TG analysis for its sublimation temperature.

$Cu(acac)_2$ (copper(II) acetylacetonate, 97%; C87851-100G, CAS Number 13395-16-9) and elemental sulfur (213292-50G, CAS Number 7704-34-9) were used as received from Aldrich.

4.2 The ALD process

Atomic layer deposition (ALD) is a chemical vapor deposition technique developed and patented (with the name Atomic layer epitaxy, ALE) in 1977 by Suntola and Antson [182]. It is based on sequential self-limiting gas-solid reactions that allow cyclic thin film growth. The basic deposition process is a reaction cycle that is comprised of the repeating of four characteristic steps:

1) A self-terminating reaction of the first reactant.

2) A purging or evacuation step for removal of nonreacted reactants and gaseous by-products from the reaction chamber.

3) A self-terminating reaction of the second reactant or a treatment to activate the surface again for the reaction of the first reactant.

4) A purging or evacuation step to evacuate the reaction chamber.

The basic growth cycle is repeated to achieve desired film thickness and results in constant material growth per cycle (GPC). The precursors chemisorb or react with the surface functional groups saturatively and no further adsorption occurs when the chemisorbed layer is formed. The precursors do not thermally decompose during the depositions. The self-limiting surface reactions are the uniqueness of ALD and lead to precise composition of the films. Films of sub-nanometer thickness control can be deposited by ALD. [183]

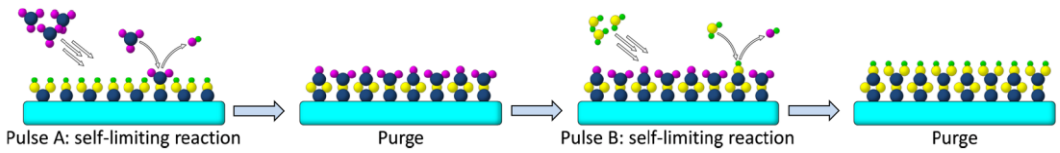

Figure 20. The four characteristic steps of the ALD process. [183]

Moreover, exceptionally uniform and pinhole free films can also be achieved over large-area substrates. ALD is preferred over traditional thin film deposition techniques in situations, where films have to be deposited on complex geometry or high aspect ratio structures, because of its unique self-saturating layer-by-layer surface reactions. A typical sputtering process may also damage the thin film (for example by high energy ion bombarding) whereas ALD is a “soft” deposition technique and usually does not physically harm the deposited films. This is because gas-phase reactions occur at relatively low temperatures (200-300°C) and the wide ALD processing window is insensitive to small temperature or precursor flow changes. [4,7,124,183–185]

Miniaturization [5,176] is a growing concept in the field of electronics industry. Miniature sized and high aspect ratio structures require atomic level control of the deposition of thin films. High conformality is achieved by using atomic layer deposition (ALD): gas phase ALD precursors coat all substrate surfaces independent of substrate geometry. Especially semiconductor devices need excellent conformality, for continuous improvement in their electrical properties. [176,183]

In addition to ALD, there are various similar methods for thin film depositions: examples include chemical vapor deposition (CVD) [26], reactive solid-phase epitaxy (R-SPE) [110], radio frequency –sputtering (RF-sputtering) [10], pulsed laser deposition (PLD) [6] and molecular beam epitaxy (MBE) [54].

4.3 Equipment for ALD

A tubular hot-walled F-120 ALD-reactor was used for all the thin film depositions in this thesis. The reactor was made by ASM Microchemistry Ltd. and the films were deposited on silicon wafer substrates (Si(100), p-type, Okmetic Oy) and a few times on borosilicate glass slides. The substrate pieces were cleaned by washing them with ethanol and blowing them dry with pressurized air before putting into the middle of the reaction chamber. One sample was deposited at a time but

sometimes a borosilicate glass slide was added to the reaction chamber beside the silicon wafer for comparison and a possibility for electric measurements.

O_3 (ozone gas), elemental sulfur, $La(thd)_2$ and $Cu(acac)_2$ were used as precursors for the thin film depositions. Fischer's O_3-generator was utilized to produce ozone from oxygen (99.99 %), with ozone flow of approximately 50 L/minute to the reactor. The powdered precursors $La(thd)_2$, $Cu(acac)_2$, and S were sublimated from open vessels and carried to the reactor chamber using N_2-gas (AGA, >99.95 %) as the carrier and purging gas. In the reactor, primary N_2 gas flow is used to transport the gaseous precursor to the substrate in the inner glass tubes of the reactor and secondary N_2 gas flow keeps the outer glass tube in correct pressure. The flow rate of the primary flow of the purging gas was 300 sccm and the secondary flow rate was 100 sccm. The pressure inside the reactor was approximately 2 – 5 mbar during the depositions.

Figure 21. Fischer's O_3-generator utilized to produce ozone from oxygen for the depositions.

4.4 Characterization methods

X-ray reflectivity (XRR) was utilized for thickness analysis of the thin films. The method is based on the reflected X-ray beams, at grazing incidence, from a flat surface. The intensity of X-rays reflected in the specular direction (reflected angle equal to incident angle) is measured. The reflection patterns have been utilized to interpret film thickness and consequently, their growth rate.

For XRR measurements, the angle of incidence was fixed at 0.5° and the 2θ was scanned from 0.1025° to 2.0°. The X'Pert Reflectivity program was used for thin film thickness analysis with the Fourier and Direct methods. This included the choosing of critical angle and measuring the approximate distances between the fringes, or selecting the start and end angle where fringes were still visible. The more fringes are present, the thicker the film is. As the cycle number increases, it is usually not possible to determine the film thickness anymore. The critical angle position is typically chosen approximately at the midpoint where intensity first begins to decrease. A visualization of this is shown in Figure 22: with these selections, the LaO film thickness was approximately 55 nm.

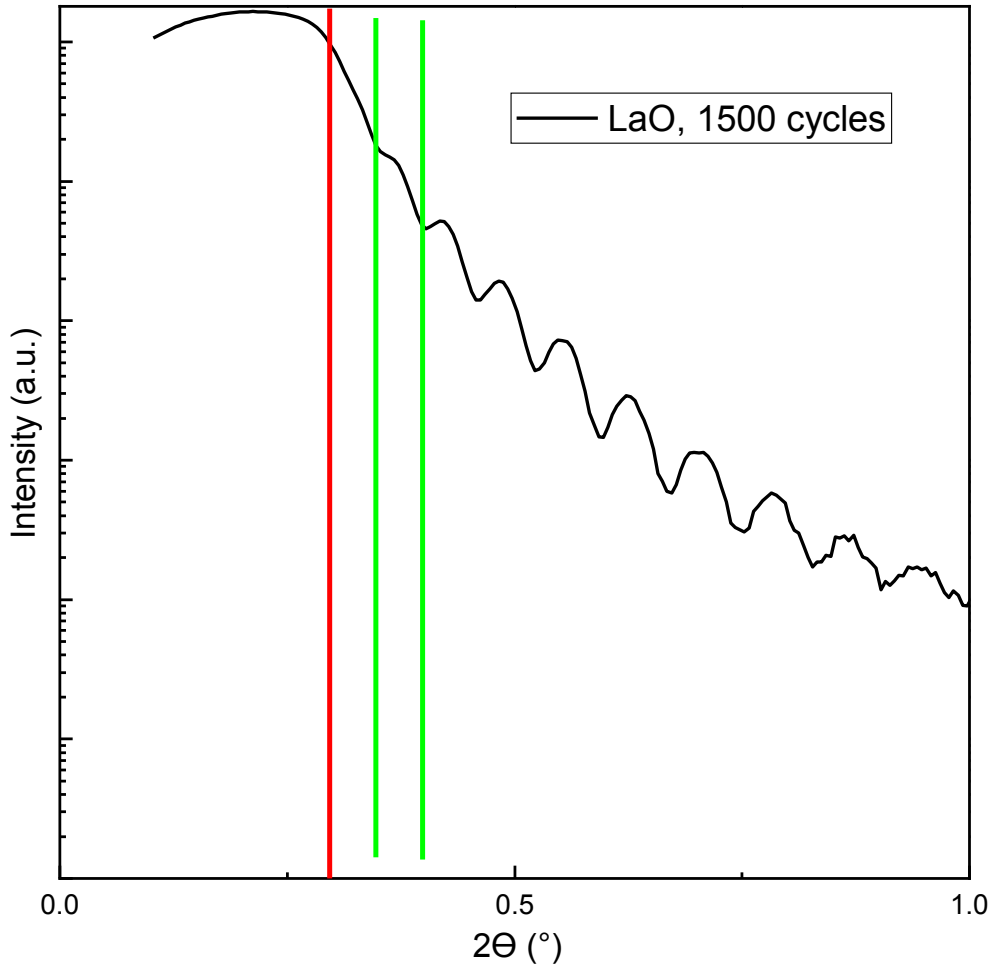

Figure 22. An XRR pattern of a LaO film. The critical angle is marked with a red line, while the first and second fringes are marked with green lines.

Grazing incidence x-ray diffraction (GIXRD) is a method for finding the structure of thin films in detail. This method has a relatively low incident angle for the X-rays in order that the majority of the X-rays reflect from the surface of the film and not from the substrate. An incidence angle of 0.5° was used in this study and the range for 2θ was typically 10 - 65°, sometimes even 5 - 80°. Peaks were identified from the GIXRD data to determine the crystallinity and composition of the thin films.

4.5 Annealing

Annealing is a step-wise heat treatment method typically utilized with polymer materials. With thin film synthesis, the method is exploited as postannealing. The thin film is deposited first and postannealing heat treatment is used for phase formation by diffusion of amorphous precursors. The material properties are changed because high temperature treatment modifies the locations of atoms in the crystal lattice and makes the structure less dislocated. This way, an as-deposited amorphous thin film may be modified to become crystalline and distinct phases are formed. [186] In this experiment, the aim was to anneal the films to see if the LaO and CuS phases could be mixed in the films and the actual LaOCuS phase composition could eventually be found.

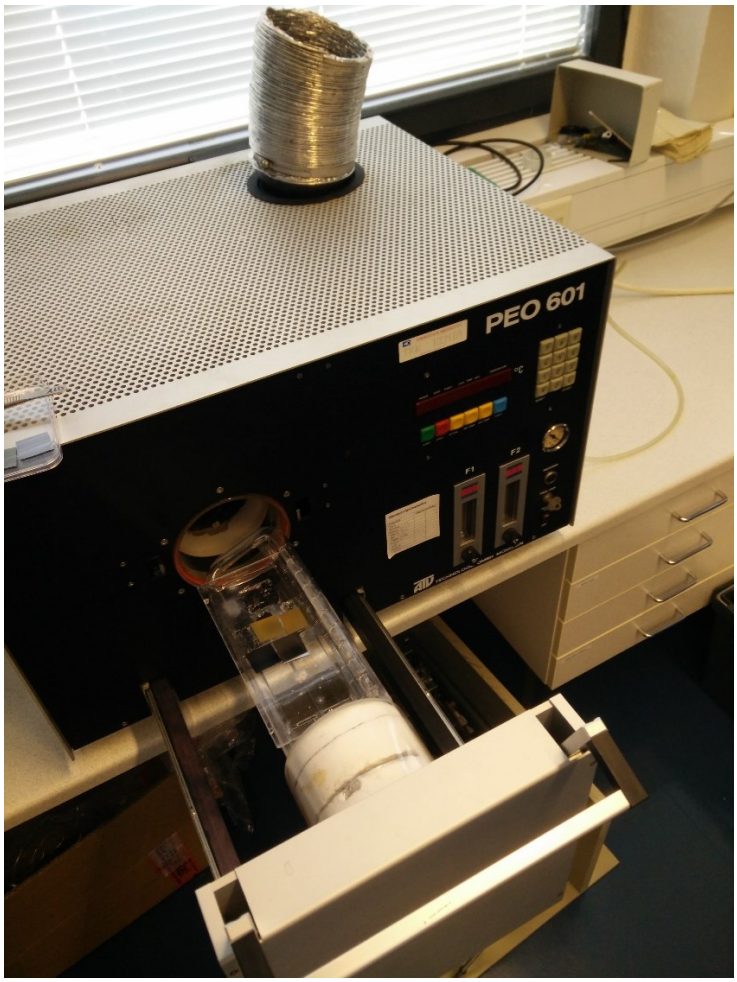

Figure 23. The ATV PEO-601 oven utilized for thin film annealing.

ATV PEO-601 oven was utilized for the annealing of films. This research included thin film annealing in argon atmosphere. The annealing was a stepwise procedure: the films were first heated to 200°C in 10 minutes, then heated to 600°C in 10 minutes, kept in 600°C for 10 minutes, cooled to 200°C in 10 minutes and finally cooled to room temperature in 10 minutes. Later, films were heated to 700°C (instead of 600°C). For most of the deposited films, annealing was crucial for the determination of their composition. This is because GIXRD measurements showed no peaks for most of the as-deposited films, except for the peaks resulting from the silicon substrate. After annealing, additional peaks were prominent in the GIXRD data and some films also showed a color change.

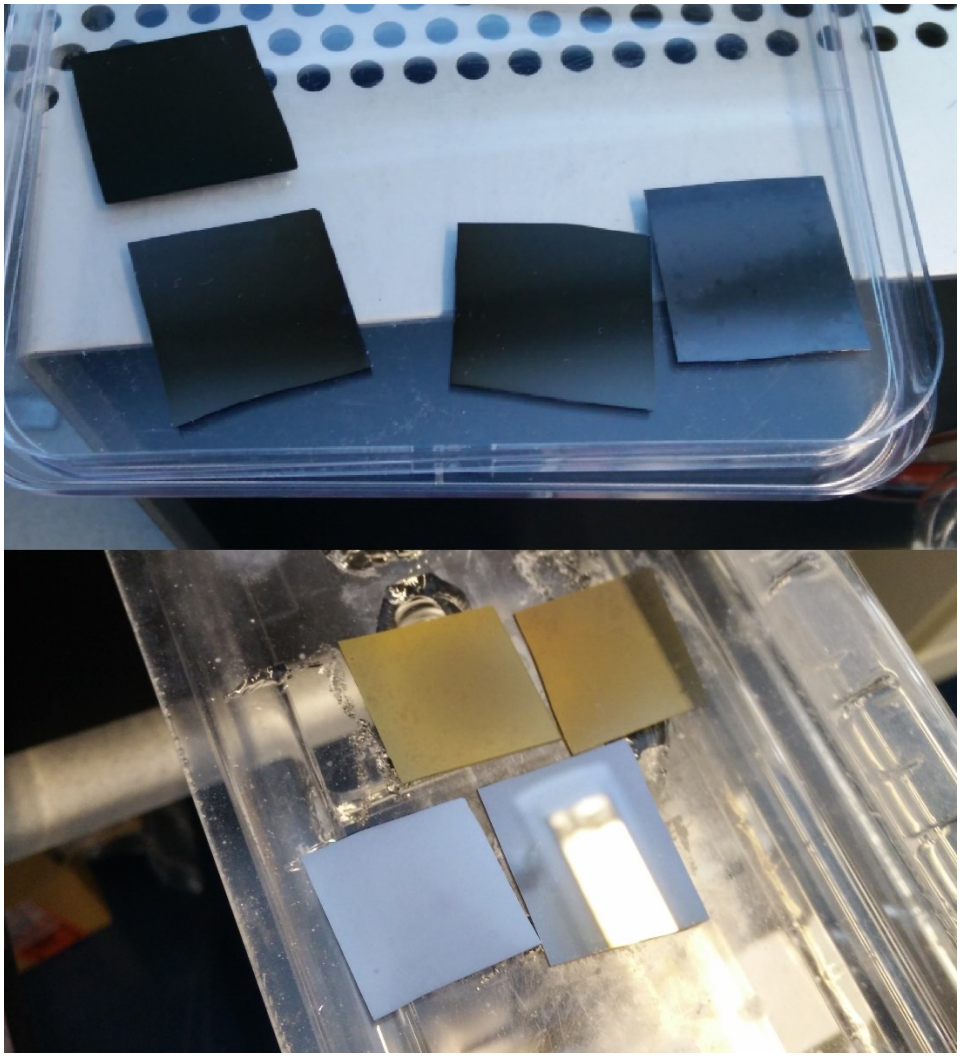

Figure 24. As-deposited films (upper picture) and the same films annealed in the oven (lower picture). A color change from dark to yellowish can be seen in two of the films.

5 Results and discussion

This chapter includes description of the thin film deposition procedure and the deposition parameters. The thin film phase composition is discussed along with the results from electrical measurements.

5.1 Thin film deposition parameters and phase composition

The depositions were completed in two different procedures. The first procedure included two separate ALD depositions: lanthanum oxide (LaO) was first deposited on a Si substrate, the film was removed from the reactor, XRR and XRD (for film thickness and crystallinity) were measured and then copper sulfide (CuS) was deposited on top of the LaO film. The second procedure included only one deposition where all the precursors were loaded in the reactor and a single deposition program was used to first deposit LaO on Si substrate and then deposit CuS on top of the LaO film.

The deposition parameters were optimized to find the optimal sublimation temperatures and to determine whether the thin film thickness was linearly dependent on the deposition temperature, cycle length and number. This research concentrated on optimizing the deposition temperature and cycle number. Other parameters were kept constant in almost every deposition.

First, LaO films were deposited separately. After this, the CuS films were deposited directly on top of the LaO films in the first deposition procedure. The sublimation temperature for $La(thd)_2$ was chosen to be 170°C. The cycle / purge ratio was 2 seconds / 3 seconds in these. All LaO films were found to be crystalline by XRD measurements. CuS film deposition parameters were not optimized separately. The following deposition sequence for LaO films was utilized:

$$La(thd)_2\ 2.0\ s + N_2\ purge\ 3.0\ s + O_3\ 2.0\ s + N_2\ purge\ 3.0\ s$$

The growth rate (GPC) of the LaO films with deposition temperatures between 230-280°C and 300 cycles was approximately 0.26 Å per cycle on average (Figure 25). The growth rate increased almost linearly with increasing deposition temperature. The growth rate was in line with previous research [187], where a GPC of 0.36 Å for LaO (La_2O_3) films was obtained with deposition temperatures between 225-275°C.

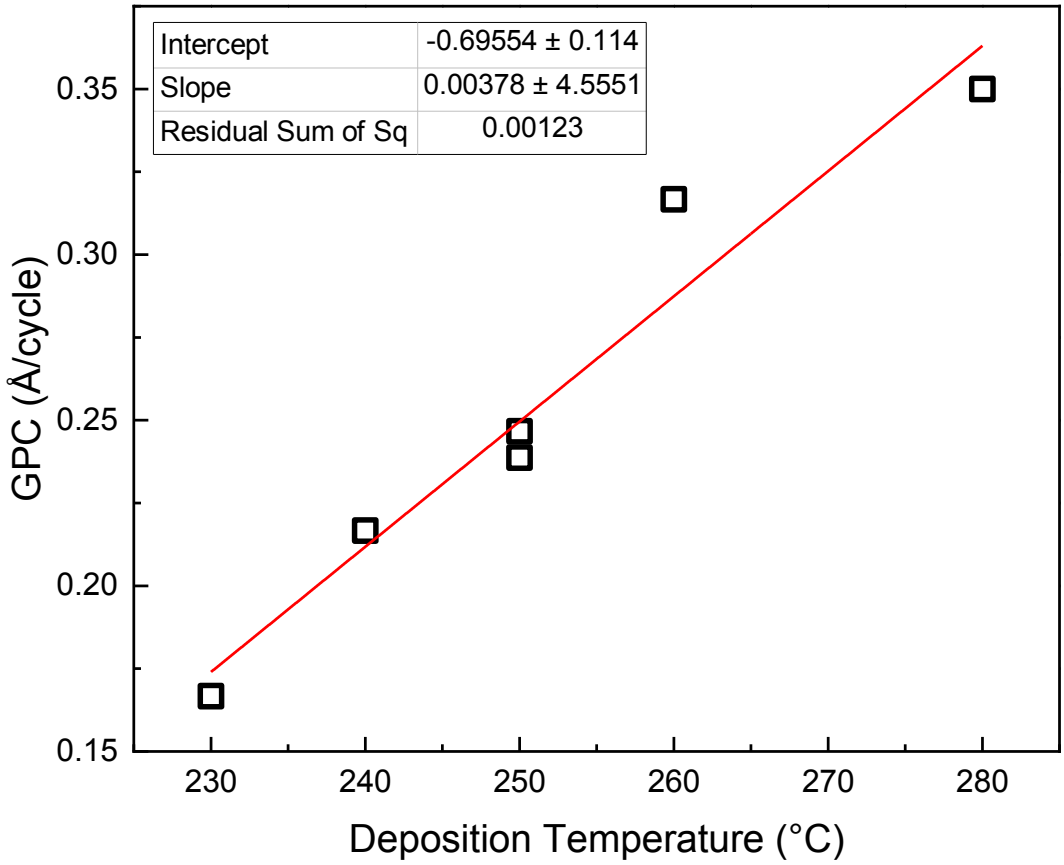

Figure 25. Growth rate (Å/cycle) versus deposition temperature plot for LaO films.

Figure 26 shows the GIXRD data of a thicker LaO film deposited with 1500 cycles (in black). It has a prominent broad peak at approximately 2θ = 25-35°, where also the bulk La_2O_3 diffractogram [188] (in red) has its most intensive peaks. Possible peaks may also be found at approximately 2θ = 40-50° but these are not as clearly observed in the LaO GIXRD data. The peaks at approximately 2θ = 45-60° most likely are a result from the Si substrate. Based on this data, it can be suggested that the phase of deposited LaO films is close to La_2O_3, but more crystalline structure is needed for exact determination of its phase composition.

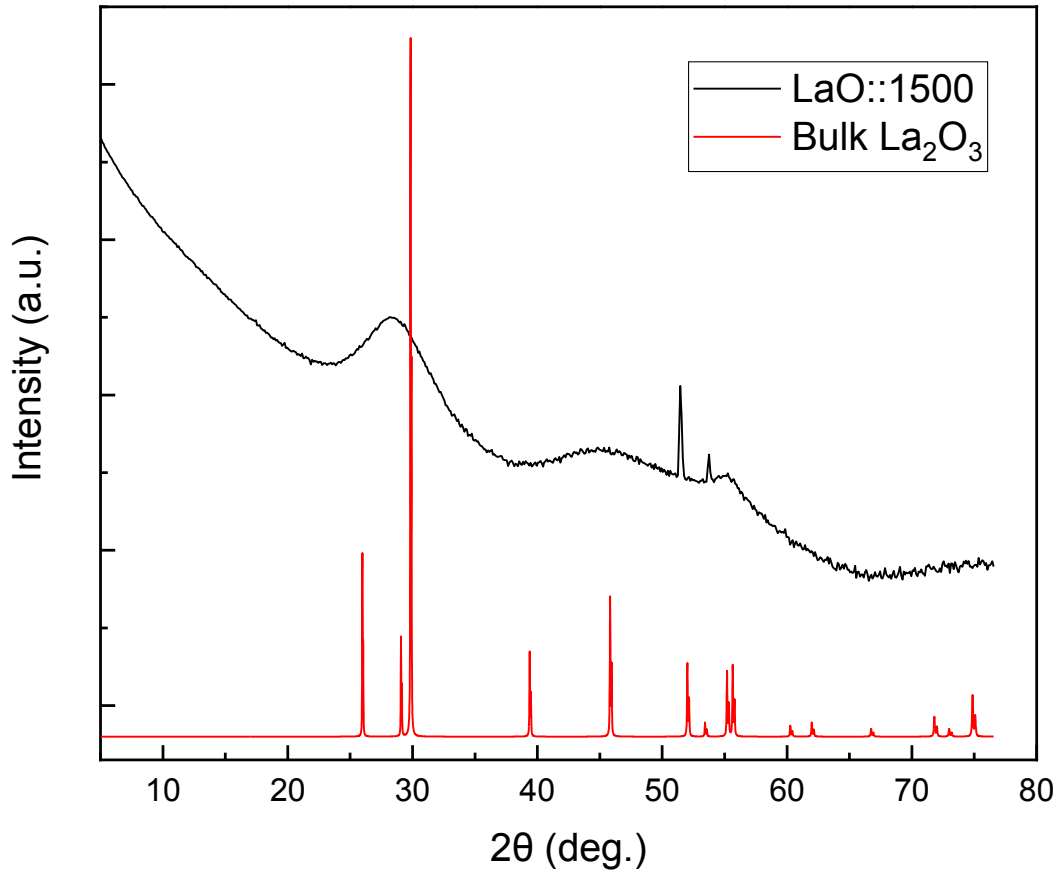

Figure 26. Comparison of the deposited LaO film (1500 cycles) GIXRD data (black) with the powder diffractogram (red) [188] of bulk La_2O_3.

For CuS films deposited separately on top of the LaO films, the sublimation temperature was chosen to be 110°C for S and 135°C for $Cu(acac)_2$ and the deposition temperature was 200°C. The cycle / purge ratio was 2 seconds / 3 seconds in these depositions. The following deposition sequence for CuS films was utilized:

$Cu(acac)_2$ 2.0 s + N_2 purge 3.0 s + S 2.0 s + N_2 purge 3.0 s

It was not possible to determine the thickness of these films accurately due to the low quality of the XRR data. The thickness seemed to increase with increasing number of cycles. See also Figure 30 for a comparison between the GIXRD data of separately and simultaneously deposited LaOCuS films.

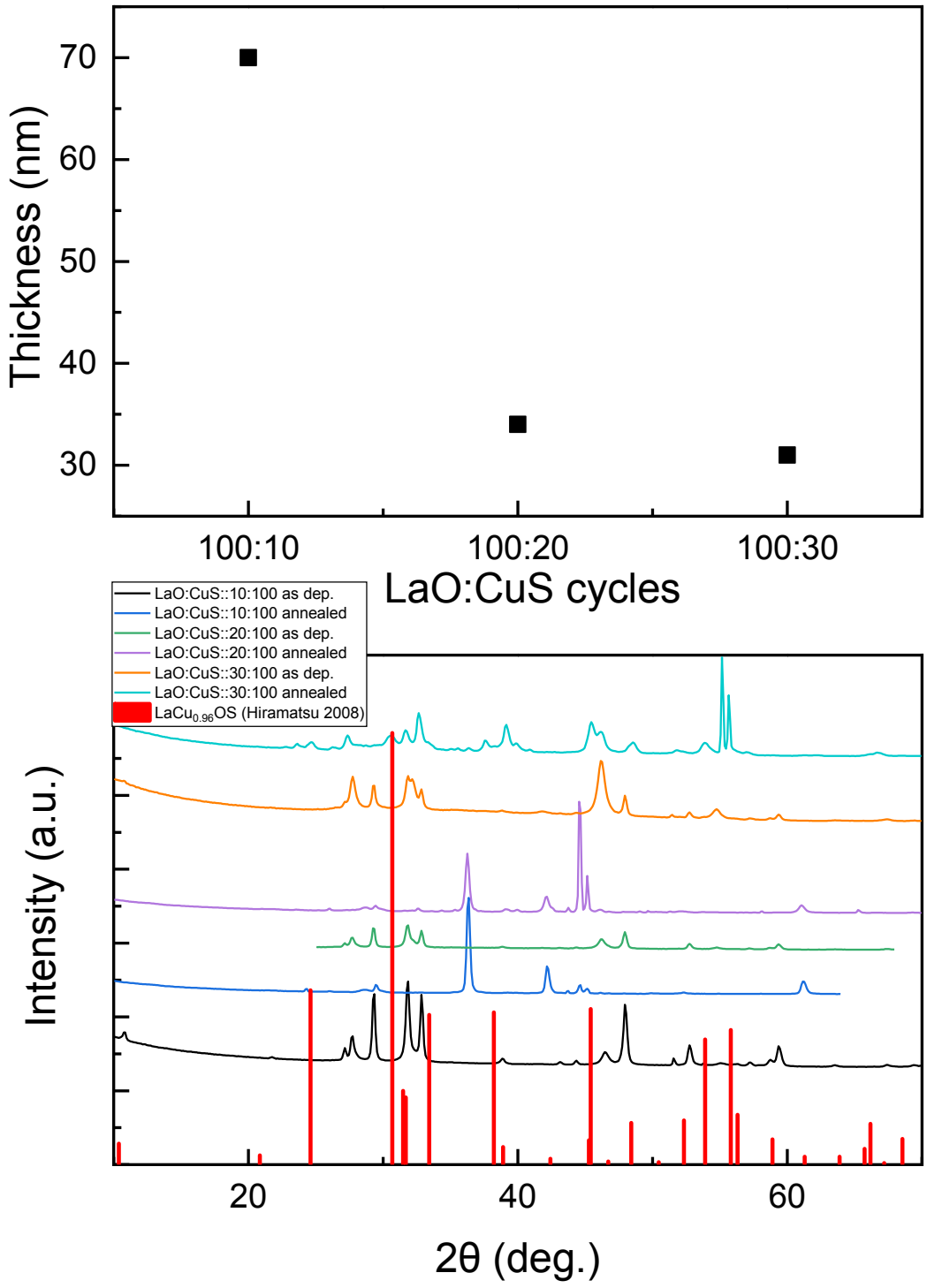

Figure 27. (Upper) The thickness of LaOCuS films deposited with supercycles versus the number of cycles. (Legend: 10:100 = 100 cycles of the first two precursors followed by 10 cycles of the last two precursors.) (Lower) The GIXRD data of annealed and as deposited LaOCuS films deposited with a supercycle and varying LaO cycles. The bulk $LaCu_{0.96}OS$ [111] XRD data is plotted for comparison.

The film thickness in simultaneous LaOCuS film depositions, with supercycles, is presented in Figure 27. The deposition temperature was 230°C in all of the depositions and the sublimation temperatures were kept the same as in the separate depositions. The cycle / purge ratio was 2 seconds / 3 seconds in these depositions. A five-minute purge of N_2 was also added in between the LaO and CuS depositions after one deposition for the rest of the depositions. The following deposition sequences were utilized for the depositions with supercycles (**x5**):

$(La(thd)_2$ 2.0 s / N_2 purge 3.0 s // O_3 2.0 s / N_2 purge 3.0 s //
$Cu(acac)_2$ 2.0 s / N_2 purge 3.0 s // S 2.0 s / N_2 purge 3.0 s) **x5**

The depositions without supercycles first resulted in a number of films that were not crystalline. This was to be expected due to the short pulse lengths for sulfur and $Cu(acac)_2$ and thus insufficient time for them to be completely sublimated and carried into the reaction chamber. Consequently, the cycle / purge ratio for these two precursors was increased to 5 seconds / 6 seconds. The deposition and sublimation temperatures were kept the same as before. GIXRD measurements confirmed that the change in cycle / purge ratio increased the crystallinity of the films. The following deposition sequence (a subcycle of the above) was utilized for the depositions without supercycles:

$(La(thd)_2$ 2.0 s / N_2 purge 3.0 s // O_3 2.0 s / N_2 purge 3.0 //)
/ N_2 purge 300.0 s /
$(Cu(acac)_2$ 5.0 s / N_2 purge 6.0 s // S 5.0 s / N_2 purge 6.0 s)

Figure 27 shows the thickness of LaOCuS films deposited with supercycles versus the number of cycles. The thickness of the films decreases with increasing CuS cycles.

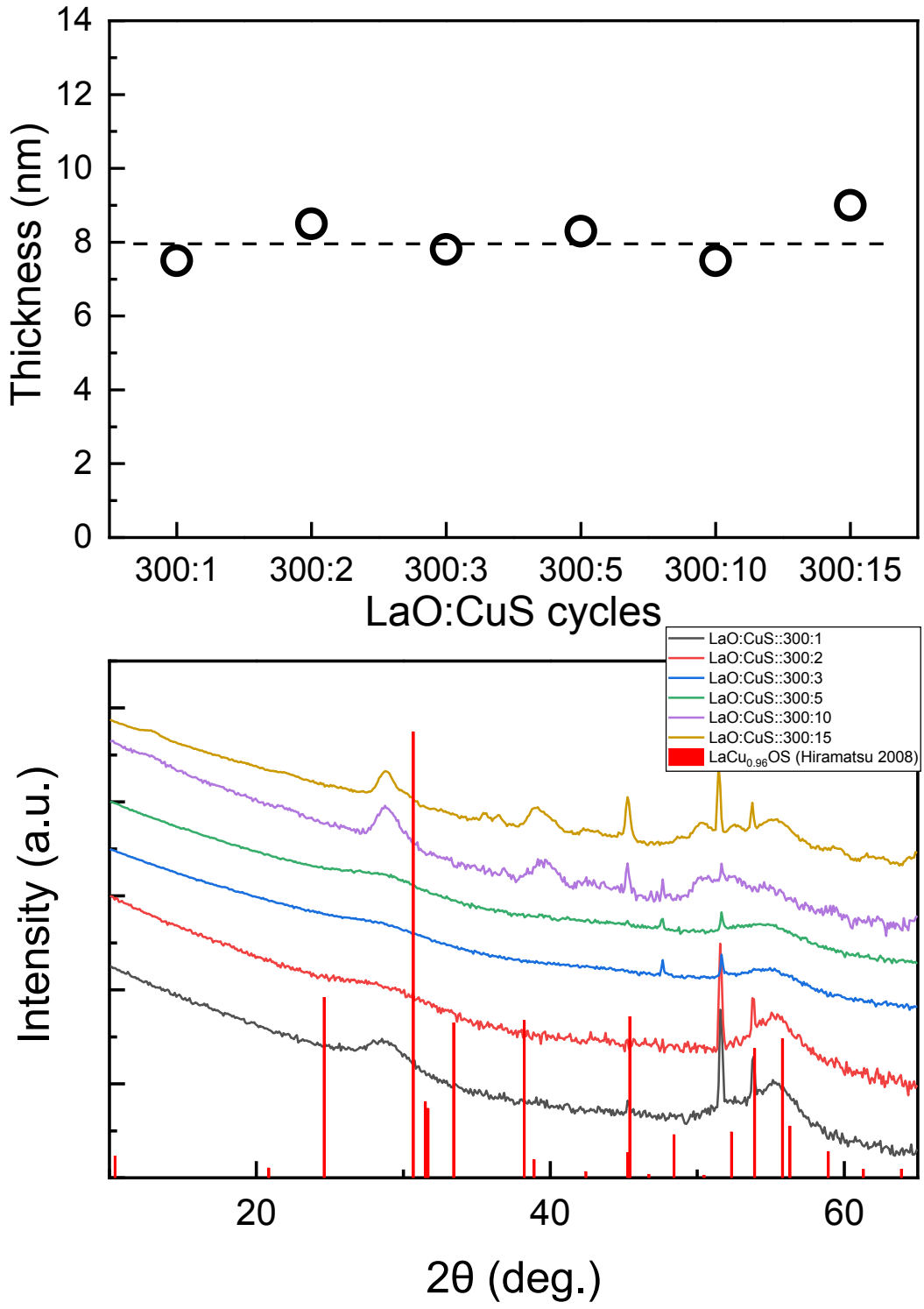

Figure 28. (Upper) The thickness of deposited LaOCuS films deposited without supercycles versus the number of cycles. (Lower) GIXRD patterns for LaOCuS films deposited with different cycles of CuS while keeping the LaO cycles at 300. These depositions included no supercycles and the bulk $LaCu_{0.96}OS$ [112] XRD data is plotted for comparison.

PANalytical X'pert PRO diffractometer with Cu K_α radiation (λ = 1.54 Å) was utilized for the XRR and GIXRD measurements and the film composition and crystallinity was determined from the GIXRD data. The database of "MATCH! Phase Identification from Powder Diffraction" program was utilized for analyzing the GIXRD data measured from the deposited thin films. The thin film GIXRD data was compared with corresponding bulk compound XRD data from the literature. The most intensive peaks at around 2θ = 30° were mainly considered when comparing the XRD data to each other. LaOCuS thin films were successfully fabricated using ALD, because there were numerous peaks visible in the GIXRD data. The data showed that partial crystallinity was present in some of the film compositions. Generally, the GIXRD data did not include enough peaks for exact determination of the phase composition. However, the peaks included in the data provide valuable information on the possible structure and phase composition of the films. Unless noted in the text, the GIXRD data is from films deposited on Si substrates.

The GIXRD data of annealed and as deposited LaOCuS films deposited with supercycles is also shown in Figure 27. Annealing changed the data considerably in some cases, such as LaO:CuS::20:100. The most intensive peak of the bulk $LaCu_{0.96}OS$ [111] is located at 2θ = 31° and various peaks of the thin film GIXRD data are located at the same position, which is an indication that the structure is close to the bulk phase. Some of the less intensive peaks around 2θ = 35 - 45° are also found in the GIXRD data.

In Figure 28, GIXRD data of films deposited without supercycles (all annealed) with varying CuS cycles are presented. Because there are considerably less cycles of CuS compared to LaO, the film thickness stays almost constant at approximately 8 nm, which is also shown in Figure 28. While the LaO cycles are kept constant at 300, the CuS cycles vary from 1 to 15. As the cycle number of CuS increases, more prominent peaks are seen especially at approximately 2θ = 30° and 2θ = 40 - 45°. This indicates that the thin film growth is more uniform with higher CuS cycles and more amorphous films are fabricated with lower CuS cycle numbers. The most

crystalline structure is achieved with CuS cycles of 10 and 15. The most intensive peak is also found in the GIXRD data of LaO:CuS::10:100 and LaO:CuS::15:100. The peaks at 2θ = 30° and 2θ = 45° are also found in both XRD data, which is a good indication that the structure is more crystalline and corresponds to the bulk phase. The phase composition is close to the bulk composition, but more peaks would be needed for the exact determination. The peaks at approximately 2θ = 45-60° most likely result from the Si substrate in all of the GIXRD data.

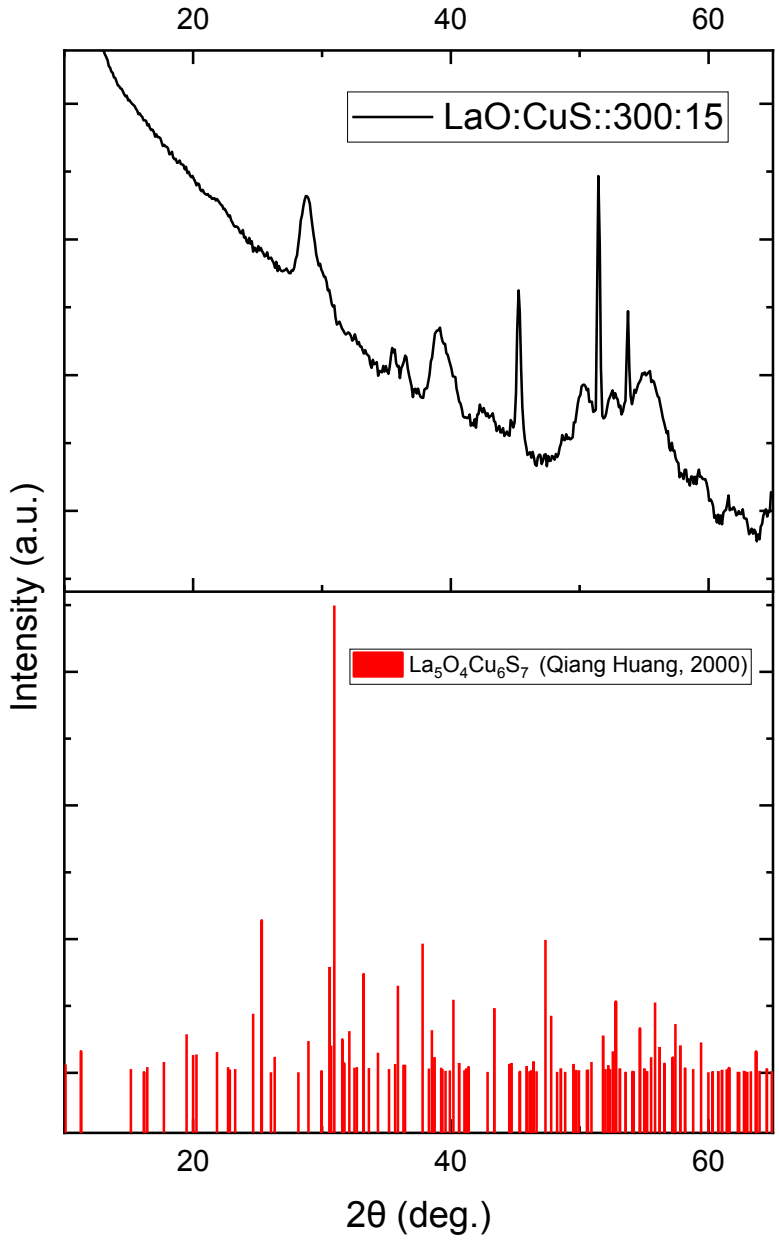

Figure 29. The GIXRD pattern for deposited LaO:CuS::300:15 compared with the XRD pattern of bulk $La_5O_4Cu_6S_7$ [189].

When comparing a single LaOCuS film (300 cycles of LaO and 15 cycles of CuS) with a different stoichiometry of a bulk LaOCuS compound [189], the most intensive peak of the bulk XRD is also found in the thin film GIXRD data (Figure 29).

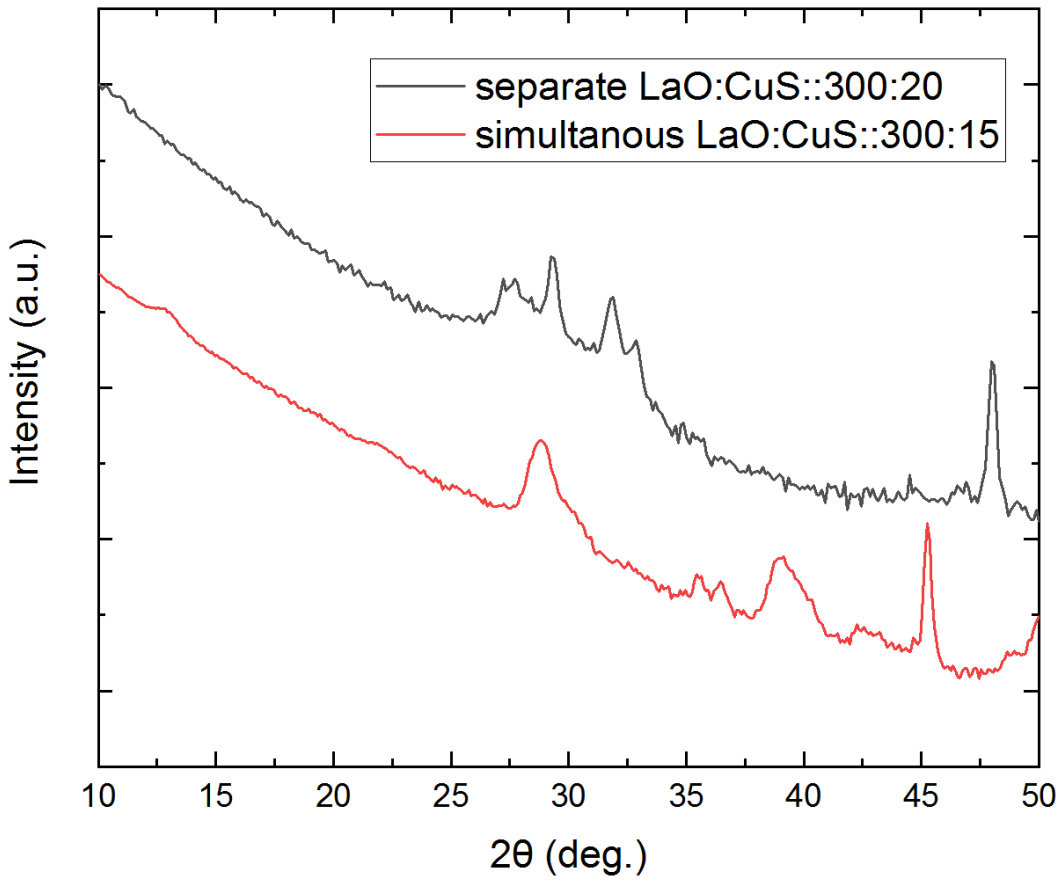

Figure 30. Comparison of two LaOCuS films deposited separately (two depositions) and simultaneously (one deposition).

As observed from Figure 30, the separately deposited LaOCuS GIXRD data includes more peaks in the 2θ = 25-35° region, whereas the simultaneous deposition has resulted in more peaks in the 2θ = 35-40° region. This could be a result from the different deposition procedure and needs more careful research in the future.

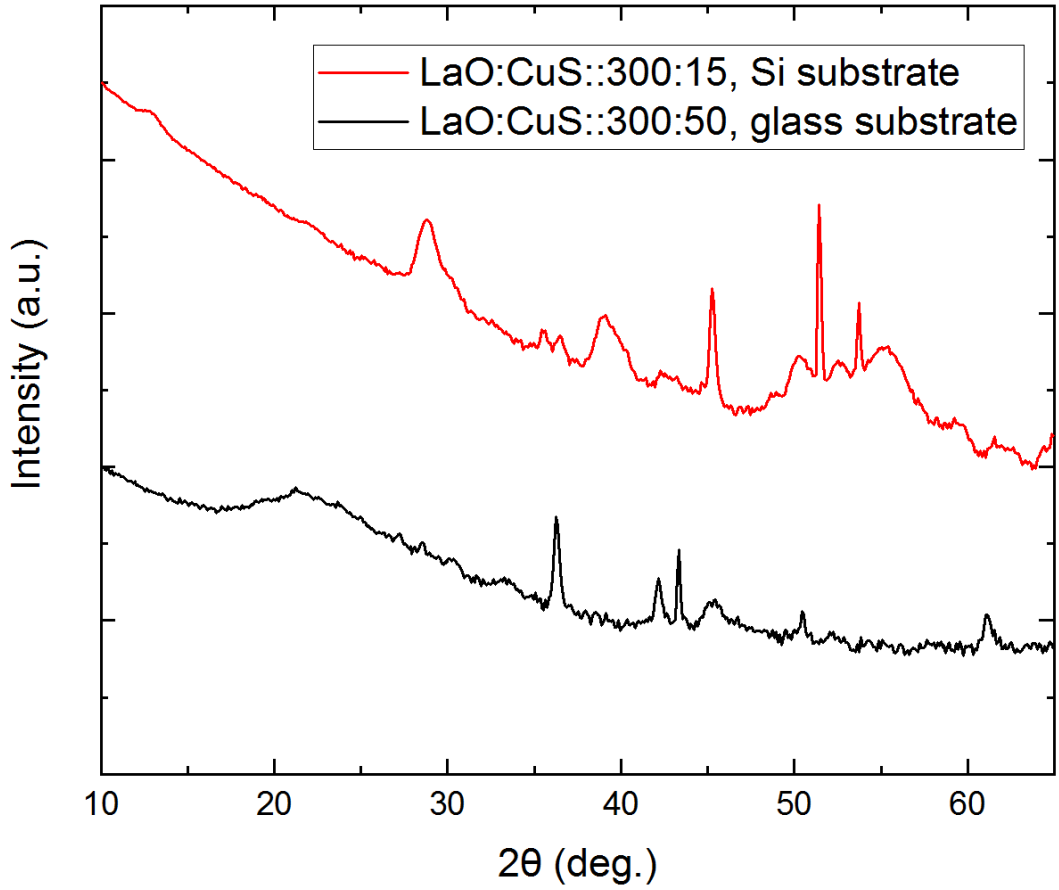

Figure 31. Comparison of two LaOCuS films deposited on a Si substrate (red) and on a borosilicate glass substrate (black).

Figure 31 shows a comparison on two films deposited on different substrates. The peak in the 2θ = 20-30° region in the borosilicate glass GIXRD data was confirmed to result from the glass itself (by measuring GIXRD from a clean borosilicate glass slab without a film), whereas there seems to be small peaks around the 2θ = 45-60° region, which are hidden in the Si substrate GIXRD data under the characteristic peaks resulting from the Si substrate.

From the overall GIXRD data, it can be concluded that more crystalline films were fabricated with depositions without supercycles (Figure 28). They had more similar peaks to the bulk XRD data of LaOCuS, whereas the depositions with supercycles (Figure 27) did not yield as consistent results. For example, the most intensive peak of the bulk XRD data at 2θ = 30° was not as clearly seen in the GIXRD data of depositions with supercycles. The most crystalline films were fabricated with cycle

numbers of LaO:CuS::300:10 and LaO:CuS::300:15 deposited on a silicon substrate with a deposition temperature of 230°C, and sublimation temperatures of 110°C for S, 135°C for $Cu(acac)_2$ and 170°C for $La(thd)_2$.

5.2 Electrical measurements

Because the films were quite resistive, a two-probe DC voltage source measurement was conducted. The measurement was performed with an Advantest R6144 Programmable DC Voltage/Current Generator with a Keithley 485 Autoranging Picoammeter on an annealed LaO:CuS::300:50 thin film with a thickness of 8 nm. The voltage range used was 0.001 – 0.1 mV. The thin film resistivity calculated from this data was approximately 2.4 Ωcm. This corresponds to a conductivity of 0.42 Scm^{-1}, which is in line with the bulk conductivities of lanthanum oxysulfides that typically vary between 0.1 and 20 Scm^{-1} [25]. Overall, the thin films were very resistive and there were difficulties in the measurements.

6 Conclusions and suggestions for further research

In summary, quaternary LaOCuS thin films were deposited with ALD, using $La(thd)_2$, O_3, $Cu(acac)_2$ and S as precursors. The LaOCuS thin film ALD process was successful and a thin film was fabricated, which is explained by the peaks that were found in the GIXRD data from the deposited films. The deposition processes were mainly based on trial and error because, to our knowledge, no one had deposited this kind of thin films before. GIXRD and XRR were utilized for thin film characterizations after depositions and annealing of the thin films. Annealing seemed to change the thin film GIXRD patterns remarkably and longer pulse length for $Cu(acac)_2$ and S were utilized for more uniform phase composition. A number of different parameters and deposition conditions were tested during the experimental part to find, which would be most efficient for this kind of thin film. There was limited time to explore each condition thoroughly, which is why they must be retested in the future more carefully.

For future work, the separate depositions could be examined more carefully because this thesis mainly concentrated on the simultaneous ones. The separately deposited films should be annealed and compared with similar annealed films deposited simultaneously to find the most crystalline thin film composition. Moreover, because the LaO thin film growth rate is very low, the cycle number should be increased in future depositions for a more even thickness of both the LaO and CuS phases. An interesting possibility would also be to deposit the films in reverse order: to deposit the CuS layer first and LaO layer second. In this case, the thickness of the LaO film should be adjusted to be as similar as possible to the thickness of the CuS layer.

For future depositions, working with different precursors is a possibility. It may be advisable to exchange $La(thd)_2$ for a different lanthanum precursor due to the larger size of $La(thd)_2$: a possible substitutive precursor smaller in size could be for example La(acac). Utilizing it could induce more uniform growth of the films and

make it possible to identify the phase more easily. The sublimation temperature for sulfur and $Cu(acac)_2$ might also have to be increased in future depositions to see if their sublimation is increased.

Different cycle numbers should be tested for the LaOCuS depositions. One possibility is to increase the cycle number for LaO because its growth is considerably lower compared to CuS. A similar thickness of the LaO and CuS phases would help in mixing the phases when annealing the films, and this would possibly produce a more crystalline and uniform phase combined of them. The exact stoichiometry of the LaOCuS thin film must also be studied in the future.

Using different annealing atmospheres might result in different film crystal structures. The annealing temperature was almost at the maximum it can be for the borosilicate glass, which softens at around 800°C, so it cannot be increased much further. There was also some inconsistency between the GIXRD data of the as deposited and annealed thin films (Figure 27): some of the films seemed to have more crystalline structure in their as deposited state even though the latter films clearly were more crystalline in their annealed state (Figure 28), which might also be due to a lower annealing temperature and different cycle numbers, as well as various problems experienced with the ALD reactor.

Four-probe electrical measurements could be conducted again in the future with thicker films, because they were not possible with the thin films deposited in this study. Two-probe measurements were more successful but the high resistivity of the films is a challenge that must be overcome in the future. Two-probe measurements should also be conducted on more than two different thin film compositions for comparison. There is a possibility to utilize a different substrate for the thin film depositions: sapphire, a different glass or aluminum. This would possibly increase the film crystallinity as well as make it easier to measure electrical properties from the films. SEM images of the films would also be interesting to compare with each other.

References

[1] T. S. Tripathi, and M. Karppinen, Atomic Layer Deposition of p-Type Semiconducting Thin Films: a Review, *Adv. Mater. Interfaces* **4** (2017) 1–16.

[2] J. R. Bakke, J. T. Tanskanen, C. Hägglund, T. A. Pakkanen, and S. F. Bent, Growth characteristics, material properties, and optical properties of zinc oxysulfide films deposited by atomic layer deposition, *J. Vac. Sci. Technol. A Vacuum, Surfaces, Film.* **30** (2012) 01A135.

[3] B. Oy, nSILVER® Anti-Tarnish Coating, https://beneq.com/sites/default/files/links/Beneq_nsilver_brochure_HiRes_20160927.pdf , 24.4.2018.

[4] J. Maula, Atomic layer deposition for industrial optical coatings, *Chinese Opt. Lett.* **8** (2010) 53–58.

[5] A. Levasseur, E. Schmidt, G. Meunier, D. Gonbeau, L. Benoist, and G. Pfister-Guillouzo, New amorphous molybdenum oxysulfide thin films their characterization and their electrochemical properties, *J. Power Sources* **54** (1995) 352–355.

[6] S. Haindl, M. Kidszun, F. Onken, A. Mietke, and T. Thersleff, Lessons From Oxypnictide Thin Films, *Int. J. Mod. Phys. B* **27** (2013) 1330001.

[7] R. L. Puurunen, Surface chemistry of atomic layer deposition: A case study for the trimethylaluminum/water process, *J. Appl. Phys.* **97** (2005).

[8] H. Kageyama, K. Hayashi, K. Maeda, J. P. Attfield, Z. Hiroi, J. M. Rondinelli, and K. R. Poeppelmeier, Expanding frontiers in materials chemistry and physics with multiple anions, *Nat. Commun.* **9** (2018).

[9] I. Ijjaali, C. L. Haynes, A. D. McFarland, R. P. Van Duyne, and J. A. Ibers, Synthesis, structure, and optical properties of the new lanthanum copper oxysulfide La3CuO2S3, *J. Solid State Chem.* **172** (2003) 257–260.

[10] H. Hiramatsu, M. Orita, M. Hirano, K. Ueda, and H. Hosono, Electrical conductivity control in transparent p-type (LaO)CuS thin films prepared by rf sputtering, *J. Appl.*

Phys. **91** (2002) 9177–9181.

[11] T. S. Tripathi, J. Lahtinen, and M. Karppinen, Atomic Layer Deposition of Conducting CuS Thin Films from Elemental Sulfur, *Adv. Mater. Interfaces* **1701366** (2018) 1701366.

[12] K. Machida, Synthesis and materials design for heteroanion compounds, *IOP Conf. Ser. Mater. Sci. Eng.* **18** (2011) 3–6.

[13] C. Barreteau, D. Bérardan, E. Amzallag, L. Zhao, and N. Dragoe, Structural and Electronic Transport Properties in Sr-Doped BiCuSeO, *Chem. Mater.* **24** (2012) 3168–3178.

[14] S. D. N. Luu, and P. Vaqueiro, Layered oxychalcogenides: Structural chemistry and thermoelectric properties, *J. Mater.* **2** (2016) 131–140.

[15] S. J. Clarke, P. Adamson, S. J. C. Herkelrath, O. J. Rutt, D. R. Parker, M. J. Pitcher, and C. F. Smura, Structures, physical properties, and chemistry of layered oxychalcogenides and oxypnictides, *Inorg. Chem.* **47** (2008) 8473–8486.

[16] T. C. Ozawa, and S. M. Kauzlarich, Chemistry of layered d-metal pnictide oxides and their potential as candidates for new superconductors, *Sci. Technol. Adv. Mater.* **9** (2008).

[17] A. Simon, Group 1 and 2 suboxides and subnitrides — Metals with atomic size holes and tunnels, *Coord. Chem. Rev.* **163** (1997) 253–270.

[18] W. J. Zhu, and P. H. Hor, Unusual Layered Transition-Metal Oxysulfides: Sr2Cu2MO2S2 (M5Mn, Zn), *J. Solid State Chem.* **321** (1997) 319–321.

[19] K. Ueda, and H. Hosono, Crystal structure of LaCuOS(1-x)Se(x) oxychalcogenides, *Thin Solid Films* **411** (2002) 115.

[20] V. Meignen, A. Meerschaut, L. Cario, and A. Lafond, Synthesis and crystal structure of a new oxysulfide Gd6+xTi4-xS10-yO6+y (where x ∼0.04 and y ∼0.27), *Zeitschrift Fur Naturforsch. - Sect. B J. Chem. Sci.* **59** (2004) 4–9.

[21] A. Baqais, A. Curutchet, A. Ziani, H. Ait Ahsaine, P. Sautet, K. Takanabe, and T. Le Bahers, Bismuth Silver Oxysulfide for Photoconversion Applications: Structural and Optoelectronic Properties, *Chem. Mater.* **29** (2017) 8679–8689.

[22] H. Zhu, T. Su, H. Li, C. Pu, D. Zhou, P. Zhu, and X. Wang, High pressure synthesis, structure and thermoelectric properties of BiCuChO (Ch = S, Se, Te), *J. Eur. Ceram. Soc.* **37** (2017) 1541–1546.

[23] A. B. Jorge, J. Oró-Solé, A. M. Bea, N. Mufti, T. T. M. Palstra, J. A. Rodgers, J. P. Attfield, and A. Fuertes, Large coupled magnetoresponses in EuNbO2N, *J. Am. Chem. Soc.* **130** (2008) 12572–12573.

[24] M. Kidszun, S. Haindl, T. Thersleff, J. Werner, M. Langer, J. Hänisch, K. Iida, E. Reich, L. Schultz, and B. Holzapfel, Fabrication of superconducting oxypnictide thin films, *EPL (Europhysics Lett.* **90** (2010) 57005.

[25] H. Hiramatsu, K. Ueda, H. Ohta, M. Hirano, T. Kamiya, and H. Hosono, Degenerate p-type conductivity in wide-gap LaCuOS1-xSex (x = 0-1) epitaxial films, *Appl. Phys. Lett.* **82** (2003) 1048–1050.

[26] B. Olofinjana, G. O. Egharevba, M. A. Eleruja, C. Jeynes, A. V. Adedeji, O. O. Akinwunmi, B. A. Taleatu, C. U. Mordi, and E. O. B. Ajayi, Synthesis and Some Properties of Metal Organic Chemical Vapour Deposited Molybdenum Oxysulphide Thin Films, *J. Mater. Sci. Technol.* **26** (2010) 552–557.

[27] I. Heikkinen, Characterization of Zinc Oxide, Sulfide and Oxysulfide Thin Films Grown By Spatial Atomic Layer Deposition, Aalto University, (2016).

[28] B. W. Sanders, and A. Kitai, Zinc Oxysulfide thin Films Grown by Atomic Layer Deposition, *Chem. Mater.* **4** (1992) 1005–1011.

[29] M. A. Negara, M. Kitano, R. D. Long, and P. C. McIntyre, Oxide Charge Engineering of Atomic Layer Deposited AlOxNy/Al2O3Gate Dielectrics: A Path to Enhancement Mode GaN Devices, *ACS Appl. Mater. Interfaces* **8** (2016) 21089–21094.

[30] IUPAC, Compendium of Chemical Terminology 2nd ed. (the “Gold Book”), *Blackwell Sci. Publ. Oxford* **2.2.3** (2014) 1670.

[31] R. K. Oogarah, E. Suard, and E. E. Mccabe, Magnetic order and phase transition in the iron oxysulfide La2O2Fe2OS2, *J. Magn. Magn. Mater.* **9** (2017) 1–14.

[32] Y. L. Pei, H. Wu, D. Wu, F. Zheng, and J. He, High thermoelectric performance realized in a bicuseo system by improving carrier mobility through 3D modulation

doping, *J. Am. Chem. Soc.* **136** (2014) 13902–13908.

[33] Y. L. Pei, J. He, J. F. Li, Fuli, Q. Liu, W. Pan, C. Barreteau, D. Berardan, N. Dragoe, and L. D. Zhao, High thermoelectric performance of oxyselenides: Intrinsically low thermal conductivity of Ca-doped BiCuSeO, *NPG Asia Mater.* **5** (2013).

[34] M. Ahmed, and G. Xinxin, A review of metal oxynitrides for photocatalysis, *Inorg. Chem. Front.* **3** (2016) 578–590.

[35] A. P. Black, H. Suzuki, M. Higashi, C. Frontera, C. Ritter, C. De, S. Athinarayanan, R. Abe, and A. Fuertes, New rare earth hafnium oxynitride perovskites with photocatalytic activity in water oxidation and reduction, *Chem. Commun.* **54** (2018) 1525–1528.

[36] A. Ishikawa, T. Takata, J. N. Kondo, M. Hara, H. Kobayashi, and K. Domen, Oxysulfide Sm2Ti2S2O5 as a stable photocatalyst for water oxidation and reduction under visible light irradiation (λ ≤ 650 nm), *J. Am. Chem. Soc.* **124** (2002) 13547–13553.

[37] H. Kabbour, E. Janod, B. Corraze, M. Danot, C. Lee, M.-H. Whangbo, and L. Cario, Structure and Magnetic Properties of Oxychalcogenides, *J. AM. CHEM. SOC* **45** (2004) 637–641.

[38] M. Guittard, S. Benazeth, J. Dugue´, S. Jaulmes, M. Palazzi, P. Laruelle, and J. Flahaut, Oxysulfides and oxyselenides in sheets, formed by a rare earth element and a second metal, *J. Solid State Chem.* **51** (1984) 227–238.

[39] T. Sambrook, C. F. Smura, S. J. Clarke, M. O. Kang, and P. S. Halasyamani, Structure and physical properties of the polar oxysulfide CaZnOS, *Inorg. Chem.* **46** (2007) 2571–2574.

[40] K. Ueda, and H. Hosono, Band gap engineering, band edge emission, and p-type conductivity in wide-gap LaCuOS 1-xSe x oxychalcogenides, *J. Appl. Phys.* **91** (2002) 4768–4770.

[41] H. J. Kim, Y.-G. Roh, and H. Jeon, Photonic Bandgap Engineering in Mixed Colloidal Photonic Crystals, *Jpn. J. Appl. Phys.* **44** (2005) L1259–L1262.

[42] K. Ueda, S. Inoue, S. Hirose, H. Kawazoe, and H. Hosono, Transparent p-type

semiconductor: LaCuOS layered oxysulfide, *Appl. Phys. Lett.* **77** (2000) 2701–2703.

[43] J. M. Polfus, T. Norby, and R. Bredesen, Protons in oxysulfides, oxysulfates, and sulfides: A first-principles study of La2O2S, La2O2SO4, SrZrS3, and BaZrS3, *J. Phys. Chem. C* **119** (2015) 23875–23882.

[44] I. R. Shein, and A. L. Ivanovskii, Electronic band structure and Fermi surface for new layered superconductor LaO0.5F0.5BiS2 in comparison with parent phase LaOBiS2 from first principles, *JETP Lett.* **96** (2013) 769–774.

[45] X. Y. Dong, J. F. Wang, R. X. Zhang, W. H. Duan, B. F. Zhu, J. O. Sofo, and C. X. Liu, Electrically tunable multiple Dirac cones in thin films of the (Lao)2(SbSe2)2family of materials, *Nat. Commun.* **6** (2015) 1–7.

[46] V. V. Bannikov, I. R. Shein, and A. L. Ivanovskii, Electronic properties and chemical bonding in quaternary arsenide oxides LaZnAsO and YZnAsO, *Mater. Chem. Phys.* **116** (2009) 129–133.

[47] M. Wintenberger, J. Dugue, M. Guittard, N. H. U. Y. Dung, and V. V. T. Tien, Ferro- and Antiferromagnetism in Oxychalcogenides (Ln = La or Nd and X = S or Se)*,', *J. Solid State Chem.* **302** (1987) 295–302.

[48] H. Yanagi, R. Kawamura, T. Kamiya, Y. Kamihara, M. Hirano, T. Nakamura, H. Osawa, and H. Hosono, Itinerant ferromagnetism in the layered crystals LaCoOX (X=P,As), *Phys. Rev. B - Condens. Matter Mater. Phys.* **77** (2008) 1–7.

[49] A. Lafond, F. Bouree, A. Meerschaut, O. Leynaud, and G. Andre, Magnetic properties of Ln2Ti2S2O5 compounds and magnetic structure of Tb2Ti2S2O5, **338** (2002) 185–193.

[50] Y. Kamihara, H. Hiramatsu, M. Hirano, R. Kawamura, H. Yanagi, T. Kamiya, and H. Hosono, Iron-based layered superconductor: LaOFeP, *J. Am. Chem. Soc.* **128** (2006) 10012–10013.

[51] J.-W. G. Bos, G. B. S. Penny, J. a Rodgers, D. a Sokolov, A. D. Huxley, and J. P. Attfield, High pressure synthesis of late rare earth RFeAs(O,F) superconductors; R = Tb and Dy., *Chem. Commun. (Camb).* **003** (2008) 3634–3635.

[52] I. U. of P. and A. Chemistry, *Nomenclature of Inorganic Chemistry: IUPAC*

Recomendations 2005, 2005.

[53] M. Kidszun, S. Haindl, E. Reich, J. Hänisch, K. Iida, L. Schultz, and B. Holzapfel, Epitaxial LaFeAsO $_{1-x}$ F $_{x}$ thin films grown by pulsed laser deposition, *Supercond. Sci. Technol.* **23** (2010) 022002.

[54] T. Kawaguchi, H. Uemura, T. Ohno, M. Tabuchi, T. Ujihara, K. Takenaka, Y. Takeda, and H. Ikuta, In situ growth of superconducting NdFeAs(O,F) thin films by molecular beam epitaxy, *Appl. Phys. Lett.* **97** (2010) 1–4.

[55] H. Hiramatsu, Y. Kamihara, H. Yanagi, K. Ueda, T. Kamiya, M. Hirano, and H. Hosono, Layered mixed-anion compounds: Epitaxial growth, active function exploration, and device application, *J. Eur. Ceram. Soc.* **29** (2009) 245–253.

[56] H. Hiramatsu, H. Kamioka, K. Ueda, H. Ohta, T. Kamiya, M. Hirano, and H. Hosono, Opto-electronic properties and light-emitting device application of widegap layered oxychalcogenides: LaCuOCh (Ch = chalcogen) and la 2CdO 2Se 2, *Phys. Status Solidi Appl. Mater. Sci.* **203** (2006) 2800–2811.

[57] R. Pöttgen, and D. Johrendt, Materials with ZrCuSiAs Type Structure, *Zeitschrift Für Naturforsch.* **161** (2008) 32.

[58] D. Phuong, Syntheses , Characterizations , and Properties of Suboxides and Layered Titanium-based Pnictide Oxide Superconductors Syntheses , Characterizations , and Properties of Suboxides and Layered Titanium-based Pnictide Oxide Superconductors Approved :, University of Houston, (2012).

[59] Z. Ren, J. Yang, W. Lu, W. Yi, G. Che, X. Dong, L. Sun, and Z. Zhao, Superconductivity at 55 K in Iron-Based F-Doped Layered Quaternary Compound Sm[O1-x Fx]FeAs, *Physics (College. Park. Md).* **967** (2008) 1–4.

[60] J. G. Bednorz, and K. A. Müller, Possible High T c Superconductivity in the Ba — La — Cu — O System, *Z. Phys. B - Condens. Matter* **64** (1986) 267–271.

[61] J. Prakash, S. J. Singh, D. Das, S. Patnaik, and A. K. Ganguli, Journal of Solid State Chemistry New oxypnictide superconductors : PrOFe 1 À x Co x As, **183** (2009) 1–6.

[62] J. Yang, Z. C. Li, W. Lu, W. Yi, X. L. Shen, Z. A. Ren, G. C. Che, X. L. Dong, L. L. Sun, F.

Zhou, and Z. X. Zhao, Superconductivity at 53.5 K in GdFeAsO1-δ, *Supercond. Sci. Technol.* **21** (2008).

[63] Z. A. Ren, G. C. Che, X. L. Dong, J. Yang, W. Lu, W. Yi, X. L. Shen, Z. C. Li, L. L. Sun, F. Zhou, and Z. X. Zhao, Superconductivity and phase diagram in iron-based arsenic-oxides ReFeAsO1-δ (Re = rare-earth metal) without fluorine doping, *Epl* **83** (2008).

[64] L. J. Li, Y. K. Li, Z. Ren, Y. K. Luo, X. Lin, M. He, Q. Tao, Z. W. Zhu, G. H. Cao, and Z. A. Xu, Superconductivity above 50 K in Tb1-x ThxFeAsO, *Phys. Rev. B - Condens. Matter Mater. Phys.* **78** (2008) 6–9.

[65] G. F. Chen, Z. Li, D. Wu, G. Li, W. Z. Hu, J. Dong, P. Zheng, J. L. Luo, and N. L. Wang, Superconductivity at 41 K and its competition with spin-density-wave instability in layered CeO1-xFxFeAs, *Phys. Rev. Lett.* **100** (2008) 1–4.

[66] Y. Ye, R. Lim, and J. M. White, High mobility amorphous zinc oxynitride semiconductor material for thin film transistors, *J. Appl. Phys.* **106** (2009).

[67] T. Yamazaki, K. Shigematsu, Y. Hirose, S. Nakao, I. Harayama, D. Sekiba, and T. Hasegawa, Amorphous ZnO_xN_y thin films with high electron Hall mobility exceeding 200 $cm^2 V^{-1} s^{-1}$, *Appl. Phys. Lett.* **109** (2016) 262101.

[68] À. R. Garcia, C. Clausell, and A. Barba, Oxynitride glasses: A review, *Bol. La Soc. Esp. Ceram. y Vidr.* **55** (2016) 209–218.

[69] Z. W. Fu, W. Y. Liu, C. L. Li, Q. Z. Qin, Y. Yao, and F. Lu, High-k lithium phosphorous oxynitride thin films, *Appl. Phys. Lett.* **83** (2003) 5008–5010.

[70] K. M. Niang, B. C. Bayer, J. C. Meyer, and A. J. Flewitt, Highly stable amorphous zinc tin oxynitride thin film transistors under positive bias stress, *Appl. Phys. Lett.* **111** (2017).

[71] M. Arbab, G. J. Marietti, P. A. Medwick, and L. A. Miller, Silicon oxynitride protective coatings, 2002.

[72] M. Yang, J. Oró-Solée, J. A. Rodgers, A. B. Jorge, A. Fuertes, and J. P. Attfield, Anion order in perovskite oxynitrides, *Nat. Chem.* **3** (2011) 47–52.

[73] M. Nisula, Y. Shindo, H. Koga, and M. Karppinen, Atomic Layer Deposition of Lithium Phosphorus Oxynitride, *Chem. Mater.* **27** (2015) 6987–6993.

[74] I. Castello, and M. Massler, EFFECT OF ZINC OXYPHOSPHATE CEMENT ON ENAMEL, *Am. J. Orthod.* **34** (1948) 271–277.

[75] A. T. Nientiedt, and W. Jeitschko, Equiatomic Quaternary Rare Earth Element Zinc Pnictide Oxides RZnPO and RZnAsO, *Inorg. Chem.* **37** (1998) 386–389.

[76] N. El Khayati, R. C. El Moursli, and J. Rodr, Crystal and magnetic structures of the oxyphosphates MFePO5 (M = Fe , Co , Ni , Cu). Analysis of the magnetic ground state in terms of superexchange interactions, *Eur. Phys. J. B* **442** (2001) 429–442.

[77] T. Watanabe, H. Yanagi, T. Kamiya, Y. Kamihara, H. Hiramatsu, M. Hirano, and H. Hosono, Nickel-based oxyphosphide superconductor with a layered crystal structure, LaNiOP, *Inorg. Chem.* **46** (2007) 7719–7721.

[78] V. S. Levushkina, D. A. Spassky, E. M. Aleksanyan, M. G. Brik, M. S. Tretyakova, B. I. Zadneprovski, and A. N. Belsky, Bandgap engineering of the LuxY1-xPO4mixed crystals, *J. Lumin.* **171** (2016) 33–39.

[79] Y. G. Kim, and H. N. G. Wadley, Lithium phosphorous oxynitride films synthesized by a plasma-assisted directed vapor deposition approach, *J. Vac. Sci. Technol. A Vacuum, Surfaces, Film.* **26** (2008) 174–183.

[80] J. Xu, C. Pan, T. Takata, and K. Domen, Photocatalytic overall water splitting on the perovskite-type transition metal oxynitride $CaTaO_2N$ under visible light irradiation, *Chem. Commun.* **51** (2015) 7191–7194.

[81] Y. Il Kim, W. Si, P. M. Woodward, E. Sutter, S. Park, and T. Vogt, Epitaxial thin-film deposition and dielectric properties of the perovskite oxynitride BaTaO2N, *Chem. Mater.* **19** (2007) 618–623.

[82] E. Carretero, R. Alonso, and C. Pelayo, Optical and electrical properties of stainless steel oxynitride thin films deposited in an in-line sputtering system, *Appl. Surf. Sci.* **379** (2016) 249–258.

[83] N. Brinkmann, D. Sommer, G. Micard, G. Hahn, and B. Terheiden, Electrical, optical and structural investigation of plasma-enhanced chemical-vapor-deposited amorphous silicon oxynitride films for solar cell applications, *Sol. Energy Mater. Sol. Cells* **108** (2013) 180–188.

[84] F. Xian, J. Ye, S. Gu, H. H. Tan, and C. Jagadish, Structural transition, subgap states, and carrier transport in anion-engineered zinc oxynitride nanocrystalline films, *Appl. Phys. Lett.* **109** (2016).

[85] J. M. Chappé, N. Martin, J. Lintymer, F. Sthal, G. Terwagne, and J. Takadoum, Titanium oxynitride thin films sputter deposited by the reactive gas pulsing process, *Appl. Surf. Sci.* **253** (2007) 5312–5316.

[86] P. Carvalho, J. Borges, M. S. Rodrigues, N. P. Barradas, E. Alves, J. P. Espinós, A. R. González-Elipe, L. Cunha, L. Marques, M. I. Vasilevskiy, and F. Vaz, Optical properties of zirconium oxynitride films: The effect of composition, electronic and crystalline structures, *Appl. Surf. Sci.* **358** (2015) 660–669.

[87] H. Le Dréo, O. Banakh, H. Keppner, P. A. Steinmann, D. Briand, and N. F. de Rooij, Optical, electrical and mechanical properties of the tantalum oxynitride thin films deposited by pulsing reactive gas sputtering, *Thin Solid Films* **515** (2006) 952–956.

[88] C. Le Paven-Thivet, A. Ishikawa, A. Ziani, L. Le Gendre, M. Yoshida, J. Kubota, F. Tessier, and K. Domen, Photoelectrochemical properties of crystalline perovskite lanthanum titanium oxynitride films under visible light, *J. Phys. Chem. C* **113** (2009) 6156–6162.

[89] F. Zhang, A. Yamakata, K. Maeda, Y. Moriya, T. Takata, J. Kubota, K. Teshima, S. Oishi, and K. Domen, Cobalt-modified porous single-crystalline LaTiO2N for highly efficient water oxidation under visible light, *J. Am. Chem. Soc.* **134** (2012) 8348–8351.

[90] J. W. George, PROGRESS IN INORGANIC CHEMISTRY - Halides and Oxyhalides of the Elements of Groups Vb and VIb, in *Prog. Inorg. Chem.*, ed. Cotton, F. A., II, INTERSCIENCE PUBLISHERS, INC., London, 1960, 33.

[91] Alexander Frank Wells, *Structural Inorganic Chemistry (3rd. ed.)*, 4th ed., CLARENDON PRESS - OXFORD Oxford University Press Ely House, London W1, Oxford, 1975.

[92] M. A. Gondal, C. Xiaofeng, and M. A. Dastageer, *Novel Bismuth- Oxyhalide- Based Materials and Their*, 2017.

[93] S. K. Poznyak, and A. I. Kulak, Photoelectrochemical properties oxyhalide films,

Electrochimica **35** (1990) 1941–1947.

[94] J. Di, J. Xia, H. Li, S. Guo, and S. Dai, Bismuth oxyhalide layered materials for energy and environmental applications, *Nano Energy* **41** (2017) 172–192.

[95] Y. N. Zhou, M. Sina, N. Pereira, X. Yu, G. G. Amatucci, X. Q. Yang, F. Cosandey, and K. W. Nam, Feo0.7F1.3/C nanocomposite as a high-capacity cathode material for sodium-ion batteries, *Adv. Funct. Mater.* **25** (2015) 696–703.

[96] S.-T. Zhang, M. Modreanu, H. Roussel, C. Jiménez, and J.-L. Deschanvres, Exploring the optical properties of Vernier phase yttrium oxyfluoride thin films grown by pulsed liquid injection MOCVD, *Dalt. Trans.* **47** (2018) 2655–2661.

[97] S. W. Kim, N. Pereira, N. A. Chernova, F. Omenya, P. Gao, M. S. Whittingham, G. G. Amatucci, D. Su, and F. Wang, Structure Stabilization by Mixed Anions in Oxyfluoride Cathodes for High-Energy Lithium Batteries, *ACS Nano* **9** (2015) 10076–10084.

[98] S. K. Sharma, V. P. Singh, V. S. Chauhan, H. S. Kushwaha, and R. Vaish, Photocatalytic Active Bismuth Fluoride/Oxyfluoride Surface Crystallized 2Bi2O3-B2O3Glass–Ceramics, *J. Electron. Mater.* (2018) 1–7.

[99] J. Li, Y. Yu, and L. Zhang, Bismuth oxyhalide nanomaterials: layered structures meet photocatalysis, *Nanoscale* **6** (2014) 8473–8488.

[100] H. et al. Gnaeyem, Bismuth oxyhalide compounds useful as photocatalysts, W02012/066545, 2018.

[101] H. Shi, W. Ming, and M. H. Du, Bismuth chalcohalides and oxyhalides as optoelectronic materials, *Phys. Rev. B* **93** (2016) 1–7.

[102] K. Kawahara, A. Chikamatsu, T. Katayama, T. Onozuka, D. Ogawa, K. Morikawa, E. Ikenaga, Y. Hirose, I. Harayama, D. Sekiba, T. Fukumura, and T. Hasegawa, Topotactic fluorination of perovskite strontium ruthenate thin films using polyvinylidene fluoride, *CrystEngComm* **19** (2017) 313–317.

[103] T. Katayama, A. Chikamatsu, H. Kamisaka, H. Kumigashira, and T. Hasegawa, Experimental and theoretical investigation of electronic structure of SrFeO3−xFx epitaxial thin films prepared via topotactic reaction, *Appl. Phys. Express* **9** (2016)

2–6.

[104] S. Y. Zheng, a M. Andersson-Fäldt, B. Stjerna, and C. G. Granqvist, Optical properties of sputter-deposited cerium oxyfluoride thin films., *Appl. Opt.* **32** (1993) 6303–9.

[105] T. Onozuka, A. Chikamatsu, T. Katayama, Y. Hirose, I. Harayama, D. Sekiba, E. Ikenaga, M. Minohara, H. Kumigashira, and T. Hasegawa, Reversible Changes in Resistance of Perovskite Nickelate NdNiO3Thin Films Induced by Fluorine Substitution, *ACS Appl. Mater. Interfaces* **9** (2017) 10882–10887.

[106] N. T. Hahn, S. Hoang, J. L. Self, and C. B. Mullins, Spray pyrolysis deposition and photoelectrochemical properties of n-type BiOI nanoplatelet thin films, *ACS Nano* **6** (2012) 7712–7722.

[107] A. Dandapat, H. Gnayem, and Y. Sasson, The fabrication of $BiOCl_x Br_{1-x}$ /alumina composite films with highly exposed {001} facets and their superior photocatalytic activities, *Chem. Commun.* **52** (2016) 2161–2164.

[108] H. Hiramatsu, K. Ueda, T. Kamiya, H. Ohta, M. Hirano, and H. Hosono, Synthesis of single-phase layered oxychalcogenide La2CdO2Se2: crystal structure, optical and electrical properties, *J. Mater. Chem.* **14** (2004) 2946.

[109] S. Bereznev, H. Kocharyan, N. Maticiuc, R. Naidu, O. Volobujeva, A. Tverjanovich, and J. Kois, One-stage pulsed laser deposition of conductive zinc oxysulfide layers, *Appl. Surf. Sci.* **425** (2017) 722–727.

[110] S. Sinha, D. K. Nandi, S. H. Kim, and J. Heo, Atomic-layer-deposited buffer layers for thin film solar cells using earth-abundant absorber materials: A review, *Sol. Energy Mater. Sol. Cells* **176** (2018) 49–68.

[111] H. Hiramatsu, H. Yanagi, T. Kamiya, and K. Ueda, Crystal Structures , Optoelectronic Properties , and Electronic Structures of Layered Oxychalcogenides M CuO Ch (M = Bi , La ; Ch = S , Se , Te): Effects of Electronic Configurations of M3+ Ions, *Chem. Mater.* **20** (2008) 326–334.

[112] M. Goga, R. Seshadri, V. Ksenofonotov, P. Gutlich, and W. Tremel, Ln2Ti2S2O5 (Ln = La , Nd , Sm , Gd): a novel series of defective Ruddlesden – Popper phases, *Chem. Commun. (Camb).* **7** (1999) 979–980.

[113] H. Hiramatsu, K. Ueda, H. Ohta, M. Orita, H. Masahiro, and H. Hideo, Preparation of transparent p-type (La1yxSrxO)CuS thin films by r.f. sputtering technique, *Thin Solid Films* **411** (2002) 125–128.

[114] D. Berthebaud, E. Guilmeau, O. I. Lebedev, A. Maignan, J. Gamon, and P. Barboux, The BiCu1−xOS oxysulfide: Copper deficiency and electronic properties, *J. Solid State Chem.* **237** (2016) 292–299.

[115] H. Hirose, K. Ueda, H. Kawazoe, and H. Hosono, Electronic structure of Sr2Cu2ZnO2S2 layered oxysulfide with CuS layers, *Chem. Mater.* **14** (2002) 1037–1041.

[116] K. Ueda, S. Hirose, H. Kawazoe, and H. Hosono, Electrical and optical properties of layered oxysulfides with CuS layers: Sr-Cu-M-O-S system (M = Zn, Ga, In), *Chem. Mater.* **13** (2001) 1880–1883.

[117] K. Momma, and F. Izumi, VESTA 3 for three-dimensional visualization of crystal, volumetric and morphology data, *J. Appl. Crystallogr.* **44** (2011) 1272–1276.

[118] Z. A. Gál, O. J. Rutt, C. F. Smura, T. P. Overton, N. Barrier, S. J. Clarke, and J. Hadermann, Structural chemistry and metamagnetism of an homologous series of layered manganese oxysulfides, *J. Am. Chem. Soc.* **128** (2006) 8530–8540.

[119] C. Rosticher, B. Viana, M.-A. Fortin, J. Lagueux, L. Faucher, and C. Chanéac, Gadolinium oxysulfide nanoprobes with both persistent luminescent and magnetic properties for multimodal imaging, *RSC Adv.* **6** (2016) 55472–55478.

[120] V. Yufit, M. Nathan, D. Golodnitsky, and E. Peled, Thin-film lithium and lithium-ion batteries with electrochemically deposited molybdenum oxysulfide cathodes, *J. Power Sources* **122** (2003) 169–173.

[121] D. Gonbeau, C. Guimon, G. Pfister-Guillouzo, A. Levasseur, G. Meunier, and R. Dormoy, XPS study of thin films of titanium oxysulfides, *Surf. Sci.* **254** (1991) 81–89.

[122] E. Backen, S. Haindl, T. Niemeier, R. H??hne, T. Freudenberg, J. Werner, G. Behr, L. Schultz, and B. Holzapfel, Growth and anisotropy of La(O, F)FeAs thin films deposited by pulsed laser deposition, *Supercond. Sci. Technol.* **21** (2008).

[123] S. H. Deulkar, J.-L. Huang, and M. Neumann-Spallart, Zinc Oxysulfide Thin Films Grown by Pulsed Laser Deposition, *J. Electron. Mater.* **39** (2010) 589–594.

[124] A. Illiberi, C. Frijters, E. Balder, P. Poodt, and F. Roozeboom, Spatial Atmospheric ALD of Functional Layers for CIGS Solar Cells, *ECS Trans.* **69** (2015) 31–37.

[125] C. Platzer-Björkman, T. Törndahl, D. Abou-Ras, J. Malmström, J. Kessler, and L. Stolt, Zn(O,S) buffer layers by atomic layer deposition in Cu(In,Ga)Se2 based thin film solar cells: Band alignment and sulfur gradient, *J. Appl. Phys.* **100** (2006) 044506.

[126] X. Wang, R. Xiao, H. Li, and L. Chen, Oxysulfide LiAlSO: A Lithium Superionic Conductor from First Principles, *Phys. Rev. Lett.* **118** (2017) 1–6.

[127] S. Ramasubramanian, M. Rajagopalan, J. Kumar, and R. Thangavel, Electronic and optical properties of mixed anion layered oxychalcogenide semiconductors: An ab initio study, *J. Appl. Phys.* **106** (2009).

[128] O. J. Rutt, G. R. Williams, and S. J. Clarke, Reversible lithium insertion and copper extrusion in layered oxysulfides, *Chem. Commun.* **88** (2006) 2869.

[129] D. Yazici, K. Huang, B. D. White, A. H. Chang, A. J. Friedman, and M. B. Maple, Superconductivity of F-substituted *Ln* OBiS $_2$ (*Ln* =La, Ce, Pr, Nd, Yb) compounds, *Philos. Mag.* **93** (2013) 673–680.

[130] I. Polat, S. Aksu, M. Altunbaş, and E. Bacaksz, The influence of diffusion temperature on the structural, optical, and magnetic properties of nickel-doped zinc oxysulfide thin films, *Phys. Status Solidi Appl. Mater. Sci.* **209** (2012) 160–166.

[131] D. C. Johnston, The puzzle of high temperature superconductivity in layered iron pnictides and chalcogenides, *Adv. Phys.* **59** (2010) 803–1061.

[132] Y. Mizuguchi, Superconductivity in BiS 2 -Based Layered Compounds, **58** (2014) 5–9.

[133] S. K. Singh, A. Kumar, B. Gahtori, Shruti, G. Sharma, S. Patnaik, and V. P. S. Awana, Bulk superconductivity in bismuth oxysulfide Bi4O4S3, *J. Am. Chem. Soc.* **134** (2012) 16504–16507.

[134] Y. Mizuguchi, S. Demura, K. Deguchi, Y. Takano, H. Fujihisa, Y. Gotoh, H. Izawa, and

O. Miura, Superconductivity in novel BiS 2-based layered superconductor LaO 1-xF xBiS 2, *J. Phys. Soc. Japan* **81** (2012) 1–5.

[135] C. Doussier-Brochard, B. Chavillon, L. Cario, and S. Jobic, Synthesis of p-type transparent laOCuS nanoparticles via soft chemistry, *Inorg. Chem.* **49** (2010) 3074–3076.

[136] K. Ueda, K. Takafuji, H. Hiramatsu, H. Ohta, T. Kamiya, M. Hirano, and H. Hosono, Electrical and optical properties and electronic structures of LnCuOS (Ln = La - Nd), *Chem. Mater.* **15** (2003) 3692–3695.

[137] M. Palazzi, Preparation and refining of the structure of (LaO) CuS, *COMPTES RENDUS L Acad. DES Sci. Ser. II* **292** (1981) 789–791.

[138] C. Bugot, N. Schneider, M. Jubault, D. Lincot, and F. Donsanti, Temperature effect on zinc oxysulfide-Zn(O,S) films synthesized by atomic layer deposition for Cu(In,Ga)Se $_2$ solar cells, *J. Vac. Sci. Technol. A Vacuum, Surfaces, Film.* **33** (2015) 01A151.

[139] H. H. Park, A. Jayaraman, R. Heasley, C. Yang, L. Hartle, R. Mankad, R. Haight, D. B. Mitzi, O. Gunawan, and R. G. Gordon, Atomic layer deposition of Al-incorporated Zn(O,S) thin films with tunable electrical properties, *Appl. Phys. Lett.* **105** (2014).

[140] S. Kim, S. Kasashima, P. Sichanugrist, T. Kobayashi, T. Nakada, and M. Konagai, Development of thin-film solar cells using solar spectrum splitting technique, *Sol. Energy Mater. Sol. Cells* **119** (2013) 214–218.

[141] S. A. Petrova, V. P. Mar'evich, R. G. Zakharov, E. N. Selivanov, V. M. Chumarev, and L. Y. Udoeva, Crystal structure of zinc calcium oxysulfide, *Dokl. Chem.* **393** (2003) 255–258.

[142] Z. Qiu, C. Rong, W. Zhou, J. Zhang, C. Li, L. Yu, S. Liu, and S. Lian, A strategy for synthesizing CaZnOS:Eu2+phosphor and comparison of optical properties with CaS:Eu2+, *J. Alloys Compd.* **583** (2014) 335–339.

[143] S. S. Bastanov, O. I. Ryabinina, K. F. Obzherina, and S. S. Derbeneva, ON THE CHEMICAL STRUCTURE OF MANGANESE OXYSULFIDES, *Izv. Akad. Nauk SSSR, Seriya Khimicheskaya* (1968) 8–14.

[144] C. Pan, J. C. Zhang, M. Zhang, X. Yan, Y. Z. Long, and X. Wang, Intrinsic oxygen vacancies mediated multi-mechano-responsive piezoluminescence in undoped zinc calcium oxysulfide, *Appl. Phys. Lett.* **110** (2017) 1–6.

[145] O. Krause, P. Dürichen, C. Näther, and W. Bensch, Directed Syntheses of New Quaternary Niobium Oxysulfides: Crystal Structures and Properties of K4Nb2S10O and Rb4Nb2S10O Compared to K4Nb2S11, *Eur. J. Inorg. Chem.* (1999) 1295–1299.

[146] F. Calvagna, J. Zhang, S. Li, and C. Zheng, Synthesis and Structural Analysis of $Ba_3V_2O_3S_4$, *Chem. Mater.* **13** (2001) 304–307.

[147] Y. Xia, F. Huang, W. Wang, Y. Wang, K. Yuan, M. Liu, and J. Shi, A novel red-emitting Mn-activated BaZnOS phosphor, *Opt. Mater. (Amst).* **31** (2008) 311–314.

[148] A. Pal, H. Kishan, and V. P. S. Awana, Synthesis and structural details of BiOCu 1-x S: Possible new entrant in a series of exotic superconductors?, *J. Supercond. Nov. Magn.* **23** (2010) 301–304.

[149] A. Ubaldini, E. Giannini, C. Senatore, and D. Van Der Marel, BiOCuS: A new superconducting compound with oxypnictide-related structure, *Phys. C Supercond. Its Appl.* **470** (2010) S356–S357.

[150] C. Deudon, A. Meerschaut, L. Cario, and J. Rouxel, Preparation and Crystal Structure Determination of La20Ti11S44O6, *J. Solid State Chem.* **120** (1995) 164–169.

[151] H. Hiramatsu, K. Ueda, K. Takafuji, H. Ohta, M. Hirano, T. Kamlya, and H. Hosono, Intrinsic excitonic photoluminescence and band-gap engineering of wide-gap p-type oxychalcogenide epitaxial films of LnCuOCh (Ln = La, Pr, and Nd; Ch = S or Se) semiconductor alloys, *J. Appl. Phys.* **94** (2003) 5805–5808.

[152] C. Boyer-Candalen, J. Derouet, P. Porcher, Y. Moëlo, and A. Meerschaut, The family of Ln2Ti2S2O5compounds (Ln=Nd, Sm, Gd, Tb, Dy, Ho, Er, and Y): Optical properties, *J. Solid State Chem.* **165** (2002) 228–237.

[153] S. Altmannshofer, and D. Johrendt, Synthesis, Crystal Structure and Magnetism of the New Oxysulfide Ce3NbO4S3, *Zeitschrift Für Anorg. Und Allg. Chemie* **634** (2008) 1361–1364.

[154] G. H. Chan, B. Deng, M. Bertoni, J. R. Ireland, M. C. Hersam, T. O. Mason, R. P. Van Duyne, and J. A. Ibers, Syntheses, structures, physical properties, and theoretical studies of CeMxOS (M = Cu, Ag; x ≈ 0.8) and CeAgOS, *Inorg. Chem.* **45** (2006) 8264–8272.

[155] T. Kobayashi, Z. J. L. Kao, and T. Nakada, Temperature dependent current-voltage and admittance spectroscopy on heat-light soaking effects of Cu(In,Ga)Se2 solar cells with ALD-Zn(O,S) and CBD-ZnS(O,OH) buffer layers, *Sol. Energy Mater. Sol. Cells* **143** (2015) 159–167.

[156] C. Stock, and E. E. McCabe, The magnetic and electronic properties of oxyselenides - Influence of transition metal ions and lanthanides, *J. Phys. Condens. Matter* **28** (2016).

[157] A. Krzton-Maziopa, Z. Guguchia, E. Pomjakushina, V. Pomjakushin, R. Khasanov, H. Luetkens, P. K. Biswas, A. Amato, H. Keller, and K. Conder, Superconductivity in a new layered bismuth oxyselenide: LaO 0.5F0.5BiSe2, *J. Phys. Condens. Matter* **26** (2014) 1–6.

[158] J. Sui, J. Li, J. He, Y.-L. Pei, D. Berardan, H. Wu, N. Dragoe, W. Cai, and L.-D. Zhao, Texturation boosts the thermoelectric performance of BiCuSeO oxyselenides, *Energy Environ. Sci.* **6** (2013) 2916.

[159] K. Ueda, H. Hiramatsu, H. Ohta, M. Hirano, T. Kamiya, and H. Hosono, Single-atomic-layered quantum wells built in wide-gap semiconductors LnCuOCh (Ln = lanthanide, Ch = chalcogen), *Phys. Rev. B - Condens. Matter Mater. Phys.* **69** (2004) 2–5.

[160] L.-D. Zhao, J. He, D. Berardan, Y. Lin, J.-F. Li, C.-W. Nan, and N. Dragoe, BiCuSeO oxyselenides: new promising thermoelectric materials, *Energy Environ. Sci.* **7** (2014) 2900–2924.

[161] J. Li, J. Sui, Y. Pei, X. Meng, D. Berardan, N. Dragoe, W. Cai, and L.-D. Zhao, The roles of Na doping in BiCuSeO oxyselenides as a thermoelectric material, *J. Mater. Chem. A* **2** (2014) 4903.

[162] S. J. Sedlmaier, S. J. Cassidy, R. G. Morris, M. Drakopoulos, C. Reinhard, S. J. Moorhouse, D. O'Hare, P. Manuel, D. Khalyavin, and S. J. Clarke, Ammonia-rich

high-temperature superconducting intercalates of iron selenide revealed through time-resolved in Situ X-ray and neutron diffraction, *J. Am. Chem. Soc.* **136** (2014) 630–633.

[163] F. Han, D. Wang, C. D. Malliakas, M. Sturza, D. Y. Chung, X. Wan, and M. G. Kanatzidis, (CaO)(FeSe): A Layered Wide-Gap Oxychalcogenide Semiconductor, *Chem. Mater.* **27** (2015) 5695–5701.

[164] H. Hiramatsu, T. Kamiya, T. Tohei, E. Ikenaga, T. Mizoguchi, Y. Ikuhara, K. Kobayashi, and H. Hosono, Origins of hole doping and relevant optoelectronic properties of wide gap p-type semiconductor, LaCuOSe, *J. Am. Chem. Soc.* **132** (2010) 15060–15067.

[165] M. Yasukawa, K. Ueda, and H. Hosono, Thermoelectric properties of layered oxyselenides La1-xSrxCuOSe (x=0 to 0.2), *J. Appl. Phys.* **95** (2004) 3594–3597.

[166] A. J. Tuxworth, and J. S. O. Evans, Synthesis, structure and properties of the oxychalcogenide series A 4O4TiSe4 (A=Sm, Gd, Tb, Dy, Ho, Er and Y), *J. Solid State Chem.* **210** (2014) 188–194.

[167] J. Wu, C. Tan, Z. Tan, Y. Liu, J. Yin, W. Dang, M. Wang, and H. Peng, Controlled Synthesis of High-Mobility Atomically Thin Bismuth Oxyselenide Crystals, *Nano Lett.* **17** (2017) 3021–3026.

[168] F. Li, J.-F. Li, L.-D. Zhao, K. Xiang, Y. Liu, B.-P. Zhang, Y.-H. Lin, C.-W. Nan, and H.-M. Zhu, Polycrystalline BiCuSeO oxide as a potential thermoelectric material, *Energy Environ. Sci.* **5** (2012) 7188.

[169] Y. Y. Liu, L. D. Zhao, Y. Zhu, Y. Y. Liu, F. Li, M. Yu, D. B. Liu, W. Xu, Y. H. Lin, and C. W. Nan, Synergistically Optimizing Electrical and Thermal Transport Properties of BiCuSeO via a Dual-Doping Approach, *Adv. Energy Mater.* **6** (2016) 1–9.

[170] L. X. Pan, Q. L. Xia, S. L. Ye, N. Ding, and Z. R. Liu, First principles study of electronic structure, chemical bonding and elastic properties of BiOCuS, *Trans. Nonferrous Met. Soc. China (English Ed.* **22** (2012) 1197–1202.

[171] J. Li, J. Sui, C. Barreteau, D. Berardan, N. Dragoe, W. Cai, Y. Pei, and L. D. Zhao, Thermoelectric properties of Mg doped p-type BiCuSeO oxyselenides, *J. Alloys Compd.* **551** (2013) 649–653.

[172] D. Feng, F. Zheng, D. Wu, M. Wu, W. Li, L. Huang, L. D. Zhao, and J. He, Investigation into the extremely low thermal conductivity in Ba heavily doped BiCuSeO, *Nano Energy* **27** (2016) 167–174.

[173] L. D. Zhao, D. Berardan, Y. L. Pei, C. Byl, L. Pinsard-Gaudart, and N. Dragoe, Bi1-xSrxCuSeO oxyselenides as promising thermoelectric materials, *Appl. Phys. Lett.* **97** (2010) 10–13.

[174] S. L. Wu, Z. A. Sun, F. K. Chiang, C. Ma, H. F. Tian, R. X. Zhang, B. Zhang, J. Q. Li, and H. X. Yang, Synthesis and physical property characterization of LaOBiSe2and LaO0.5F0.5BiSe2superconductor, *Solid State Commun.* **205** (2015) 14–18.

[175] S. D. N. Luu, and P. Vaqueiro, Synthesis, characterisation and thermoelectric properties of the oxytelluride Bi2O2Te, *J. Solid State Chem.* **226** (2015) 219–223.

[176] S. M. George, G. S. M., S. M. George, and G. S. M, Atomic Layer Deposition: An Overview, *Chem. Rev.* **110** (2010) 111.

[177] K. Kukli, M. Peussa, L.-S. Johansson, E. Nykänen, and L. Niinistö, Controlled Growth of Yttrium Oxysulphide Thin Films by Atomic Layer Deposition, *Mater. Sci. Forum* **315–317** (1999) 216–221.

[178] J. Penttinen, Alkali- ja maa-alkalimetalleihin perustuvat metalli-orgaanisen runkorakenteen ohutkalvot ALD / MLD-menetelmällä. Alkali and Earth Alkaline - based Metal-Organic Framework Thin Films by ALD/MLD, Aalto University, (2016).

[179] M. Nisula, and M. Karppinen, Atomic/Molecular Layer Deposition of Lithium Terephthalate Thin Films as High Rate Capability Li-Ion Battery Anodes, *Nano Lett.* **16** (2016) 1276–1281.

[180] M. E. Alnes, E. Monakhov, H. Fjellvåg, and O. Nilsen, Atomic layer deposition of copper oxide using copper(II) acetylacetonate and ozone, *Chem. Vap. Depos.* **18** (2012) 173–178.

[181] MERCK, and SIGMA-ALDRICH, 155756 ALDRICH 2,2,6,6-Tetramethyl-3,5-heptanedione 98%, https://www.sigmaaldrich.com/catalog/product/aldrich/155756?lang=fi&region=FI , 20.6.2018.

[182] T. Suntola, United States Patent (19) 54 METHOD FOR PRODUCING COMPOUND THIN FILMS, (1977).

[183] N. P. Dasgupta, X. Meng, J. W. Elam, and A. B. F. Martinson, Atomic Layer Deposition of Metal Sulfide Materials, *Acc. Chem. Res.* **48** (2015) 341–348.

[184] M. Leskelä, and M. Ritala, Atomic Layer Deposition Chemistry: Recent Developments and Future Challenges, *Angew. Chemie - Int. Ed.* **42** (2003) 5548–5554.

[185] E. Ahvenniemi, and M. Karppinen, Atomic/molecular layer deposition: a direct gas-phase route to crystalline metal–organic framework thin films, *Chem. Commun.* **52** (2016) 1139–1142.

[186] R. Eason, *Pulsed Laser Deposition of Thin Films - Applications-Led Growth of Functional Materials*, John Wiley & Sons, Inc., 2007.

[187] M. Nieminen, M. Putkonen, and L. Niinistö, Formation and stability of lanthanum oxide thin films deposited from β-diketonate precursor, *Appl. Surf. Sci.* **174** (2001) 155–165.

[188] C. Wang, M. Tan, C. Feng, Z. Ma, S. Jiang, Z. Xu, G. Cao, K. Matsubayashi, and Y. Uwatoko|, La2Co2Se2O3: A Quasi-Two-Dimensional Mott Insulator with Unusual Cobalt Spin State and Possible Orbital Ordering, *J. AM. CHEM. SOC.* **132** (2010) 7069–7073.

[189] F. Q. Huang, P. Brazis, C. R. Kannewurf, and J. A. Ibers, Synthesis, structure, electrical conductivity, and band structure of the rare-earth copper oxychalcogenide La5Cu6O4S7, *J. Solid State Chem.* **155** (2000) 366–371.